INVESTIGATION OF BIOLOGICAL ROLES OF NEURAMINIDASE 3 AND N-ACETYLGALACTOSAMINYLTRANSFERASE ENZYMES IN GLYCOLIPID METABOLISM

A Thesis Submitted to
The Graduate School of
İzmir Institute of Technology
in Partial Fulfillment of the Requirements for the Degree of

MASTER OF SCIENCE

in Molecular Biology and Genetics

by
Hatice Hande BASIRLI

July 2020
İzmir

ACKNOWLEDGEMENTS

In the beginning, I would like to thank to the people who contributed to my thesis in different ways. First of all, I would like to express my deepest regards and thanks to my supervisor Prof. Dr. Volkan SEYRANTEPE for his patient, encouraging, and understanding guidance and extensive knowledge throughout my graduate studies and thesis writing.

I would like to thank to The Scientific and Technological Research Council of Turkey (TÜBİTAK) (215Z083) for their financial support of my thesis research.

I have very special thanks to my friends and co-workers Melike CAN, Tuğçe ŞENGÜL, and Deniz AK for their precious friendship, help, and encouragement in every day. I am also grateful to my other co-workers Nurselin ATEŞ, Orhan Kerim İNCİ, and Berkay DAĞALP for their help and kindness during my thesis. I especially thank to Seçil AKYILDIZ DEMİR for mentoring me throughout my research. I am also grateful to the undergraduate members of Seyrantepe Laboratory for their voluntary support and learning enthusiasm.

At last but not least, I am deeply grateful to my grandparents Fehmiye YILDIZ and Osman YILDIZ for their endless love, infinite believe, and support to me throughout my life. I would like to thank to my dear mother Vildan YILDIZ for raising me with endless love and support. If I am here, this is all your success.

ABSTRACT

INVESTIGATION OF BIOLOGICAL ROLES OF NEURAMINIDASE 3 AND N-ACETYLGALACTOSAMINYLTRANSFERASE ENZYMES IN GLYCOLIPID METABOLISM

Gangliosides are sialic acid containing biomolecules and perform important functions by locating on cell membranes. Their catabolism regulated by sialidases while their synthesis was performed by glycosyltransferases. Neu3 reacts with gangliosides on plasma-membrane and acts in cellular processes. Neu3 mice model was studied without signs of altered brain activity and phenotypic alterations. In further studies, significance of Neu3 sialidase in bypass mechanism shown in Tay-Sachs disease mice model named as Hexa-/-Neu3-/- mice. Galgt enzyme produces 0-, a-, b-, and c-series of complex gangliosides. *Galgt* deficiency led to progressive axonal degeneration, decreased myelin volume, altered axo-glial junction integrity, male infertility and hindpaw-clasping in mice. However, the studies for showing In this study, we investigated altered ganglioside metabolism, ER-stress, oxidative stress, and apoptosis mechanisms in cortex, thalamus, and cerebellum tissues of 3- and 6-month-old Neu3-/-, Galgt-/-, and Neu3-/-Galgt-/- mice compared to age-matched WT control by performing molecular biological techniques (TLC, RT-PCR, and Western Blot analyses). Furthermore, we performed histopathologic and immunohistochemical analyses to examine the alterations in myelination, neuron number, and glyco-conjugate content, morphological abnormalities, and apoptosis in brain sections of single and double deficient mice models. We also performed behavioral assays like rotarod, passive avoidance and open field to show altered brain functions and behavioral abnormalities like anxiety, reduced motor balance, strength, and locomotory activity in addition to problems in memory formation. In line with these studies, we found that Neu3 and Galgt enzymes acts in the regulation of ganglioside metabolism in a region-specific and age-dependent manner.

ÖZET

NÖROMİNİDAZ 3 VE N-ASETİLGALAKTOZAMİNİLTRANSFERAZ ENZİMLERİNİN GLİKOLİPİD METABOLİZMASINDAKİ BİYOLOJİK ROLÜNÜN ARAŞTIRILMASI

Gangliositler siyalik asit içeren biyomoleküller olup hücre zarında önemli işlevleri yerine getirir. Gangliosit sentezi glikosiltransferazlarla gerçekleştirilirken katabolizmaları sialidazlarla düzenlenmiştir. Neu3 sialidazı gangliositler üzerinde etkili olup hücresel işlemlerde rol alır. Neu3 fare modelinde, değişmiş beyin aktivitesi ve fenotipik değişiklikler gözlenmemiştir. Daha sonra yapılan çalışmalarda, Neu3 enziminin Hexa-/-Neu3-/- fare modelinde Tay-Sachs hastalığı patolojisine sebep olduğu belirtilmiştir. Galgt enzimi, 0-, a-, b- ve c-serisi kompleks gangliosidleri üretir. Galgt eksikliği, ilerleyici aksonal dejenerasyona, azalmış miyelin hacmine, değişen akso-glial bağlantı bütünlüğüne, erkek kısırlığına ve farelerde arka pençeye neden oldu. Biz bu çalışmada, 3- ve 6 aylık Neu3-/-, Galgt-/- ve Neu3-/- Galgt-/- fare modellerinin korteks, talamus ve beyincik dokularında değişen gangliosit metabolizmasını, ER stres, oksidatif stres ve apoptoz mekanizmalarını yaş-uyumlu WT kontrolü ile kıyaslayarak moleküler biyolojik teknikler (TLC, RT-PCR ve Western Blot analizleri) ile araştırdık. Ayrıca miyelinasyon, nöron sayısı ve gliko-konjugat içeriği, morfoloji ve apoptoz analizlerini tek ve çift gen eksiği olan fare modellerinin beyin kesitlerinde histopatolojik ve immünohistokimyasal teknikler uygulayarak gerçekleştirdik. Ayrıca değişen beyin fonksiyonlarını ve anksiyete, azalan motor kontrolü, güç ve hafıza oluşturma gibi davranış anormalliklerini göstermek için rotarod, pasif kaçınma ve açık alan gibi davranış analizleri yaptık. Bu çalışmalar sonucunda, Neu3 ve Galgt enzimlerinin gangliosit metabolizmasının düzenlenmesinde bölgeye ve yaşa bağlı olarak etkili olduğunu düşünüyoruz.

Dedicated to my grandparents,
Fehmiye & Osman YILDIZ…

TABLE OF CONTENTS

LIST OF FIGURES

Figure **Page**

Figure **Page**

Figure **Page**

LIST OF TABLES

Table **Page**

CHAPTER 1

INTRODUCTION

1.1. Gangliosides

One group of lipid-containing biomolecules named as glycolipids are formed by a glycosidic linkage bonding one or more carbohydrate moieties to hydrophobic lipid residues (Hirabayashi 2012). Sphingolipids are the most abundant lipid molecules found in plasma membrane of many organism. They perform significant functions for regulating cellular mechanisms like differentiation, cell death, division and signaling (Chen *et al*. 2010). They are categorized under neutral lipids containing a sphingoid base backbone called sphingosine. Combinations of sphingosine with fatty acids result in ceramide groups. After formation of ceramide backbone, diverse groups in neutral or charged, and glycosylated or phosphorylated forms could bind to increase complexity of sphingolipids (Pralhada *et al*. 2013; Ohanian and Ohanian 2001). Once hydrophobic lipid residues are sphingoid base or ceramide in a glycolipid, they are then specified as glycosphingolipids (Holst 2007). These biomolecules could have distinct patters of hydrophobic moieties and a various forms of carbohydrate components resulting in a diversity. The variation in the carbohydrate moieties of glycosphingolipids (GSLs) defines a classification into following series as ganglio-, isoganglio-, lacto-, neolacto-, lactoganglio-, globo-, isoglobo-, muco-, gala-, neogala-, mollu-, arthro-, schisto- and spirometo-series (Iwabuchi *et al*. 2015).

The sialic acid (N-acetylneuraminic acid or N-glycolylneuraminic acid) carrying molecules called gangliosides are a group of acidic glycosphingolipids (Robert *et al*. 2011). The syntheses of this class of glycosphingolipids are initiated in Endoplasmic reticulum after which the carbohydrate moieties are sequentially added to the hydrophobic lipid residues in the Golgi apparatus for further modification. These modifications are performed by the actions of a series of glycosyltransferases adding sialic acid residues sequentially to the lactosylceramide (LacCer) or to the galactosylceramide (GalCer) forming G_{M4}. In 2012, Kolter named this synthesis pathway as “combinatorial ganglioside biosynthesis” (Kolter 2012) where sialylation of LacCer is

initiated in the Golgi and TGN membranes resulting in simple gangliosides G_{M3}, G_{D3} and G_{T3}. Once these molecules are formed, the complex gangliosides are generated through the enzymatic activity of membrane-linked glycosyltransferases. As a result of this biosynthesis, 0-, a-, b- and c-series gangliosides with no-, one- sialic acid residue and two-, three-sialic acid residues are obtained. Degradation of gangliosides are generated in lysosomes and endosomes via the cleavage of terminal sugars sequentially toward the ceramide core by glycohydrolases (Palmano *et al*. 2015). The ganglioside biosynthesis and degradation pathways were shown in the Figure 1.1. The gangliosides are localized in body fluids and tissues but they are abundantly found in nervous system as a member of outer leaflets of plasma membranes or of microdomains on cell surface together with cholesterol and sphingomyelin. Through their localization in special microdomains called as lipid rafts, caveolae, or GSL-rich microdomains or interactions with other lipids, they perform important roles like cell to cell recognition, signal transduction and cell adhesion (Xu *et al*. 2010).

One class of gangliosides named as ganglio-series gangliosides are expressed differentially throughout the brain development such as predominant expression of simple gangliosides -G_{M3} and G_{D3} in embryonic brains of rodents and humans. While the brains continue to develop, the complex gangliosides -G_{M1}, G_{D1a}, G_{D1b} and G_{T1b} start to substitute the former ones by an up-regulation in their expression in contrast to down-regulated expression of the simple gangliosides (Xu *et al*. 2010). This differential expression occurs mostly in a region-specific manner so that it affects neurodevelopmental stages such as neuritogenesis, synaptogenesis, myelination and axogenesis. Due to the importance of the gangliosides in both the neuronal development and signal transduction, they are involved in the pathophysiology of many diseases. For instance, in Guillain-Barré syndrome, the gangliosides on the cell surface lead to autoimmune response. The involvement of the gangliosides is also presented in the lysosomal storage disorders like G_{M1} gangliosidosis and G_{M2} gangliosidosis (Sandhoff disease and Tay-Sachs disease, respectively) where deficiencies in certain glycosyltransferases or their co-activators lead to accumulating glycosphingolipids or gangliosides in lysosomes (Sandhoff and Harzer 2013).

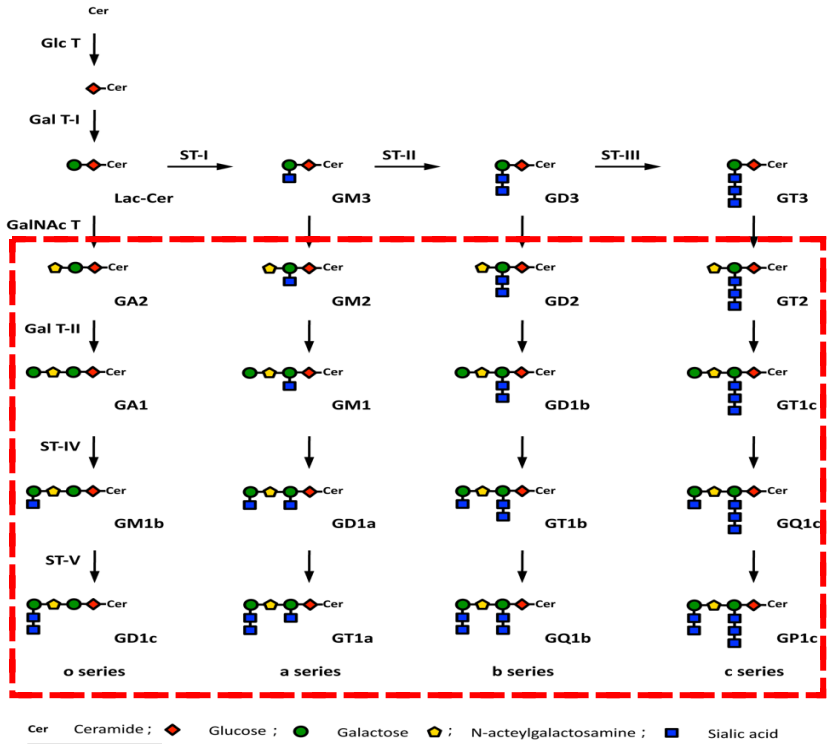

Figure 1.1. The ganglioside biosynthesis pathway in human and the dashed-boxed shows the 0-, a-, b-, and c- series of complex gangliosides by courtesy of Fougeray *et al* (Fougeray *et al*. 2016)

1.1.1. Gangliosides and Signaling Pathways

The gangliosides residing on the plasma membrane in special structures as caveolae and lipid rafts showed important roles in signaling pathways. The gangliosides were studied by d'Azzo *et al*. in 2006 for understanding their importance in adaptive stress responses like apoptosis. According to their investigations, once a stress factor was detected by cells, the gangliosides elevated in their concentration to induce cell death program. They performed their roles of either proliferation or cell death by acting in subcellular regions such as ER and mitochondria through increasing or decreasing their concentrations and modifying their sugar backbone (d'Azzo *et al*. 2006).

By taking important roles on the cell membranes, the gangliosides could lead to detrimental outcomes. The alterations in the ganglioside content and configuration could result in the changes in membrane dynamics and arrangements or the activities of other membrane proteins. Because they have an amphipathic characteristic, they could reside on not only the outer leaflets of cell membranes but also mitochondria and endoplasmic

reticulum in small portions. The ganglioside content could vary in cell type- or species-specific manner in addition to changes during development and the cell state (Heffer-Lauc *et al*. 2005). The amphipathic feature of gangliosides and variety in their hydrophobic parts, they could localize in special membrane domains like lipid rafts and caveolae while they could spread in an asymmetric manner over the cell membranes. The gangliosides having diversity and complexity in their structures and membrane localizations perform special roles by being coreceptors or receptors of bacteria, viruses, toxins and cytokines apart from acting as a part of important signaling pathways such as signal transduction, cell adhesion, and cell recognition (Ledeen and Gusheng 2002). Moreover, their specific actions have also been revealed in the stress response like apoptosis through increase in their concentrations. Therefore, it was deduced that gangliosides controlling many signaling mechanisms could determine differentiation, cell division, or cellular death. While the exact mechanisms for their roles in these pathways have not been elucidated yet, their actions are deduced to occur in membrane parts like caveolae and lipid rafts where the gangliosides could cooperate other membrane proteins by changing in concentration or types (Miljan and Bremen 2002). In addition to their important roles in membrane domains, their actions have been concluded in mitochondria and endoplasmic reticulum where they affect opposing cellular pathways like apoptosis versus proliferation through organizing their concentrations locally or modifying the sugar backbones. Their activities in those sub-cellular compartments could eventually cause ER stress conditions, mitochondrial apoptosis induction, or both of them once the compositions, concentrations, and localizations of the gangliosides are altered (Heffer-Lauc *et al*. 2005).

Their roles in endoplasmic reticulum membrane have been shown to modulate Ca^{2+} flux through the ER membrane. Since the ER is primary storage region for intracellular Ca^{2+} in nerve cells, this compartment is really important for the control of cellular pathways requiring Ca^{2+} ion like protein folding after translation by the ER-resident proteins (Berridge, Bootman, and Roderick 2003; Ledeen and Gusheng 2002). This signaling mechanism is checked by a mechanism called Unfolded Protein Response (UPR) or ER-stress response in which certain ER chaperons such as BiP normally interacting with UPR sensors as IRE1, ATF6, and PERK on ER membrane are activated (Schröder and Kaufman, 2005). The active BiP removal from its interactors cause the activation of those molecules by homodimerization and trans-autophosphorylation of PERK and IRE1 homodimerization while ATF6 is directed to Golgi for being proteolyzed

in to an active transcription factor (Bonilla *et al*. 2002). Then, after being translocated into nucleus, it binds to promoters of ER-responsive elements for the expression of ER-chaperons like BiP, Calreticulin and Calnexin while this transcription factor also induces CHOP/GADD153 as the proapoptotic transcription factor reducing antiapoptotic Bcl2 expression. On the other hand, the IRE1 activation causes a proteolytic cleavage into ribonuclease and kinase activity bearing soluble C-terminal fragments from which some of them enters into nucleus for inducing ER-responsive genes while the ribonuclease part splices an intron of XBP1 mRNA to create an active XBP1 transcription factor for activating ER-stress related genes (Patil and Walter, 2001; McCullough *et al*. 2001). Moreover, by the actions of IRE1 recruited TRAF2 (tumor necrosis factor receptor–associated factor 2) protein which binds to activate JNK, the proapoptotic mechanisms are activated. Apart from the actions of IRE1 and ATF6, the PERK acts to terminate translation. Depending on the types or levels of stressors, the activations of ER-stress controlling chaperones or proapoptotic molecules are detected in cells. Therefore, the importance of the regulation of Ca^{2+} in ER is concluded through those observations (Harding *et al*. 2000).

The studies have showed that the gangliosides perform regulatory actions on the Ca^{2+} of ER through their localization on the ER membranes. The roles of GlcCer in Gaucher disease for calcium mobilization, G_{M2} on the SERCA pumps of ER membrane, and accumulation of G_{M1} in G_{M1} gangliosidosis causing Ca^{2+} store depletion in ER but not the molecular mechanisms have been deduced (d'Azzo *et al*. 2006; Babcock and Hille 1998). In the further studies, by the double deficiency of Galgt and β-galactosidase enzymes in the animal model resulting in deficient G_{M1} ganglioside, there were no signs of ER-stress activated proapoptotic signaling. The elevation in G_{M1} content in ER could lead to ER-stress response by either influencing Ca^{2+} transport through the ER membrane or regulating ER-membrane proteins like Ca^{2+} channels or pumps. Especially, the last probability has been related with the G_{M2} activity on SERCA pump in Sandhoff disease mice. Through accumulation of gangliosides within the nerve cells could probably alter ER membrane composition and Ca^{2+} homeostasis resulting in ER-stress response and apoptotic neuron death (d'Azzo *et al*. 2006; Babcock and Hille 1998; Boya *et al*. 2002).

The ER and mitochondria cooperation for controlling intracellular calcium ion content alters the apoptosis pathway which is also controlled by the changes in ganglioside content and composition on those subcellular membranes. The significantly

increased GM1 ganglioside in ER would then influence the very closely localized mitochondrial membranes through the stimulating calcium ion content of this organelle. According to the studies, it was indicated that ER-released Ca^{2+} causes deterioration in mitochondrial membrane permeability (MMP) since the permeability transition pore (PTP) opening is generated. The opening of this pore could occur due to the negative actions of elevated Ca^{2+} content, reactive oxygen species, altered mitochondrial pH, and increased concentrations of ganglioside G_{D3} (Malisan and Testi 2002). These factors lead to the releasing of cytochrome c and apoptosis inducible factor while the released cytochrome c activates caspases and nucleases and acts to induce apoptosome formation in cytosol. In the studies of Scorrano et al., it was investigated that G_{M3} and G_{D1a} gangliosides were not as effective as the G_{D3} for acting on PTP opening while the acetylated G_{D3} prevented the proapoptotic actions of G_{D3} ganglioside. In the further studies, antagonists of G_{D3} as the PT inhibitors indicated the pore-level activity of this ganglioside. Moreover, overexpressed calnexin -ER chaperone- keeps G_{D3} synthase in ER for preventing the transportation of G_{D3} toward the mitochondria (Scorrano *et al*. 1999).

Actions of gangliosides are not restricted to those molecules since their actions in proapoptotic or antiapoptotic elements of Bcl2 family proteins have been indicated. These proteins are involved in ER-stress mediated apoptosis induction by localizing in both ER and mitochondria where they could control Ca^{2+} composition. Antiapoptotic Bcl2 protein residing on ER membrane prevents the Ca^{2+} efflux toward mitochondria to decrease calcium ion levels while the proapoptotic Bax and Bak of ER are oligomerized due to Ca^{2+} mediated ER stress after which they activate Caspase 12 for inducing apoptotic program. Ratio of Bax and Bak to Bcl2 could be a determination factor for ER stress conditions due to Ca^{2+} content. Concentration and compositional changes of gangliosides in nerve cells should be controlled to regulate cell fate decisions (Rippo *et al*. 2000).

In addition to ER stress mediated mitochondrial deterioration terminating with apoptosis, the direct action of G_{D3} ganglioside on mitochondria was also investigated in the studies. According to these investigations, the action of CD95- and ceramide-mediated apoptotic induction could be understood. In this case, conversion of ceramide into G_{D3} is a critical step for initiation of Fas mediated apoptotic cell death because G_{D3} elevation results in the disturbed mitochondrial membrane potential (De Maria 1997). At the end, the mitochondrial pores would be open to release its content as cytochrome c, AIF, mitochondrial caspases, and ATP. Through the release of cytochrome c and ATP which are cofactors of Apaf-1, Apaf-1-regulated induction of caspase-9 is initiated

whereas AIF functions to influence nucleus mediated apoptosis. After isolation of mitochondria and its induction by G_{D3}, the results have indicated that G_{D3} ganglioside works to disturb mitochondrial membrane potential and to cause apoptosis. mitochondrial depolarization, loss of oxidative phosphorylation, and reactive oxygen species (ROS) overgeneration (Malisan and Testi 2002).

The excessively generated reactive oxygen species could then lead to oxidative stress which is another stress factor for the initiation of apoptosis unless they are prevented by antioxidant defense enzymes such as Catalase, TTase1, and SOD2. Catalase works in catalyzing of hydrogen peroxide into water and oxygen while SOD2 functions as an antiapoptotic molecule in the antioxidant defense system. Finally, the TTase1 of glutaredoxin family works as the part of antioxidant defense mechanism enzyme. In the studies of Malisan *et al*. with the liver mitochondria, it was obtained that ganglioside G_{D3} acted for induction of ROS, cytochrome c, caspase 9, and AIF release in contrast to other gangliosides such as G_{M3} and G_{D1a}. From the analyses with isolated mitochondria, it was deduced that G_{D1a}, G_{D1b}, G_{T1b}, and G_{Q1b} could induce cytochrome c release but G_{M1}, G_{M2}, and G_{M3} could not. Moreover, through the G_{D3} treatment but not G_{M3} and G_{D1a} treatments, the released factors from mitochondria to cytosol resulted in DNA fragmentation. The opening of mitochondrial channels and the releasing of its content were show to be regulated by the actions of antiapoptotic Bcl2 family proteins that affect the G_{D3} targets like G_{D3} synthase. Apart from the anti-apoptotic forms of Bcl2 family, the proapoptotic types like Bax could act together with the G_{D3} ganglioside for apoptotic signaling (Malisan and Testi 2002; García-Ruiz *et al*. 2000).

1.2. Sialidases

The removal of terminally associated acidic monosaccharides from carbohydrate portions of glycoconjugates like glycoproteins or glycolipids is performed by certain glycosidases called sialidases or neuraminidases. The enzymes acting on sialic acid removal from G_{M2} to generate G_{A2} ganglioside which is further catabolized into LacCer by HEXB in the mouse neurons are called sialidases. These enzymes work on monosialylated or polysialylated glycolipids (gangliosides) in order for desialylating those biomolecules. As mentioned before, those enzymes are encoded by *Neu1*, *Neu2*,

Neu3 and *Neu4* genes whose products are distributed in different cell structures with distinct enzymatic activities (Seyrantepe *et al*. 2008).

They are existed in vertebrates and certain microorganisms such as viruses, fungi and bacteria. After the studies with the rat tissues, four distinct forms of mammalian sialidases have been characterized together with their specific functions, subcellular localizations and enzymatic features. According to the results of molecular cloning studies, the subcellular localizations of the mammalian sialidases have been revealed as lysosomes, cytosol, plasma membrane for NEU1, NEU2 and NEU3, respectively. The localization of the last mammalian sialidase called NEU4 is mitochondria and Endoplasmic reticulum or lysosomes (Monti *et al*. 2002). Their pH ranges change for their specific enzymatic activities on their substrates, as well. The optimal enzymatic activities have been detected at the pH levels of 4.4-4.6, 6.0-6.5, 4.6-4.8 and 3.2-4.8 for NEU1, NEU2, NEU3 and NEU4, respectively. In addition to the distinctions in their subcellular localizations and enzymatic properties, they are differentiated in terms of their substrates like oligosaccharides and glycopeptides for NEU1, oligosaccharides, glycoproteins and gangliosides for NEU2, gangliosides for NEU3 and oligosaccharides, glycoproteins and gangliosides for NEU4 (Monti *et al*. 2010). These sialidase groups take significant roles in several cellular mechanisms like metabolism of gangliosides or glycoproteins, cellular differentiation and proliferation, and cellular adhesion through acting on their specific substrates (Monti *et al*. 2010).

1.2.1. Neuraminidase 3 (Neu3)

According to studies on ganglioside catabolism pathways, it was presented that the degradation by desialylation to convert G_{D1a} to G_{M1a}, G_{M3} to lactosyl ceramide etc. was primarily conducted by sialidases (Monti *et al*. 2010).

Among four neuraminidases, Neu3 is the one with the highest activity toward the gangliosides *in vitro*. The cloning studies of sialidase Neu3 was initiated by Miyagi et al. in 1999 from bovine brain library (Miyagi *et al*. 1999). When expression levels of the gene were analyzed, relatively high levels in human brain and muscles, and also in mouse heart in addition to substantial levels in all tissues were shown. As the expression pattern of *Neu3* was studied, it was shown that heart, brain, spleen, kidney, testis and lung tissues express this sialidase mostly. Especially cerebral cortex, granule cell layer, Purkinje cell

layer and deep cerebellar nucleus within the cerebellum are the regions of brain to express *Neu3* according to *in situ* hybridization studies (Hasegewa *et al*. 2000).

The sialidase 3 or neuraminidase 3 is mostly found in the structures called caveolae microdomains of endosomal membranes and plasma membrane. This protein was also detected on the membranes of exosomes (Zanchetti *et al*. 2007). The enzyme was initially deduced to be a peripheral membrane protein but in the recent studies, it was revealed that it is a S-acylated transmembrane protein having a C-terminus exposed to cytosol and the remaining parts found in the extracellular space (Papini et al. 2004). Because of its cell-surface localization, it acts in several cellular pathways like cell adhesion, cell signaling, cell-cell recognition and differentiation. By residing outer leaflet of plasma membrane and inner portion of endosomal structures, it could metabolize the gangliosides locating on adjacent cells. Principally, the sialidase Neu3 acts on G_{M3} and disialo-gangliosides like G_{D1a} (Ha *et al*. 2004) but it has lower activity toward G_{M1} or G_{M2} mostly in *in vitro* studies (Wang *et al*. 2004).

In biochemical studies, the plasma membrane associated sialidase was indicated to play roles in differentiation and proliferation control in neuroblastoma cells (Kopitz *et al*. 1994, 1998, 2001) in addition to participating in the neurite formation in mice and human neuroblastoma cell lines by using cDNA clone of NEU3. Moreover, regeneration and regulation of neurons in rat hippocampus were analyzed to show the involvement of Neu3 sialidase (Hasegawa *et al*. 2000).

In the studies by administrating radiolabeled G_{D1a} ganglioside to murine Neu3-transfected cells, it was investigated that enzyme hydrolyzed ganglioside G_{D1a} as the substrate in living cells at neutral pH. Since Neu3 enzyme has a unique specificity to its substrates and interactions with plasma membrane, it was deduced to be a potentially significant enzyme for many cell surface mechanisms (Papini *et al*. 2004).

The regulation of apoptosis in human fibroblasts generated by the production of ceramides from G_{M3} in plasma membranes via degrading sugar units from the ganglioside. In this study, the overexpression of Neu3 resulted in higher levels of ceramide which acts in cell apoptosis and cell differentiation pathways. In addition to that, G_{M3} synthase mRNA levels and enzyme activity were also increased to detach sugar units from G_{M3} ganglioside (Valaperta *et al*. 2006).

The involvement of Neu3 enzyme in cancerous cell survival was shown by performing knock-down of NEU3 in cancer cell lines through siRNA transfection. The reduced NEU3 expression in cancer cell lines resulted in apoptosis initiation so NEU3

had role in tumor development. Moreover, because of the highly elevated expression levels of NEU3, its participation in human cancers like renal, ovarian, prostate and colon cancers was investigated. In order for the evaluation of tumor developing activity of NEU3 in colitis-associated colon cacinogenesis, the mouse model with *Neu3* deficit was generated by Yamaguchi *et al*. in 2012 (Yamaguchi *et al*. 2012). Through generation of this mouse model, the studies that were performed to understand susceptibleness to tumorigenesis in colon cancer revealed a reduction in the occurrence of colitis-related colon carcinogenesis in the absence of *Neu3*. However, in this mice model, apart from tumorigenesis involvement, there were no deficiency in brain activity, infertility and any phenotypic alterations detected (Yamaguchi *et al*. 2012).

The further studies by Kappagantula *et al*. in 2014 performed to show activity of Neu3 sialidase on gangliosides of axons and its role in axonal regeneration in CNS (retinal) and PNS (sensory) axons (Kappagantula *et al*. 2014). According to the results, after only PNS axotomy in adult rat, conversion of G_{D1a} to G_{M1} acting as an important regulator of axonal regeneration through the sialidase activity of Neu3 was observed. In the studies, pharmacologically blocked Neu3 activity, downregulated expression of Neu3 by siRNA or depletion of all gangliosides were all resulted in inhibited axonal regeneration in PNS. In contrast, they did not investigate changes in G_{M1}/G_{D1a} ratio after axotomy in CNS axons although Neu3 sialidase was present. On the other hand, exogenous Neu3 sialidase exposure resulted in increased G_{M1} ganglioside in CNS axons so that axonal regeneration was induced. Therefore, they concluded that polysialylated gangliosides were essential regulators of axonal regeneration (Kappagantula *et al*. 2014).

The recent studies by Seyrantepe et al. in 2018 with the animal model of Neu3 deficiency, a double deficient mice strain was generated by crossing Hexa-/- mice with Neu3-/- mice to understand the role of Neu3 sialidase within the by-pass mechanism in ganglioside degradation pathways. In the resulting double deficient model, there were massively stored G_{M2} ganglioside and alterations in terms of biochemical, clinical, and pathological features resembling to Tay-Sachs disease patients. According to their results, they deduced that Neu3 sialidase is a significant regulator of ganglioside degradation pathway in mice so that the Hexa-/-Neu3-/- mouse strain could be presented as the Tay-Sachs disease mice model (Seyrantepe *et al*. 2018).

These investigations have presented the importance of Neu3 sialidase in the control of cell differentiation, neurite formation and regeneration of neurons, axonal regeneration and ganglioside degradation pathway by being a part of the plasma

membrane and specifically acting towards the gangliosides. Moreover, its importance comes from activity toward sialoglyco-conjugates and from its involvement in many biological pathways such as T-cell activation, cell adhesion, neuronal differentiation, cell motility and adhesion, and monocyte differentiation (Yamaguchi *et al*. 2012).

1.3. N-acetlygalactosaminyltransferase Enzyme

β-1,4-N-acetylgalactosaminyltransferase or GM2/GD2 synthase (GalNacT) is the enzyme for catalyzing the generation of the complex gangliosides from the simple gangliosides (Takamiya *et al*. 1996). The resulting ganglioside metabolism pathway and TLC plate image was shown in Figure 1.2.

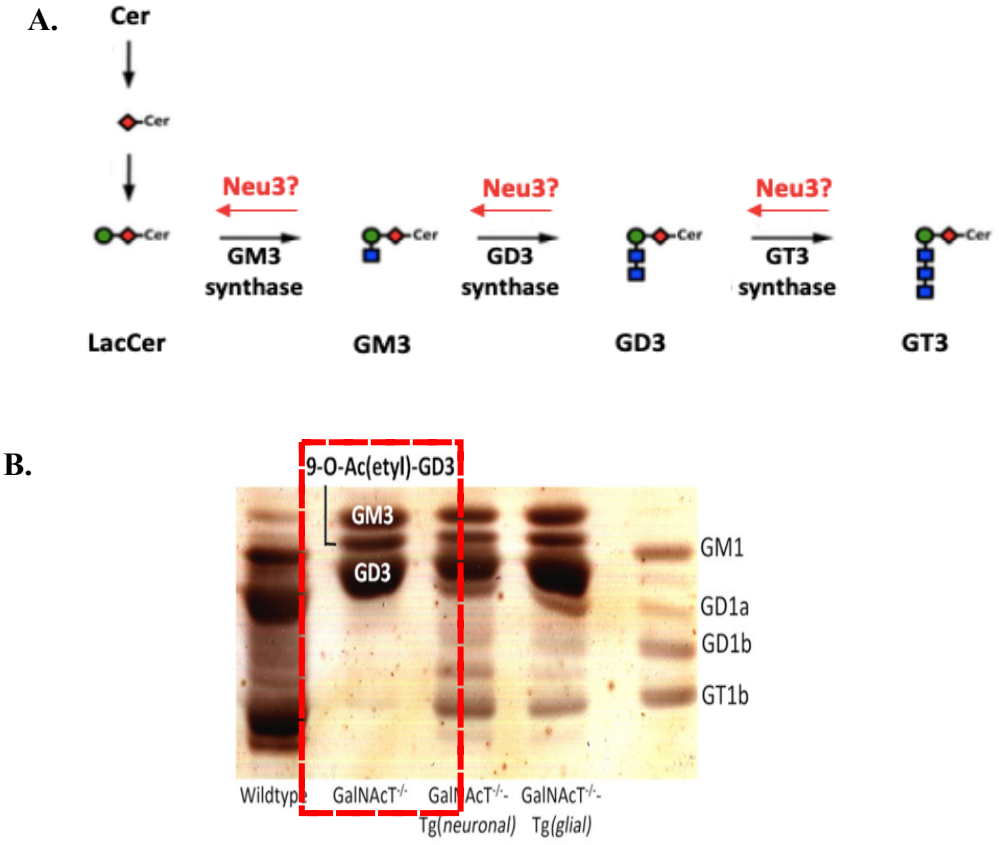

Figure 1.2. The ganglioside biosynthesis pathway when Galgt is blocked and potential role of Neu3 sialidase in degradation of simple gangliosides shown in red arrows (A) and TLC image (B) of GalNacT-/- mice shown in dashed-box by courtesy of Yao *et al*. (Yao *et al*. 2014)

In order for investigating the roles of gangliosides in nervous system by especially controlling synaptogenesis and neuritogenesis, two separate groups established a mouse model with the lack of all complex gangliosides. In 1996 by Takamiya *et al*. and in 1998 by Liu *et al*., the animal model was generated through the disruption of the gene encoding β-1,4-N-acetylgalactosaminyltransferase which is responsible for the biosynthesis of complex gangliosides. As a result, the mice model had the absence of complex gangliosides which are synthesized from LacCer, G_{M3}, G_{D3}, and G_{T3} gangliosides (Takamiya *et al*. 1996; Liu *et al*. 1999). However, the resulting phenotype of the mice model did not show any expected circumstances such as alterations in gross behavioral features and major histological deficiencies in nervous system. This mouse strain was born normally and grew without any evident neurological defects. The limited deficiencies were observed in the neural conduction velocity which was reduced from the tibial nerve to the somatosensory cortex (Takamiya *et al*. 1996). According to those observations, it was deduced that complex gangliosides were only required for the normal functioning of neurons but they were not involved in organogenesis and morphogenesis of the brain. In the TLC analyses on this mouse model, it was revealed that the simple gangliosides especially G_{M3}, and G_{D3} were expressed at higher levels for compensating the absence of the complex gangliosides (Takamiya *et al*. 1996; Liu *et al*. 1999).

The studies on this mice model were continued by Sheikh *et al*. for further investigation of central and peripheral nervous system. Moreover, they aimed to clarify the possible correlations between myelin associated glycoprotein (MAG) deficient mice model and G_{M2}/G_{D2} synthase deficient mice model. The gene encoding myelin associated glycoprotein which was a receptor specifically binding to complex gangliosides like G_{D1a} and G_{T1b} was disrupted (Sheikh *et al*. 1999). Since this receptor protein was localized in the peripheral and central myelin producing glial cells especially the adaxonal glia, it was associated with axonal-glial communications. In the mouse, axonal atrophy and demyelination in sciatic nerves, and degenerating axons were detected. Because complex gangliosides were ligands for this receptor protein, the complex ganglioside defective animal was suspected to have similar pathological alterations to MAG-deficient mice (Sheikh *et al*. 1999). The studies of Takamiya *et al*. showed only minor deficiencies in nervous systems such as reduction in conduction velocity of G_{M2}/G_{D2} synthase deficient mice while in their studies, they were mainly focused on 10-week-old mice (Takamiya *et al*. 1996). However, the MAG-deficient mice revealed the abnormalities in their

phenotypes at older ages so that Sheikh *et al*. proposed their studies by increasing ages of G_{M2}/G_{D2} synthase deficient mice groups. The studies were based on the alterations in conduction velocity which was controlled by myelination and diameter of axons (Sheikh *et al*. 1999). According to their studies, the complex ganglioside defective mice had altered central myelination and degenerated axons in CNS and PNS while demyelination was observed in PNS. Degeneration of axons were observed in optic and sciatic nerves. The central and peripheral nervous systems were affected by axonal degeneration through Wallerian degeneration. As a result, complex gangliosides were significant components of nervous system for initiating CNS myelination and for preventing axonal degeneration (Sheikh *et al*. 1999).

In 2000, Chiavegatto *et al*. revealed behavioral neuropathies in complex ganglioside deficient model were worsened progressively. These neuropathies included altered balance, strength, coordination and reflexes in mice model. In addition to behavioral deficiencies, the G_{M2}/G_{D2} synthase defective mice were observed to have progressive gait disorders that were evaluated by stride length, hindpaw print length, stride width, and rearing tests, According to results, there were an apparent reduction in rearing, stride length and stride width while hindpaw print length was increased in the mouse model. As the mouse model got older, the catalepsy and tremor were also visualized. The studies of Chiavegatto *et al*. confirmed significance of the complex gangliosides for maintaining neural physiology of mice and axon and myelin contents in brain (Chiavegatto *et al*. 2000; Sugiura *et al*. 2005). In parallel with all those developments, the mice model revealed age-dependent deficits in both brain tissues and behavioral features like axonal degeneration (Yamashita *et al*. 2005), demyelinating CNS and PNS causing reduction in conduction velocity (Sheikh *et al*. 1999), altered motor functions such as problems in balance, strength, coordination and reflexes (Chiavegatto *et al*. 2000).

Wu et al. in 2011 investigated that the phenotypes observed in Galgt-/- mice represented the phenotypes in Parkinson's disease patients. This model could be a possible animal model for studying Parkinsonian symptoms in addition to the chemical induced animal models of the disease. In this study, it was shown that GM1 ganglioside was the vital ganglioside for disease progression that was previously indicated in the mice and primate studies. The GM1 ganglioside was a potential treatment molecule for performing replacement therapies in the dopaminergic cells of Parkinson's disease patients (Wu *et al*. 2011).

In 2013 Boukhris *et al*. and in 2014 Wakil *et al*. studied the gene mutations in Galgt and their correlations with the Hereditary Spastic Paraplegia (HSP) 26. According to structural annotation analyses, it was revealed that the mutations in the gene encoding G_{M2}/G_{D2} synthase resulted in Hereditary Spastic Paraplegia 26 that is a severe neurodegenerative disorder. As a comparison between the mice model and the symptoms in patients with HSP, age-dependent neurodegeneration resulting in reduction of sensory nerve abilities, altered gait, increasing tremors, ataxia and reducing nerve conduction velocity was observed. Moreover, in each case, there was male sterility while females were all reproducing (Boukhris *et al*. 2013; Wakil *et al*. 2014).

From now on, the β-1,4-N-acetylgalactosaminyltransferase enzyme deficient mice was named as Galgt-/- in this study.

1.4. Lysosomal Storage Diseases

The lysosomes containing certain hydrolytic enzymes such as glycosidase, sulfatases, phosphatases, proteases, nucleases and lipases are membrane-covered organelles. These membrane-enclosed cellular structures provide an acidic pH for the activity of the enzymes. Any alterations in genes encoding the proteins like enzymes, integral membrane proteins, enzyme activators and membrane transporters of lysosomes result in lysosomal storage disorders. These types of diseases inherited to off-springs mostly as autosomal recessive traits affect the functionality of lysosomes (Ferreira and Gahl 2017). The lysosomal dysfunction occurs due to altered expression of lysosomal genes, malformed proteins and accumulating substrates within the lysosomes. At the end, the cells with the dysfunctional lysosomes are directed to cell death. Glycogen in the Pompe disease, glycosaminoglycans in mucopolysaccharidoses, and sphingolipids in G_{M1} gangliosidosis, G_{M2} gangliosidoses, Niemann-Pick disease types A and B, Gaucher disease, Fabry disease, and Krabbe disease are defined under lysosomal storage disorders according to the accumulating substrates in the lysosomes because of the non-functional hydrolytic enzymes. In addition to the substrate and enzyme dysfunctionality, the defects in an activator protein cause one form of G_{M2} gangliosidoses (Sun 2018).

1.4.1. Tay-Sachs Disease

Tay-Sachs disease which is categorized under G_{M2} gangliosidosis is a progressively neurodegenerative fatal disorder caused by the mutated version of *HEXA* gene encoding *β*-Hexosamidase A enzyme (heterodimer of α and β subunits) (Yamanaka *et al.* 1994). The mutated *HEXA* gene normally encodes α subunit of the enzyme so the resulting mutation generated non-functional A (acidic) enzyme. Since the enzyme working on catabolism of G_{M2} ganglioside with its activator and ganglioside binding protein (G_{M2}AP) is malfunctional, excessively accumulating G_{M2} ganglioside is detected in the lysosomes of patients, especially in the central nervous system. Tay-Sachs disease which is inherited through autosomal recessive manner begins at the early ages of the patients -3 to 5 months (Solovyeva *et al.* 2018). The disease symptoms include motor dysfunctionality and mental retardation ending with the death due to the stored G_{M2} in membranous cytoplasmic bodies (MCBs). These cytoplasmic structures continue to fill cell cytoplasm of neurons leading to the deficiencies in cellular architecture. Ongoing lysosomal storage of G_{M2} ganglioside induces expanding microglia cells, macrophage and astrocyte activity together with the inflammatory pathways in brains of patients (Solovyeva *et al.* 2018).

According to accumulation levels of those inclusions within the lysosomes, the disease is sub-grouped into three different forms showing distinctions in the age of onset and severities. In most studies, the infantile or early-onset form of the disease is mostly considered because it is the one encountered abundantly. In another form of Tay-Sachs disease, the children at the age of 3–10 years are exposed to the symptoms of juvenile onset such as ataxia, spasms and hypotension and terminally death at the ages of 15. In the final version called as late-onset Tay-Sachs disease, the patients show pathology of the disease less severely but with a broader range including abnormal gait and weakness in muscles (Solovyeva *et al.* 2018). On the contrary to early- and juvenile-onsets of the disease, patients with this subtype of Tay-Sachs disease show decreased aggressiveness in disease symptoms because of the small mutations in *HEXA* gene resulting in the highest residual enzyme activity (5–20% of normal enzyme activity). Disease symptoms are revealed at later ages like 20-30 years of age together with gradually decreasing motor and mental functions (Solovyeva *et al.* 2018).

1.4.2. Tay-Sachs Disease Mouse Model

The generation of Tay-Sachs disease mouse model was studied by three distinct research groups each trying to knock *HEXA* gene out for obtaining Hexa-/- mouse model (Yamanaka *et al.* 1994; Cohen-Tannoudji *et al.* 1995; Phaneuf *et al.* 1996).

In this mouse model, there has been a complete lack of β-Hexosaminidase A enzyme activity. On the other hand, in this *HEXA*-deficient mouse, the clinical symptoms analyzed in TSD patients have not been observed and the model have shown a normal lifespan since the ganglioside accumulation and membranous cytoplasmic body production occurred limitedly in the nervous system with no signs of accumulation in the cerebellum, and the anterior horn of the spinal cord (Yamanaka *et al*. 1994). According to studies with electron microscopy, the accumulating G_{M2} in lysosomes and resulting membranous balloon shaped neurons constituted age-dependently because of the elevated HexB enzyme activity. As a result of those observations, it was deduced that metabolic pathways affecting G_{M2} ganglioside accumulation and MCB generation in mice and humans are different from each other (Cohen-Tannoudji *et al*. 1995). These conclusions were further confirmed by comparing two G_{M2} gangliosidosis animal models as Hexb-/- lacking HEXA and HEXB activity with Hexa-/-. Since the Hexb-/- mice shows all the motor and mental retardation phenotypes found in human patients in contrast to the other one with no behavioral phenotypes (Phaneuf *et al*. 1996). For generation of TSD mouse model with all clinical phenotypes, firstly the models for understanding G_{M2} ganglioside catabolism pathway in Hexa-/- mice was considered. In the model 1, G_{M2} catabolism is performed by functional HEXB hydrolyzing N-acetylgalactoseamine to form G_{M3} ganglioside as a product. In the second model, sialic acid removal from G_{M2} by a sialidase is generated to obtain G_{A2} ganglioside that is further catabolized by HEXB cleaving N-acetylgalactoseamine to yield LacCer (Phaneuf *et al*. 1996).

1.5. The aim for the study

The importance of gangliosides in the signaling pathways in brain has been assessed in the previous studies. Their regulation is conducted by sialidases and glycosyltransferases. Neu3 -membrane sialidase- and Galgt -complex ganglioside

synthesizing enzyme- were combined in a mouse model in this study. The aim was to evaluate the novel roles of Neu3 sialidase on the simple gangliosides when the complex gangliosides were removed. Moreover, the purpose was investigating regulation of ganglioside metabolism in distinct brain regions of the 3- and 6-month-old WT, Neu3-/-, Galgt-/-, and Neu3-/-Galgt-/- mice by Neu3 sialidase and Galgt enzyme.

CHAPTER 2

MATERIALS AND METHODS

2.1. Animals

Galgt gene deficient mice were provided by our collaborator Prof. Roger Sandhoff (Hochschule Mannheim-Mannheim University of Applied Sciences, Institut für Instrumentelle Analytik und Bioanalytik, Germany) through the project "Intensified Cooperation (IntenC): Promotion of German-Turkish Higher Education Research" (Project number: 113T025). The animal was named as Galgt-/- in this study. The Neu3 deficient mice model that was generated after the deletion of exon3 in Neu3 gene (Yamaguchi *et al*. 2012) was supported by Prof. Taeko Miyagi (Division of Cancer Glycosylation Research, Institute of Molecular Biomembrane and Glycobiology, Tohoku Pharmaceutical University, Sendai, Japan). Neu3 and Galgt doubly deficient mice were generated in our laboratory through the proper breedings. To obtain doubly deficient mice, the breedings and crossings have been made between brothers and sisters in this study. For the maintenance and breeding of the mice groups, the ethical concerns specified by Turkish Council on Animal Care accredited animal facility of İzmir Institute of Technology were applied. The housing of animals was organized by keeping a 12h dark/light circulation at constant temperature and humidity while feeding of the animals were made as ad libitum. The animal care and their uses in the studies were confirmed by the Animal Care and Use Committee of İzmir Institute of Technology, İzmir, Turkey. The mice breedings were performed as shown in Figure 2.1. For revealing age-dependency of ganglioside accumulation, and its effects in terms of phenotypic, biological and biochemical aspects, 3- and 6-month-old mice groups were used.

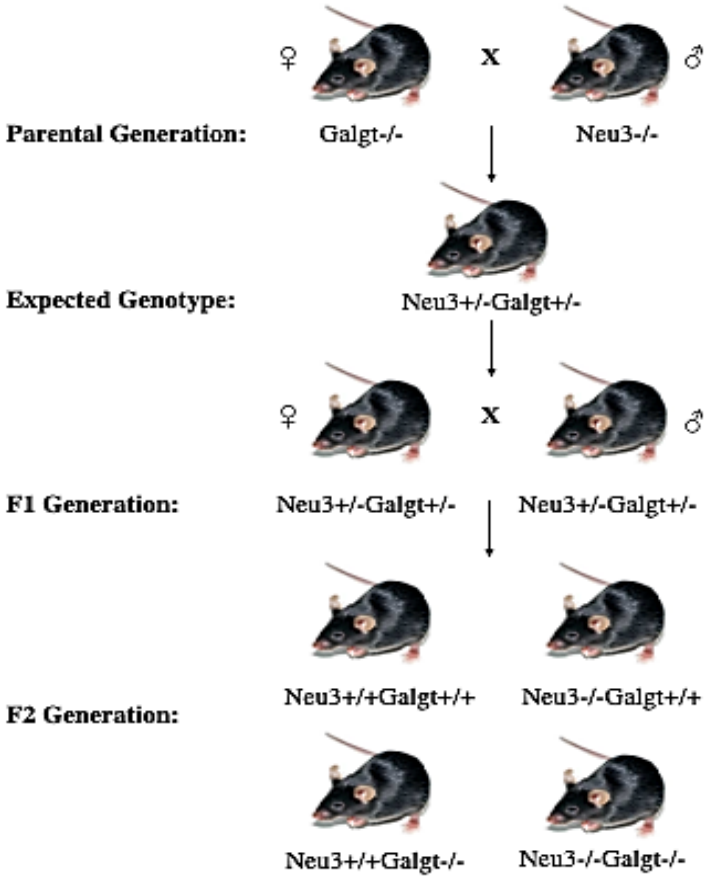

Figure 2.1. The breeding scheme of Neu3-/- and Galgt-/- mice

2.2. DNA Isolation for Genotyping

Genotyping of mice groups were generated by the DNA isolation protocol which has been already optimized in our laboratory. DNA was extracted from mouse tail in two days. For the first day, the mice tails cut when they were weaned from their parents at one-month-old age were placed into 1.5ml Eppendorf tubes including 250µl of tissue lysis buffer (containing 10% 1M Tris pH 7.6, 2.5% 0.2M EDTA, 20% SDS, 4% 5M NaCl) and 6µl of proteinase K solution (25 mg/ml solution). Then, the samples were subjected to overnight incubation in a shaking incubator at 55°C and 70rpm. In the second day, the samples were centrifuged at 13,000rpm for 10minutes at room temperature to obtain supernatants. The supernatants were pulled into a new 1.5ml Eppendorf tubes after which 1volume of 100% isopropanol was added onto them for DNA precipitation. After gentle inversion of the mixture, extracted DNAs were seen. The extracted DNA samples were taken into new 1.5ml Eppendorf tubes containing 250µl of 70% ethanol for ethanol

wash. After that, centrifugation was done at 15,000rpm for 1minute at room temperature in order to obtain DNA pellets and to discard ethanol. The DNA pellets were left to air-dry and later they were dissolved in 100µl of dH_2O. Next, the samples were incubated at 55°C for 1hour after when they were stored at -20°C.

2.2.1. Genotyping of Mice

In the next part of genotyping, the PCR was run for detecting wild type and mutant alleles of Neu3 and Galgt independently by using isolated DNA samples. For this aim, the previously designed genotyping primers shown in Table 2.2 were used. PCR for Neu3 was generated in the condition of 1 cycle of 3 minutes at 94°C; 35 cycles of 50 seconds at 94°C, 45 seconds at 58°C, 2 minutes at 72°C; and 1 cycle of 10 minutes at 72 °C. The Neu3 PCR mixture was prepared by adding 100 ng genomic DNA together with 0.4 μM of each primer listed in Table 2.2, 0.4 mM of each dNTPs, 10X reaction buffer including 2mM $MgCl_2$ and 2.5 units of Taq polymerase (GeneDireX, Inc., Taiwan). For performing the genotyping of Galgt, two different PCR reactions were prepared because one PCR reaction was for wild type allele and the other one for knock-out allele. For the wild type allele of Galgt, the conditions were 1 cycle of 3 minutes at 94°C; 34 cycles of 45 seconds at 94°C, 30 seconds at 65°C, 3 minutes at 72°C; and 1 cycle of 10 minutes at 72°C. The knock-out PCR reaction conditions were 1 cycle of 3 minutes at 94°C; 34 cycles of 45 seconds at 94°C, 30 seconds at 58°C, 3 minutes at 72°C; and 1 cycle of 10 minutes at 72°C. The PCR mixture for WT allele of Galgt were prepared with 100 ng genomic DNA. 50 µl of reaction mixture of WT allele was included 0.4 μM of each primer, 0.5 mM of each dNTPs, 10X reaction buffer without $MgCl_2$, 3mM $MgCl_2$ and 2.5 units Taq polymerase (GeneDireX, Inc., Taiwan). Then, the genotyping of KO allele of Galgt was performed with 100 ng genomic DNA together with 0.4 μM of each primer, 0.4 mM of each dNTPs, 10X reaction buffer containing 2mM $MgCl_2$ and 2.5 units of Taq polymerase (GeneDireX, Inc., Taiwan).

Table 2.1. The sequences of the primers used for genotyping of the mice groups

Gene	Primer Name	Primer Sequence	Product Size
Neu3	Neu3-F	AAGCAGAGAACATTCTTGAGAGAGCACAGC	WT allele: 1100bp KO allele: 600bp
	Neu3-552R	TCGTGCTTTACGGTATCGCCGCTCCCGATT	
	Neu3-553R	GTGAGTTCAAGAGCCATGTTGCTGATGGTG	
Galgt	Galgt-WT-F1	CGTGGAGCACTACTTCATGC	WT allele: 608bp KO allele: 1600bp
	Galgt-WT-R1	CTCTCCTCCCCTACCAGGTC	
	Galgt-KO-F1	TCGTCCTGCAGTTCATTCAG	
	Galgt-KO-R1	ATATGGCTCCATCGGGCCTC	

2.3. Tissue Handling

Brain samples from 3- and 6-month-old WT, Neu3-/-, Galgt-/- and Neu3-/-Galgt-/- mice were collected by doing either brain dissection or PFA fixation.

2.3.1. Brain Dissection

For fulfilling the analyses in this study, wild type, single- and double- deficient mice groups were sacrificed with CO_2 when they reached to the targeted ages (3- or 6-month old). At the expected ages of mice groups, the total brains were removed and the brains were divided into right and left hemispheres. Then, cortex, thalamus and cerebellum of each hemisphere shown in Figure 2.1. were obtained by a dissector blade. After that, these samples were directly treated in liquid nitrogen, and preserved frozen under -80°C. The separated brain regions were used for isolation of acidic and neutral gangliosides, and their analyses through the thin layer chromatography, for performing RT-PCR to obtain relative gene expression levels and western blotting to visualize protein expression levels, for doing the urinary oligosaccharide analyses through the thin layer chromatography and for conducting DNA fragmentation assays.

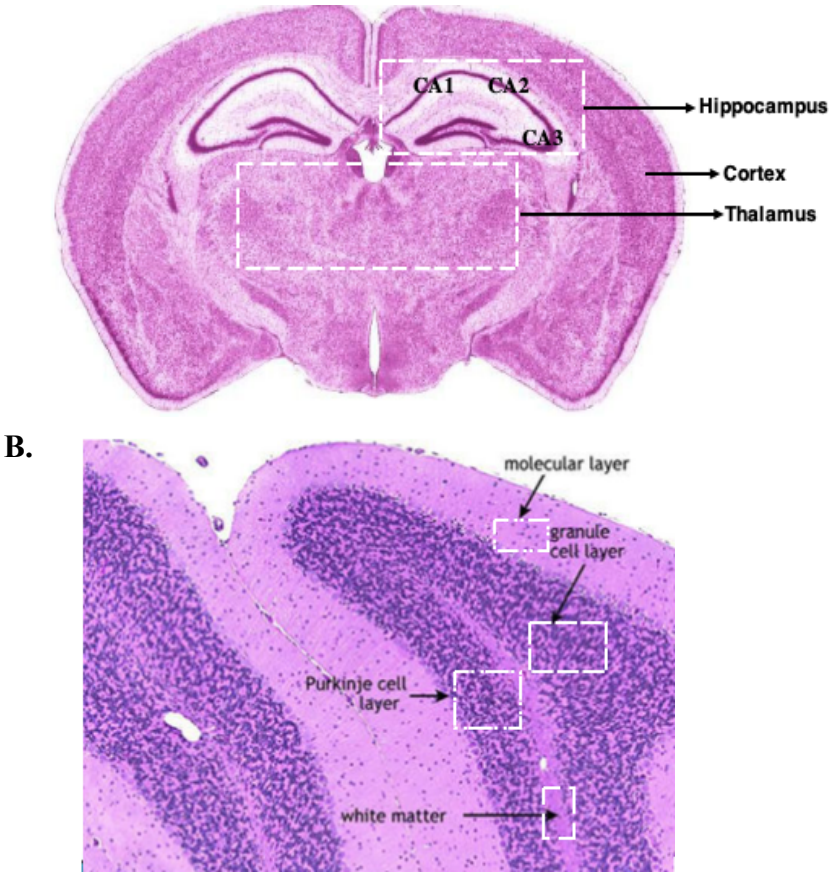

Figure 2.2. The hippocampus, cortex, and thalamus (A) and cerebellum (B) regions in a coronal section of mouse brain by courtesy of Woods *et al* (Woods *et al*. 2013)

2.3.2. Fixation

In order to perform immunohistochemical or histopathological analyses, the fixed brain samples were prepared. For this purpose, the animals of targeted ages for each genotype (8 animals in total) were anesthetized by doing intraperitoneal injection of Ksilazol and Basilazin mixture in required amounts. Before starting trans cardiac perfusion, the anesthetized animals were fixed to be immobilized by tapes while they were lying on their back. Then, an incision was done through the abdomen of mice and through the rib cage in order to open the thoracic cavity and the heart of the animals. Later, a needle was placed to the bottom-left ventricle while the top-right atrium was cut by a sharp scissors. Thus, through the needle ~10ml of 0.9% NaCl solution (pH 7.4) was inserted into the circulation system so all blood was drained from the mice organs. After this procedure, NaCl solution was replaced by ~10ml of freshly prepared 4%

paraformaldehayde in 1xPBS in order to fix the mice. The decapitation of the PFA fixed mice were done and brain excision was performed. The brains were initially kept in 5ml of 4% paraformaldehyde solution in 1xPBS overnight at +4°C. In the second day, the sucrose gradient was done by incubating the brains in 5ml of 10%, and 20% sucrose in 1X PBS solution (pH 7.4) sequentially in 2 hours at +4°C. The final gradient was generated by keeping the brains in 30% sucrose in 1X PBS solution (pH 7.4) overnight at +4°C. In the third day, embedding of the brains was done by using OCT (optimal cutting temperature) containing cryomolds so that they were stored frozen at -80°C. After obtaining OCT embedded fixed brains, 10μm coronal sections were got through Leica Cryostat (CM1850-UV, Leica, Wetzlar, Germany) at -20°C and these sections were collected on adhesive-coated HistoBond slides. The slides were then kept at -80°C until being used for further analyses.

2.4. Ganglioside Isolation from the Brain

Isolation of acidic and neutral gangliosides and their visualization were generated by using 3- and 6-month-old mice brains for genotypes according to the protocol optimized in our laboratory. The protocol was described below (Sandhoff *et al*. 2002).

2.4.1. Neutral and Acidic Ganglioside Isolation

For extraction of gangliosides, 50mg of brain tissues -cortex, cerebellum or thalamus- from each genotype at targeted age groups (8 samples totally) placed into borosilicate tubes was homogenized in 2ml of dH_2O via the ultra turax homogenizer (IKA T10, Sigma, Darmstadt, Germany) at 6000rpm for 30 seconds. Then, homogenized samples were exposed to sonication by sonicator (Bandelin-sonopuls, Berlin, Germany) for 4 cycles of 1.5minutes after placing the tubes into ice-cold water. Next, the samples were left to dry by using a N_2 flow in the Reacti-Therm Heating module (Thermo, Massachusetts, USA) in heated water at 55°C for speeding up the evaporation. When the pellet was obtained after evaporation of entire water, the extraction procedure was started by adding 3ml of 100% acetone over it. Then, the samples were vortexed and centrifuged

at 2000rpm for 5 minutes. This step was performed twice so that phospholipids and other membrane lipids could be removed completely. After that, pellets were washed by adding 1.5ml of chloroform:methanol:water (10:10:1) solution and by centrifuging at 2000 rpm for 5 minutes. By repeating this step twice and collecting every supernatant into new neutral glass tubes with Pasteur pipettes, the first part of ganglioside collection was generated. For the second part, 2ml of a chloroform:methanol:water (30:60:8) solution was used and the samples were centrifuged at 2000rpm for 5 minutes. This step was done twice and supernatants were put over the previously collected supernatants after each centrifugation, as well. At the end, the collections contained both acidic and neutral gangliosides which were separated by using the DEAE Sephadex A-25 ion exchange columns. For this aim, the columns were prepared freshly by incubating 1 gr of DEAE Sephadex A-25 resin (GE Health Care, Little Chalfont, United Kingdom) into 10ml of chloroform: methanol:0.8M sodium acetate (30:60:8) solution for 5 minutes. Then, resin and solution mixture were centrifuged at 2000rpm for 1 minute. After the solution removal, resin was washed with the same solution twice. In addition to these applications, the resin was left for overnight incubation in 10ml of chloroform: methanol:0.8M sodium acetate (30:60:8). On the next day, the removal of the solution and washing of the resins with 10ml of chloroform:methanol:water (30:60:8) were performed twice. After all those procedures, the DEAE Sephadex A-25 resin were ready for use. The next part of acidic-neutral ganglioside separation required closure of tips of glass Pasteur pipettes with glass woolen before loading enough amounts of the resin. The amount of the resin was determined by marking 2cm-long area over the glass woolen and this area was filled with the resin in order to generate separation column. After washing the columns with 1ml of chloroform:methanol:water (10:10:1) solution, and 1ml of chloroform:methanol:water (30:60:8) solution, and placing new neutral glass tubes, the total ganglioside samples were loaded. Afterwards, column washing was done with 4ml of 100% methanol and the resulting solutions in the neutral tubes were neutral gangliosides. These elution solutions were then subjected to evaporation by a N_2 flow in the Reacti-Therm Heating module (Thermo, Massachusetts, USA) including heated water at 55°C, and stored at +4°C until the TLC analyses. Next step was performed to obtain acidic samples which were eluted into new neutral glass tubes by 5ml of 500mM potassium acetate in methanol. The acidic ganglioside elution was continued by performing desalting procedure with the Supelclean LC-18 column (Supelco, Sigma, Darmstadt, Germany). In this part, specific columns

called LC-18 columns were located in the Chromabond Vacuum manifold (Macherey-Nagel, Düren, Germany) fixed to 5Hg. The desalting procedure was started by equilibrating the columns by washing them with 2ml of methanol, and with 2ml of 500mM potassium acetate in methanol solution. Later, the acidic ganglioside samples were added onto the columns and the column bound samples were washed with 10ml of dH_2O. New neutral tubes were located under the columns for elution of desalted acidic gangliosides with 4ml of methanol and 4ml of chloroform:methanol (1:1) under low vacuum (<5 Hg). Finally, the eluted samples were directed to evaporation by a N_2 flow in the Reacti-Therm Heating module (Thermo, Massachusetts, USA) in 55°C water so that pellets were stored at +4°C until being used.

2.4.2. Thin Layer Chromatography (TLC)

The Thin Layer Chromatography abbreviated as TLC was performed to distinguish gangliosides according to their weights and structures. For this purpose, 20cm x 20cm silica TLC plates (Merck, New Jersey, USA) were incubated in an incubator at 100°C for 30minutes in order to remove humidity. Then, the TLC tank (Camag, Muttenz, Switzerland) was prepared by using TLC running solution containing Chloroform:methanol: 0.2% $CaCl_2$(30:65:8) and by placing it into the tank. The tank was incubated for 2hour 15minutes at room temperature. Afterwards, the acidic and neutral ganglioside samples that were stored at +4°C in N_2-dried forms were loaded onto the silica plates with the Linomat 5 (Camag, Muttenz, Switzerland) machine automatically. For this loading procedure, the pellets were suspended in 100µl of chloroform: methanol: water (10:10:1) solution. Then, acidic samples were loaded as 45µl whereas neutral samples were loaded as 20µl on the TLC plate. The plates were located into the pre-incubated tanks to run for 10cm at room temperature.

2.4.3. Orcinol Staining of Plates

After running of the TLC plates of both neutral and acidic samples, the visualization was generated by using Orcinol (Sigma, Darmstadt, Germany) stain which was prepared freshly before using. In order to prepare orcinol solution, 0.06g of orcinol,

3.75ml of sulphuric acid and 11.25ml of dH_2O were mixed in in TLC sprayer (Sigma, Darmstadt, Germany), and left to cool at room temperature. The plates were then dyed by orcinol mixture and placed over TLC plate heater (Camag, Muttenz, Switzerland) heated at 120°C for making the bands visible. After the staining procedure, the bands showing specific gangliosides were compared with brain ganglioside standards (Avanti Polar Lipids, Alabaster, Alabama, USA). Finally, the plates were scanned with the HP scanner system and later the band intensities were measured by NIH ImageJ program.

2.5. DNA Fragmentation Analyses

The cortex, thalamus and cerebellum brain regions of both 3- and 6-month-old mice of each genotype were subjected to DNA fragmentation analyses (Huang *et al*. 1997) to visualize presence or absence of fragmented DNAs and their correlation with apoptosis. For this purpose, each brain region was initially incubated overnight in 500µl of tissue lysis buffer including 10% 1M Tris pH 7.6, 2.5% 0.2M EDTA, 20% SDS, 4% 5M NaCl with 12µl Proteinase K solution in shaking incubator at 37℃ and 70rpm. In the following day, the phenol-chloroform extraction procedures were applied to the samples by adding 1 volume of phenol:chloroform:isoamyl alcohol (25:24:1) and shaking the mixture for 20seconds. The samples were then centrifuged at 13000rpm for 10minutes at room temperature. After collecting the supernatant into new Eppendorf tubes, the same procedure was repeated with the supernatants in three times totally. Then, 1 volume of chloroform was added on the collected supernatants and resulting mixtures were centrifuged for 10minutes at 13000rpm and room temperature. These steps were also repeated once more for collecting the supernatants. For precipitation of DNA molecules, 0.1 volume of 3M sodium acetate of collected samples and 2.5 volumes of 100% ethanol of sample and sodium acetate mixture were mixed and shaken to observe DNA. The precipitated DNA was kept in -80℃ for at least 1hour. After that, the samples were centrifuged at 13000rpm and +4℃ for 30minutes so DNA pellets were obtained by removing the supernatant. The DNA wash was performed by adding 150µl of 70% ethanol, centrifuging the samples at 13000 rpm and +4℃ for 10minutes and repeating these steps once more. After removing the supernatant and drying the excess ethanol for 10-15minutes at room temperature, the samples were dissolved in ~100µl of TE buffer.

The samples were then measured with nanodrop to calculate the amounts needed to load 2μg DNA to agarose gel. For loading DNA samples, 2% agarose gel was prepared and gels were run at 40V for 2hours.

2.6. Relative Gene Expression Analysis by Real-Time PCR

The next biochemical analysis performed for this study was measurement relative gene expression levels of apoptosis, oxidative stress and ER stress related genes through RT-PCR. For apoptosis, *Bax* (pro-apoptotic), *Bcl-Xl* and *Bcl-2* (anti-apoptotic) were analyzed through specific primers. For oxidative stress analyses, *TTase-1*, *SOD2* and *Catalase* were used while for ER stress gene expression analyses, *Calnexin*, *ATF6* and spliced *XBP-1* gene expression analyses were performed by using their specific primers. The normalization of expression levels was generated by the glyceraldehyde-3-phosphate dehydrogenase (GAPDH) which was chosen as the internal control. Firstly, the brain samples from 3- and 6-month-old mice -cortex, cerebellum or thalamus- were weighed as 50mg and mixed with 500μl of Genezol Reagent (Geneaid, New Taipei City, Taiwan) for cortex and 250μl of Genezol Reagent (Geneaid, New Taipei City, Taiwan) for cerebellum and thalamus in 2ml Eppendorf tubes. After placing RNAse-free beads into the tubes, homogenization was started by using tissue homogenizator (Retsch MM100) for 30seconds at 1^{-25} frequency. When homogenization was finished, the samples were waited at room temperature for 5 minutes and the supernatants were replaced into new 1.5ml Eppendorf tubes. Afterwards, 200μl of chloroform for 1000μl of Genezol were added onto the supernatants. The mixtures were shaken for 10seconds before being centrifuged at 15000g for 15minutes at +4°C in order to perform phase separation. Next, resulting supernatant containing RNA samples was transferred into new tubes for RNA precipitation by adding 1 volume of 100% isopropanol and then inversing the mixture several times. After incubating the samples at room temperature for 10minutes, they were centrifuged for 10minutes at 15000g and at +4°C. In this time, supernatant was removed to wash RNA pellets with 1ml of 70% ethanol and centrifugation at 16000g for 5 minutes at +4°C. The supernatant was discarded, as well and RNA pellet was left to dry at 55°C for 5-10minutes. Finally, RNA suspension was done by adding 20-50μl nuclease-free water and by incubating the samples in water bath at 50°C for 10-15minutes. After

suspending RNA samples, RNA concentration measurements were performed with Nanodrop spectrophotometer (ND-1000) at 260nm.

2.6.1. The cDNA Synthesis

After the isolation of RNA samples, the next step was to convert these RNA molecules into cDNAs through EvoScript Universal cDNA master (Cat# 07912455001, Roche, Mannheim, Germany) The conditions were organized for 50ng/µl total cDNA product. Reaction conditions were arranged for 50 ng/µl total cDNA product. For each reaction; 1 X RT buffer, 4 mM dNTP mix, 1X RT Random primers, 50 units MultiScribe Reverse Transcriptase were mixed with water and RNA dependent on RNA concentration that was measured in NanoDrop. Total mixtures were prepared as 20 µl volumes. PCR conditions for cDNA conversion were 1 cycle of 15minutes at 42°C; 1 cycle of 5minutes at 85°C; and 1 cycle of 15minutes at 65°C. After that, for the confirmation of cDNA conversion, housekeeping gene GAPDH were used to perform confirmation PCR in which 25µl reaction mixture was prepared by using 0.8mM of GAPDH gene primers, 10mM of each dNTPs, 1x reaction buffer with $MgCl_2$ and 1.75 units of GeneDireX Taq Polymerase for each 50ng of cDNA. The reaction conditions were 1 cycle 2minutes at 95°C; 30cycles of 20seconds at 95°C; 15seconds at 65°C; and 22 seconds at 72°C; and 1 cycle of 3minutes at 72°C were done. To complete confirmation, PCR products were run on 1% agarose gel for 30minutes at 95Volts.

2.6.2. Real-Time PCR

In the Real-Time PCR, the genes given in the Table 2.3 were used to analyze the expression levels in the brain regions of age-matched mice of 4 genotypes. For this purpose, Roche LightCycler 96 system with Roche LightCycler 480 SYBR Green I Master Mix was used. The reaction mixture optimized to 20µl including 0.4µM each primer shown in Table 2.3 and 1x Roche LightCycler 480 SYBR Green I Master Mix and 50ng cDNA was directed to 1 cycle of 10 minutes at 95 ˚C; and 45 cycles of 20 seconds at 95 ˚C; 15 seconds at 60 ˚C; 22 seconds at 72 ˚C. The samples were placed in three

replicates in order to get averages of the gene expression levels. The values were analyzed through One-way ANOVA on GraphPad Prism to obtain statistical changes.

Table 2.2. The primer sequences used for gene expression analyses by RT-PCR

	Gene	Primer Sequence	Product Size
ER Stress Markers	*ATF6*	F:5'- TGGAAGTGGGAAGATCGGGA -3' R:5'- AGGACAGAGAAACAAGCTCGG -3'	354bp
	Calnexin	F:5'- ATTGCCAACCCCAAGTGTGA -3' R:5'- TCCAGCATCTGCAGCACTAC -3'	362bp
	XBP-1	F:5'- TCCGCAGCACTCAGACTATG -3' R:5'- GACTCTCTGTCTCAGAGGGGA -3'	360bp
Oxidative Stress Markers	*SOD2*	F:5'- GTGTCTGTGGGAGTCCAAGG -3' R:5'- CCCCAGTCATAGTGCTGCAA -3'	339bp
	Catalase	F:5'- TTCGTCCCGAGTCTCTCCAT -3' R:5'- GAGGCCAAACCTTGGTCAGA -3'	351bp
	Ttase 1	F:5'- CTGCAAGATCCAGTCTGGGAA -3' R:5'- CTCTGCCTGCCACCCCTTTTAT -3'	322bp
Apoptotic Markers	*Bcl-2*	F:5'- CGCAGAGATGTCCAGTCAGC -3' R:5'- TATGCACCCAGAGTGATGCAG -3'	369bp
	Bcl-XL	F:5'- TCAGCCACCATTGCTACCAG -3' R:5'- GTCTGAGGCCACACACATCA -3'	356bp
	Bax	F:5'- AGGATGCGTCCACCAAGAA-3' R:5'- CTTGGATCCAGACAAGCAGC -3'	306bp
	GAPDH	F:5'- CCCCTTCATTGACCTCAACTAC-3' R:5'- ATGCATTGCTGACAATCTTGAG-3'	347bp

2.7. Western Blot

By using cortex, thalamus and cerebellum brain regions of 3- and 6-month-old mice group from all genotypes, the western blot was performed after doing protein isolation and Bradford assay and then SDS-PAGE.

2.7.1. Protein Isolation

The protein lysates from the brain regions listed above were obtained by initially homogenizing the samples in tissue lysis buffer containing 1% Triton X-100, 50mM HEPES, 150mM NaCl, 10% Glycerol, 50mM Tris-Base, 1% PMSF, 1% protease

inhibitor with mini homogenizer. The proteins from cortex and cerebellum regions were extracted with 500µl whereas the isolation from thalamus required 100µl lysis buffer. After homogenizing the samples mechanically, the chemical homogenization of protein lysis buffer was performed by keeping the samples on ice for 1hour and vortexing in every 10minutes. The samples were centrifuged at 14000rpm for 15minutes at 0^{o}C after 1hour incubation. At the end of this centrifugation, the supernatant including proteins was obtained and collected into new Eppendorf tubes.

2.7.2. Bradford Assay

In the next step, the isolated protein samples were prepared for concentration measurement with Bradford assay. For this purpose, the protein samples were diluted in dH_2O in the ratio of 1:80 (2µl protein in 158µl dH_2O) and kept over ice. In order to draw a proper standard curve, the BSA solutions in 100µg/ml, 80µg/ml, 40µg/ml, and 20µg/ml concentrations were prepared. 50µl of both the BSA solutions and the diluted protein samples were loaded into the 96-well plate so that 200µl of 5x Bradford reagent (Cat no 39222, SERVA Electrophoresis, Heidelberg, Germany) were added onto them. The blank samples, dH_2O and protein lysis buffer for BSA solutions and the protein samples, respectively were also loaded as 50µl and mixed with 200µl of 5x Bradford Reagent. The 96-well plate were then directed to measurement at 595nm with iMark™ Microplate Absorbance Reader (Cat no 1681130, Bio-Rad Laboratories, California, USA). After drawing the standard curve with the absorbance values of serially diluted BSA samples, the concentrations and required amounts of the protein samples were calculated. The protein stocks in dH_2O were prepared to contain 20µg of each protein.

2.7.3. SDS-PAGE

After pouring the prepared resolving gel between glass plates for SDS-PAGE according to the amounts shown in Table 2.4, the polymerization of the gel was waited at room temperature. When the resolving gel becomes solidified, the stacking gel that was prepared with the values shown in Table 2.4 was placed on top of the resolving gel and the combs were put into the stacking part. The stacking gel was waited to solidify so that

the combs were removed and the gel was placed into the running tank containing running buffer (0.25M Tris-Base, 1.92M Glycine, 1%SDS) in the required levels. Before loading 20μg-protein samples, they were mixed with protein loading buffer including 40% Glycerol, 240mM Tris-HCl pH 6.8, 8% SDS, 0.04% Bromophenol Blue, 5% β-mercaptoethanol in 4:1 ratio. This mixture was then boiled at 95℃ for speeding the activity of β-mercaptoethanol. The samples were loaded into the wells for running them at 80V for ~2hours and separating the proteins through SDS-PAGE after which they were subjected to transfer onto the 0.2μm-pore sized nitrocellulose paper (Cat no 1620112, Bio-Rad Laboratories, California, USA). The transfer procedure was performed by locating the protein gel and nitrocellulose membrane within transfer sandwich that was placed into the transfer tank containing transfer buffer (48mM Tris-Base, 39mM Glycine, 20%Methanol, pH 9.2). The transferring was arranged at 0.25A for 1hour in transfer buffer. The blots with protein samples were later blocked by shaking in 5% milk in 1xPBS-T (containing 0.005% Tween20) for 1hour at room temperature. For removal of blocking solution, the blots were washed in 1xPBS-T for 5minutes in three times so that they were incubated for 1hour at room temperature in anti-BiP (Cell Signaling Technologies, 1:1000), anti-Caspase 9 (Cell Signaling Technologies, 1:1000), anti-Caspase 3 (Cell Signaling Technologies, 1:1000), and anti-Fas-ligand (Cell Signaling Technologies, 1:1000) and anti-β-actin (Cell Signaling Technologies, 1:1000) diluted in red solution (5%BSA, 0.02% NaAzide, Phenol Red, in PBS-T pH 7.5). After primary antibody incubation, the blots were washed with 1xPBS-T for 5 minutes in three times in order to place HRP-conjugated secondary antibody (Cat no 115-035-003, Jackson ImmunoResearch Lab, Cambridge, UK) over the blots for 1hour incubation at room temperature. In the next step, the blots were dipped in 1xPBS-T for 5minutes in three times to remove excess secondary antibody. The visualization of protein bands was performed by Luminata™ Forte Western HRP Substrate (Cat no WBLUF0500, Millipore, Darmstadt, Germany) and a chemiluminescence imaging system (Fusion SL, Vilber). The intensities of protein bands were calculated by NIH Image J program so the statistical analyses were obtained by Two-way ANOVA on GraphPad Prism.

Table 2.3. The quantities of the reagents for the preparation of resolving gel (10%) and stacking gel (5%)

Resolving Gel (10%)	**Stacking Gel (5%)**
3 ml Lower buffer (1.5M Tris-HCl, pH: 8.8)	1.5 ml Upper buffer (1M Tris-HCl, pH: 6.8)
4 ml Acrylamide (30%)	1 ml Acrylamide (30%)
5 ml Water	3.5 ml Water
60 µl SDS (10%)	60 µl SDS (10%)
60 µl APS (10%)	60 µl APS (10%)
6 µl TEMED	6 µl TEMED

2.8. The Histopathological Analyses

The fixed coronal brain sections on HistoBond slides of 6-month-old WT, Neu3-/-, Galgt-/-, and Neu3-/-Galgt-/- mice were directed to histopathological evaluations by staining the samples with Cresyl Echt Violet, Hematoxylin-Eosin, Periodic acid-Schiff's reagent, and Luxol Fast Blue dyes.

2.8.1. Cresyl Violet Staining

The brain slices collected by HistoBond slides of 6-month-old group were chosen for staining with Cresyl Echt Violet (ScyTek Laboratories, Utah, USA) dye. Then, they were put over ice for 15minutes and they were placed into humidified chambers for incubation at 55℃ for 15minutes. The slides were washed in 1xPBS for 5minutes and dried with KimWipes (KimTech, Irving, Texas, USA) after which they were covered with 20μl of cresyl violet stain for incubation at room temperature for 5minutes. For removal of excess dye, the slides were rapidly dipped up into dH_2O for two times. Later, the slides were washed within 100% ethanol for three times. After drying all remaining ethanol over the tissues, the slides were mounted with Richard-Allan Scientific™ Cytoseal™ XYL (Cat no 8312-4, ThermoFisher Scientific, United Kingdom) and covered by coverslips. By nail-polishing the edges of the slides, they were kept at +4°C until the images of cortex, hippocampus, thalamus and cerebellum regions were taken by light microscopy (BX53, Olympus, Tokyo, Japan) for further histopathologic analyses.

2.8.2. Hematoxylin and Eosin Staining

For another histopathological staining called Hematoxylin-Eosin staining (Merck, Darmstadt, Germany) the fixed slides of 6-month-old group were chosen, put over ice for 15minutes and placed into humidified chambers for incubation at 55℃ for 15minutes. They were washed with dH_2O for 2minutes and excess water was removed by drying the slides. Then, they were treated with hematoxylin for 3minutes at room temperature after which the dye was removed by washing in dH_2O for 5minutes followed by rinsing in tap water for 5minutes in two times. The differentiation was performed by placing the slides into jar containing 1% HCl in 70% ethanol. This solution was removed by rinsing the slides in running tap water for 5minutes and then washing with dH_2O for 2minutes. After drying the water off, counterstaining with Eosin (Merck, Darmstadt, Germany) was done by incubating the slides for 1minute. The excess dye was removed by dipping the slides into the jars containing 95% ethanol for 2 minutes in two times. The slides were then located into the jars with 100% ethanol for 2 minutes in two times. When the liquids were evaporated completely, the mounting was performed by using Richard-Allan Scientific™ Cytoseal™ XYL (Cat no 8312-4, ThermoFisher Scientific, UK) and covered by coverslips. At the end, the slides were covered by nail-polishing the edges, and they were placed at +4°C until the images of cortex, hippocampus, thalamus and cerebellum regions were taken by light microscopy (BX53, Olympus, Tokyo, Japan) for further histopathologic analyses.

2.8.3. Periodic Acid-Schiff Staining

The PFA fixed brain sections of 6-month-old WT, Neu3-/-, Galgt-/-, and Neu3-/-Galgt-/- mice on Histobond slides were chosen and directed to Periodic acid-Schiff staining (Merck, Darmstadt, Germany) procedure. The brain slides were initially put over ice for 15minutes and they were placed into humidified chambers for incubation at 55℃ for 15minutes. Then, the slides were washed in 1xPBS for 5minutes after which they were dried with KimWipes (KimTech, Irving, Texas, USA). The brain sections were then incubated in Carnoy's solution containing Ethanol: Chloroform: Acetic acid in 6:3:1 ratio in 10 minutes at room temperature. After washing the slides in distilled water for 2

minutes and drying them with KimWipes, the slices were subjected to periodic acid solution (0.5%) in 30µl for each brain sample for 5 minutes at room temperature. The slides were washed in running tap water for 3 minutes so they were waited in distilled water in the next 2 minutes. After drying off the excess water, Schiff's reagent (Merck, Darmstadt, Germany) was applied onto the brain slices in 30µl for 12 minutes at room temperature. The reagent was then removed in running tap water for 5 minutes and in distilled water for 2 minutes. Next, the counterstaining procedure was performed by staining tissues with Hematoxylin solution (Merck, Darmstadt, Germany) for 1.5 minutes at room temperature so that excess dye was removed by rinsing slides in running tap water for 5 minutes. Later, the slides were localized into the jar containing 70% ethanol for 1 minute and two times. This procedure was continued with placing the slides into 96% and 100% ethanol solutions subsequently. After the evaporating the excess ethanol, the slides were mounted with Richard-Allan Scientific™ Cytoseal™ XYL (Cat no 8312-4, ThermoFisher Scientific, United Kingdom) and covered by coverslips. By nail-polishing the edges of the slides, they were kept at +4°C until the images of cortex, hippocampus, thalamus and cerebellum regions were taken by light microscopy (BX53, Olympus, Tokyo, Japan) for further histopathologic analyses.

2.8.4. Luxol Fast Blue Staining

The PFA fixed brain sections of 3- and 6-month-old WT, Neu3-/-, Galgt-/-, and Neu3-/-Galgt-/- mice on Histobond slides were chosen and directed to Luxol Fast Blue staining procedure. First of all, the brain slides were initially were put over ice for 15 minutes after which they were placed into humidified chambers for incubation at 55℃ for 15 minutes. Later, the slides were washed in 1xPBS for 5 minutes after which they were dried with KimWipes (KimTech, Irving, Texas, USA). The slides were then incubated in Luxol Fast Blue (ScyTek Laboratories, Utah, USA) dye placed as 30 µl for 2hours in the incubator at 56℃ in the humidified chamber. By exposing the slides to 95% ethanol, the removal of excess dye was performed so the slides were rinsed in distilled water to remove additional dyes. Then, for differentiation, the samples were placed into lithium carbonate solution for 30 seconds at room temperature. The differentiation was continued by placing the brain slices into 70% ethanol for 30seconds until the gray matter was shown clearly while the white matter was observable so rinse the slides were rinsed

in distilled water. The counterstaining was performed by applying Cresyl Echt Violet (ScyTek Laboratories, Utah, USA) dye on the slices for 30 seconds at room temperature. After the removal of the dye by rinsing the slides in distilled water, the differentiation was generated by placing them into 95% ethanol for 5minutes at room temperature. After locating the slides into 100% ethanol for 5minutes twice and evaporating the remaining ethanol, the slides were mounted with Richard-Allan Scientific™ Cytoseal™ XYL (Cat no 8312-4, ThermoFisher Scientific, United Kingdom) and covered by coverslips. By nail-polishing the edges of the slides, they were kept at +4°C until the images of cortex regions were taken by light microscopy (BX53, Olympus, Tokyo, Japan) for further histopathologic analyses.

2.9. TUNEL Staining

The 6-month-old mice fixed brain slices on HistoBond slides were chosen and prepared for staining with DeadEnd™ Fluorometric TUNEL System (Cat no G3250, Promega, United States) by keeping them over ice for 15minutes and then incubating them in humidified chambers in incubator at 55℃ for 15minutes. The staining procedure was performed by following the manufacturer's instructions. For this purpose, the slides were washed in 1xPBS for 5minutes at room temperature. After that, they were subjected to 4% PFA fixation in 1xPBS for 15minutes at room temperature. The PFA was removed by washing the slides with 1xPBS for 10minutes at room temperature and the slides were dried with KimWipes (KimTech, Irving, Texas, USA). The brain tissues were encircled by liquid blocker PAP pen (Sigma, Darmstadt, Germany) for preventing leakage of solutions. The slides were incubated in 20µl of Proteinase K solution diluted in 1xPBS in 1:500 ratio from 10mg/ml stock solution for permeabilization of cell membranes for 20minutes at room temperature in humidified chamber. When the incubation was finished and excess PK solutions were removed, the slides were firstly washed in 1xPBS for 5minutes and secondly fixed in 4% PFA in 1xPBS for 5minutes at room temperature. The tissues on slides were grouped as experimental tissues and one negative control and additionally one slide was chosen as positive control. The positive control slide was initially equilibrated with in DNase I buffer containing 40mM Tris HCl (pH: 7.9), 10mM NaCl, 6mM $MgCl_2$ and 10mM $CaCl_2$ for 5minutes at room temperature so that the slides were added 5.5-10units/ml DNase I in DNase I buffer for 10minutes incubation at room

temperature. After washing these slides in dH_2O for 2minutes in two times, the positive control slides and the others were equilibrated with 20µl of equilibration buffer supplied with the assay kit for 10minutes at room temperature. The equilibrated slides were then incubated with 50µl/5cm^2 of rTDT incubation buffer including equilibration buffer, nucleotide mix and rTDT enzyme in predicted amounts by the manufacturer whereas negative control slides were treated without rTDT enzyme. The incubation with 10µ of rTDT incubation buffer was done at 37°C for 1hour in humidified chamber. For stopping the reaction, 1:10 diluted SSC buffer in dH_2O from 20x stock were added onto the tissues and left for incubation at room temperature for 15minutes. Afterwards, the slides were washed in 1xPBS for 5minutes in three times to remove excess reaction buffers. After drying the liquids over the tissues, the slides were treated with Propidium Iodide which was initially diluted from 1mg/ml stock in 1:1000 ratio in 1xPBS in order to stain nuclei. After the PI treatment was performed at room temperature in dark for 15minutes, the slides were washed in dH_2O for 5minutes in three times to remove excess stain. Then, the slides were dried to be mounted with anti-fade PI mounting medium and covered with coverslips. After nail-polishing the edges, the slides would be kept at +4°C until the fluorescent images of cortex, hippocampus, thalamus and cerebellum regions were taken by fluorescent Microscopy (BX53, Olympus, Tokyo, Japan) with the specific filters. At the end, the localization analyses of red and green fluorescence were performed through NIH Image J program and statistical analyses were performed by One-way ANOVA on GraphPad Prism.

2.10. The Immunohistochemical Analyses

The fixed coronal brain sections on HistoBond slides of 3- and 6-month-old WT, Neu3-/-, Galgt-/-, and Neu3-/-Galgt-/- mice were chosen for applying immunohistochemical analyses as anti-CNPase and anti-NeuN antibody staining.

2.10.1. Anti-CNPase Antibody Staining

The fixed brain sections on HistoBond slides of both targeted ages were chosen according to required brain regions for staining with anti-CNPase antibody. Then, they

were placed over ice for 15minutes and after that they were put into humidified chambers for incubating them in incubator at 55℃ for 15minutes. The slides were then placed into coplin jars for being fixed in 4% PFA in 1xPBS in 15minutes. Next, they were washed in 1xPBS for 5minutes in three times. The slides were located into coplin jars containing ice-cold 100% methanol for 10minutes in order to permeabilize the cell membranes. Afterwards, the slides were washed in 1xPBS for 5minutes in order to remove excess methanol. The brain tissues were then dried with KimWipes (KimTech, Irving, Texas, USA) and they were encircled by liquid blocker PAP pen (Sigma, Darmstadt, Germany) to prevent leakage of solutions. In order to prevent non-specific binding of primary antibody, the slides were blocked by a blocking solution including 0.3% Triton X-100, 0.3M Glycine, 4% BSA in mg and 10% normal goat serum in 1xPBS in humidified chamber at room temperature for 1hour. The primary antibody was prepared by 1:100 dilution in blocking buffer. After blocking of brain tissues, they were left to dry so anti-CNPase primary antibody (Cat no D83E10-5664S, Cell Signaling Technology, United States) was added in 20µl for overnight incubation in humidified chamber at +4°C. In the next day, the primary antibody was removed and the slides were washed with 1xPBS in three times for 5minutes for removal of excess primary antibody. After drying of excess 1xPBS, the secondary antibody (Cat no ab150077 Alexa Fluor®-488, Abcam, green, Cambridge, United Kingdom) which was diluted in 1:500 ratio in blocking buffer was added over the brain tissues in 20µl for 1hour incubation at room temperature in humidified chamber in dark. At the end of this incubation period, the secondary antibody was removed by washing the slides in 1xPBS in three times for 5minutes. Finally, the tissues were dried and mounted through Fluoroshield mounting medium DAPI (Cat No ab104139, Abcam, Cambridge, United Kingdom) for staining the nuclei and covered with coverslips. After covering the edges of slides with nail-polish to keep samples fixed, they were stored at +4°C. Then, the fluorescent images of cortex, hippocampus, thalamus and cerebellum regions were taken by fluorescent Microscopy (BX53, Olympus, Tokyo, Japan) with the specific filters. The intensities of images were analyzed through NIH Image J program and statistical analyses were performed by One-way ANOVA on GraphPad Prism.

2.10.2. Anti-NeuN Antibody Staining

The brain slices collected by HistoBond slides of both targeted ages were chosen for staining with either anti-NeuN antibody (Cat no D4G4O-24307S, Cell Signaling Technology, United States). Then, they were prepared for staining by firstly keeping them over ice for 15minutes and secondly incubating them in humidified chambers in incubator at 55℃ for 15minutes. After this incubation process, the slides were washed in 1xPBS for 10minutes at room temperature. Afterwards, the slides were placed into coplin jars containing ice-cold acetone for permeabilization of the cell membranes for 15minutes. In order to remove excess acetone, the slides were washed twice in 1xPBS for 5minutes at room temperature. Later, the slides were dried by using KimWipes (KimTech, Irving, Texas, USA) for covering the environment of the tissues with liquid blocker PAP pen (Sigma, Darmstadt, Germany). Thus, the slides were covered by blocking buffer containing 0.3% Triton X-100, 0.3M Glycine, 4% BSA in mg and 10% normal goat serum in 1xPBS in humidified chamber at room temperature for 1hour. After the blocking process, the anti-NeuN primary antibody which were diluted in blocking buffer in 1:50 ratios, were added over the tissues in 20µl to incubate them overnight in humidified chamber at +4°C. In the next day, following the primary antibody removal, the 1xPBS wash was done for 5 minutes in three times and excess liquid was removed by KimWipes. The slides were then placed into humidified chambers for incubating them in secondary antibody (Cat No ab175471 Alexa Flour 568, red, Abcam, Cambridge, United Kingdom) in dark for 1hour at room temperature. The slides were washed with 1xPBS for removing excess antibody in three times for 5minutes so that the slides were mounted by Fluoroshield mounting medium DAPI (Cat No ab104139, Abcam, Cambridge, United Kingdom) for staining the nuclei and covered with coverslips after being dried. Following nail-polishing of the edges, the slides were stored at +4°C until the fluorescent images of cortex, hippocampus, thalamus and cerebellum regions were taken by fluorescent Microscopy (BX53, Olympus, Tokyo, Japan) with the specific filters. The intensities of images were analyzed through NIH Image J program and statistical analyses were performed by One-way ANOVA on GraphPad Prism.

2.11. Behavioral Tests

For observing whether the changes in the ganglioside pattern could alter the locomotory functions, memory or anxiety of the mice, two age groups for each genotype were examined by performing three behavioral tests as Rotarod Test, Passive Avoidance Task and Open Field Test.

2.11.1. Rotarod

Rotarod Test (Hamm *et al*. 1994) was applied to control the alterations in the motor neurons and their function by using an accelerating Rotarod (Pan-Lab Harvard Aparatus, Barcelona, Spain). The mice group of two ages for each genotype (5-8 from each group) were initially subjected to training at a speed of 4rpm on a 5-line Rotarod unit. After that, mice were tested by increasing acceleration mode from 4 to 40rpm over 5minutes. The testing period was repeated in three times and between the repeating trials animals were left to rest for 15minutes. The staying durations in the trials on the rotating rod were recorded for each animal. The results were analyzed with the help of Two-way ANOVA supplied by GraphPad Prism.

2.11.2. Passive Avoidance Task

WT (n=5), Neu3-/- (n=5), Galgt-/- (n=5) and Neu3-/-Galgt-/- (n=5) mice at the ages of 3- and 6-month-old were used for performing Passive avoidance task by using A Shut Avoid Vol. 1.8 (Harvard Apparatus, USA). The task system was comprised of two boxes being separated by a guillotine door as either dark or light compartments. In the first day, the animals were given a habituation period in which the animals were placed into the light box to discover both boxes and when the animals passed to the dark part, the door was closed. The door closure did not occur unless the animals put all paws to the dark compartment. In the second day, the training procedure was generated by again placing the animal to the light compartment. After that, the animals were waited to pass to the dark part so that the door was closed and the animals were given a 0.2 mA foot

shock for 1second. In the final part, the animals were tested for their learning and memory for the electric shock on the dark compartment. For this purpose, the animals were put into the light box and waited for their passage into the dark compartment. The times for the entry into this box were recorded and used to measure the escape latency of the animals from the electric shock. This latency time was arranged to be 300s maximally. The time for entries from light compartment to dark one was recorded in each day in order to compare any difference between those time points. The results were analyzed with the help of Two-way ANOVA supplied by GraphPad Prism (Nordquist *et al*., 2017).

2.11.3. Open Field Test

For the final behavioral test, the animals were used in groups of 10 for WT, Neu3-/-, Galgt-/- and Neu3-/-Galgt-/- genotypes at the ages of 3- and 6-month-old. The analyses were performed in a 40x40cm box having four walls in 40cm from all sides. In order to record the assay, a digital camera was located above the box and when the mouse was placed, its movement was measured. After locating the animal from one corner of the box, the recording was started and continued for 5minutes. The exploration of the animals, their locomotory functions and anxiety levels were analyzed through this camera records and the PanLab SMART Video Tracking System v0.3 (Harvard Apparatus, USA). This tracking program enabled a square center and a periphery in order to calculate the time of animals standing in center, periphery and total area. These measurements were then analyzed for their statistics through Two-way ANOVA supplied by GraphPad Prism (Thompson and Kim 1996).

CHAPTER 3

RESULTS

3.1. Mice Genotyping

By using PCR with Neu3, Galgt wild type and Galgt knock-out allele-specific primers, the genotypes were determined for WT, Neu3-/-, Galgt-/- and Neu3-/-Galgt-/- mice groups Table 2.1. For performing Neu3 PCR with Neu3F, Neu3-552R and Neu3-553R, the primers Neu3-F, and Neu3-553R were used to obtain a DNA fragment of 1022bp for WT allele whereas the primers Neu3F, and Neu3-552R were required to get a DNA fragment of 601bp for KO allele Figure 3.1.

In order for obtaining Galgt PCR results with Galgt allele-specific primers, the primers Galgt WT-F1, and Galgt WT-R1 were used to get a DNA fragment of 608bp for WT allele while Galgt KO-F, and Galgt KO-R primers were used to obtain a DNA fragment of 1600bp for KO allele Figure 3.2.

From the WT and Neu3-/- and female Galgt-/- mice groups, the offspring were obtained while according to literature, Galgt-/- male mice were completely infertile. Therefore, in order for obtaining Galgt-/- offspring, Galgt-/- female mice and Galgt+/- male mice were bred. Moreover, Neu3-/-Galgt-/- mice were generated by crossing Neu3-/-Galgt-/- female mice with Neu3-/-Galgt+/- male mice.

3.2. Body Weight Analyses

After obtaining all mice groups of four genotypes, the body weight measurements were performed weekly by starting from 6 weeks up to 24 weeks for both female and male mice. According to the measurements, there were no significant changes between WT, Neu3-/-, Galgt-/- and Neu3-/-Galgt-/- mice strain in female (Figure 3.3 A) and male (Figure 3.3 B). However, the slightly occurring weight loss was observed in Galgt-/- mice for both genders. The gross body measurements Figure 3.3 C were also performed for 6-

month-old WT, Neu3-/-, Galgt-/- and Neu3-/-Galgt-/- mice but there were not significant differences among the genotypes.

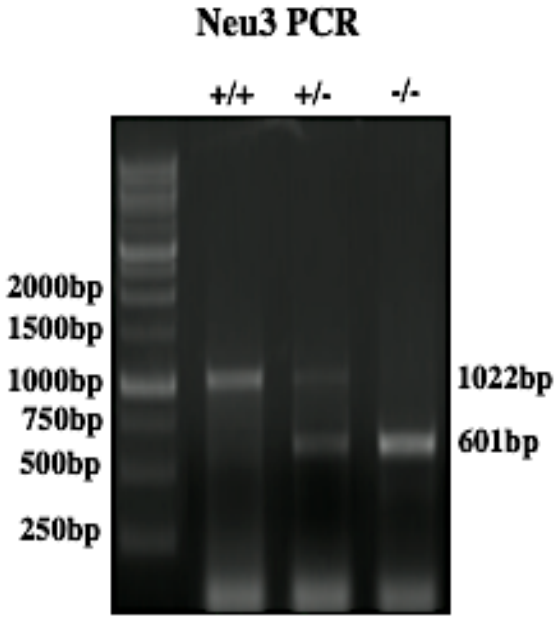

Figure 3.1. Gel images for the visualisation of Neu3 PCR product

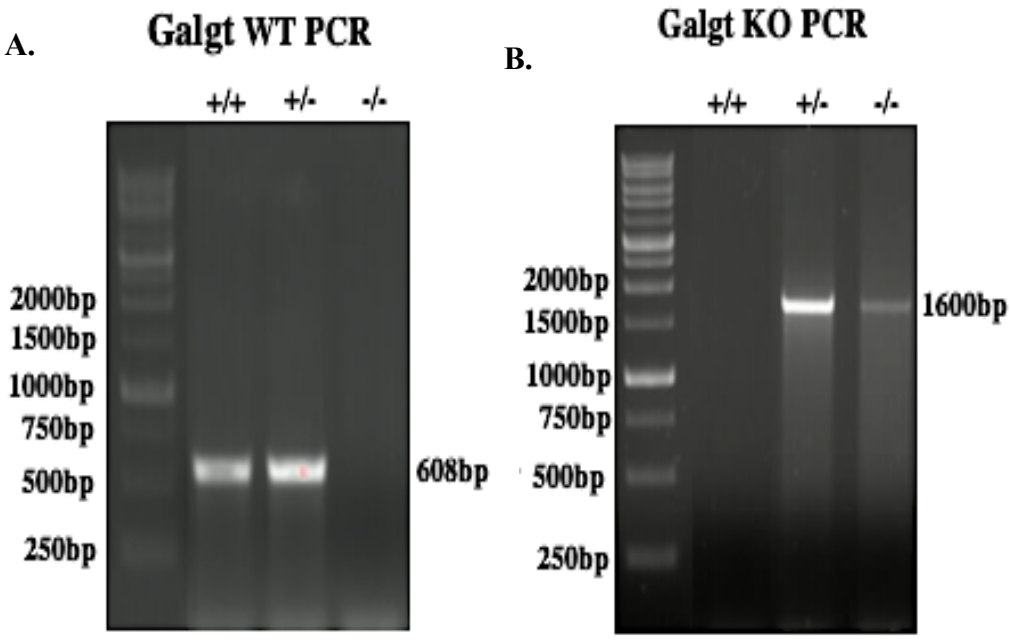

Figure 3.2. Gel images for the visualisation of Galgt WT PCR product (A) and Galgt KO PCR product (B)

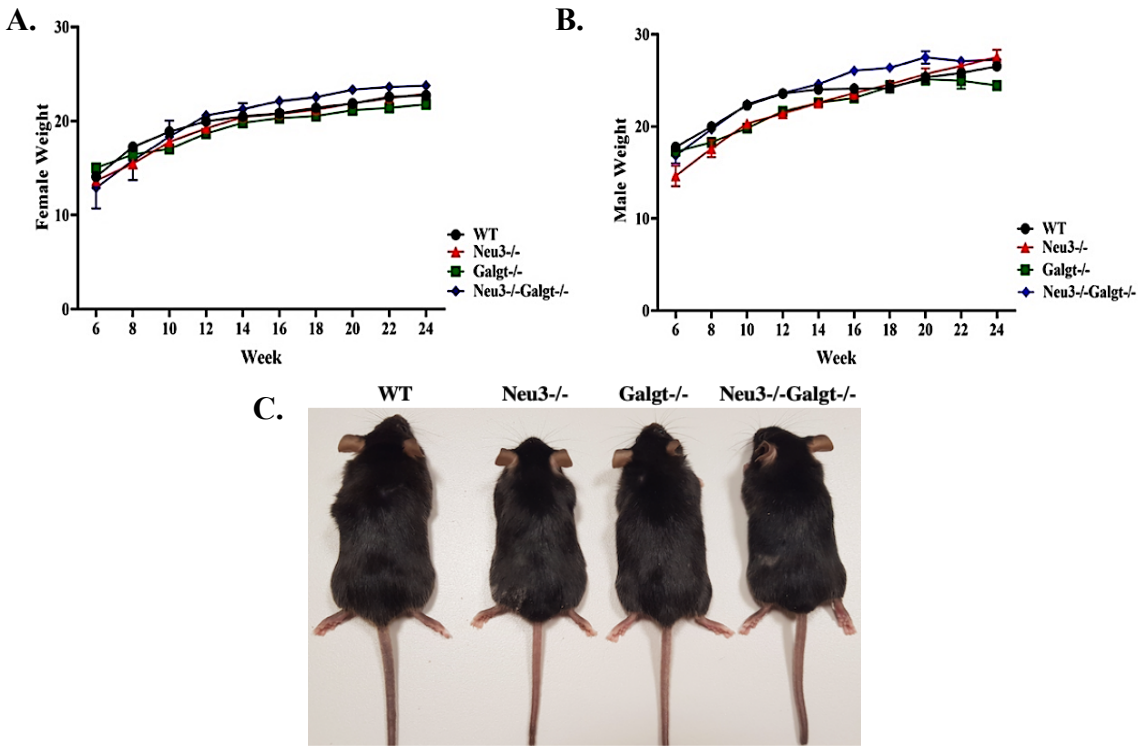

Figure 3.3. Weight measurements performed for WT, Neu3-/-, Galgt-/- and Neu3-/-Galgt-/- female (A) and male (B) mice from 6 weeks to 24 weeks. The gross appearance of 6-month-old WT, Neu3-/-, Galgt-/- and Neu3-/-Galgt-/- male mice (C). Data show mean ± SEM of measurements. Significant levels of data were determined using the two-way ANOVA. (n=8, *p<0.05, **p<0.025, ***p<0.001 and ****p<0.0001)

3.3. TLC Analysis for Acidic and Neutral GSLs

Since Neu3 sialidase has specific activity toward gangliosides and Galgt is required for the synthesis of complex gangliosides from the simplest ones, it would be important to show the any changes in ganglioside pattern in the single or the double-deficient mice. Thin Layer Chromatography analyses on cortex and cerebellum regions of 3- and 6-month-old WT, Neu3-/-, Galgt-/- and Neu3-/-Galgt-/- mice groups were generated by using the optimized TLC procedure of our laboratory requiring DEAE Sephadex A25 Ion Exchange Column in order to separate acidic and neutral gangliosides. Acidic glycosphingolipids in cortex of 3- (Figure 3.4 A) and 6-month-old (Figure 3.4 B) for WT, Neu3-/-, Galgt-/- and Neu3-/-Galgt-/- mice were evaluated on TLC plates.

According to the TLC results of acidic gangliosides in cortex, there were presence of only complex gangliosides as G_{M1}, G_{D1a}, G_{D1a}, G_{D1b}, and G_{T1b} for WT and Neu3-/- in

contrast to presence of only simple gangliosides G_{M3}, G_{D3}, and G_{D3} isoform called o-acetyl G_{D3} in Galgt-/- and Neu3-/-Galgt-/- for 3- (Figure 3.4 A) and 6-month-old mice (Figure 3.4 B). The neutral GSLs were also analyzed in cortex of 3- (Figure 3.7 A) and 6-month-old (Figure 3.7 B) WT, Neu3-/-, Galgt-/- and Neu3-/-Galgt-/-.

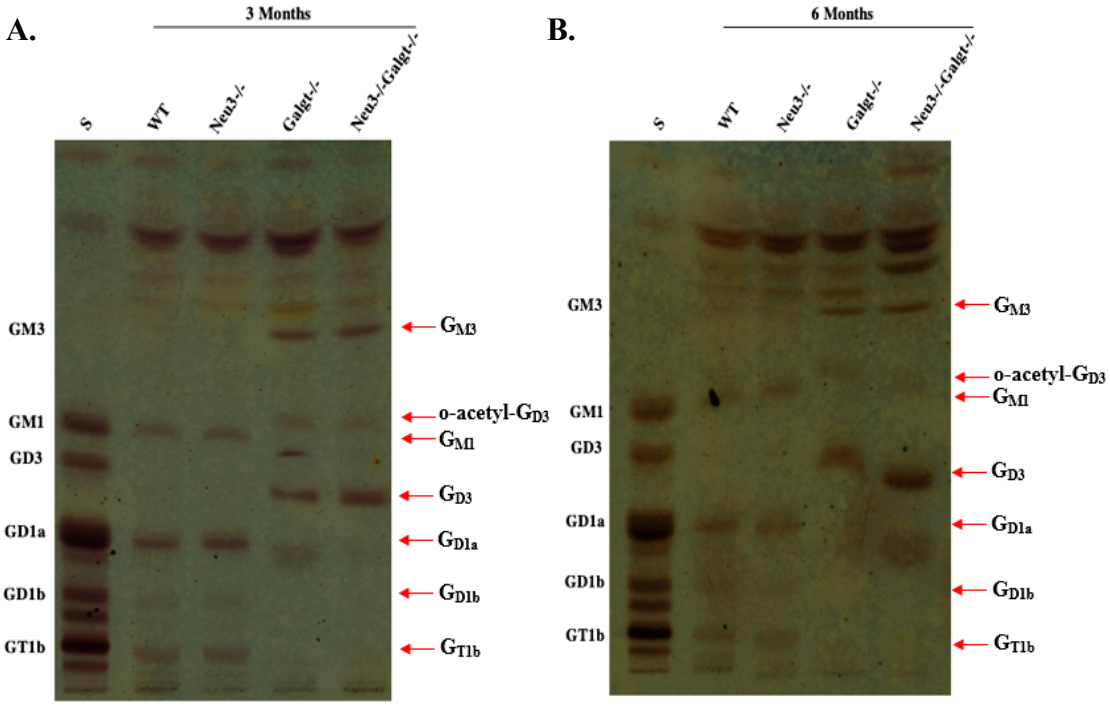

Figure 3.4. TLC plate images for 3-month-old (A) and 6-month-old (B) WT, Neu3-/-Galgt-/- and Neu3-/-Galgt-/- mice for acidic GSLs of the cortex region. The S shows the ganglioside standards with indicated gangliosides and the red arrows are the representative of the presence of G_{D3} isoform o-acetyl G_{D3}. (n=3 for 3- and 6-month old mice)

According to band intensities, G_{M1} levels were decreased in 6-month-old Neu3-/- compared to 3-month-old Neu3-/- (1.5-fold) and in 6-month-old Neu3-/- compared to WT as 1.5-fold (Figure 3.5 A). There were not any changes in G_{D1a} levels (Figure 3.5 B) between WT and Neu3-/- for both ages, the changes in 3-month-old Neu3-/- for G_{D1b} ganglioside were detected as 1.6-fold while 1.7-fold in 6-month-old Neu3-/- compared to WT counterparts (Figure 3.5 C). The G_{T1b} levels of Neu3-/- mice at 3- and 6-month-old ages were changed as 1.5-fold and 1.6-fold, respectively compared to WT of the same ages (Figure 3.5 D).

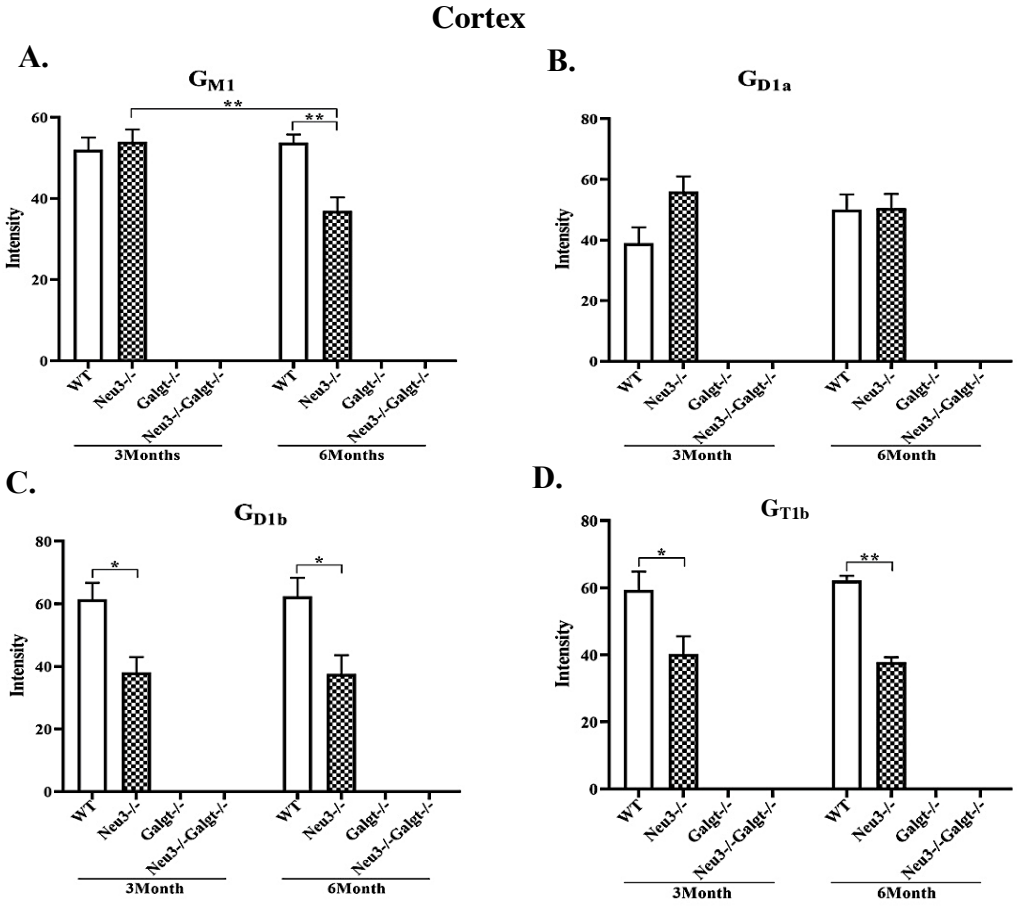

Figure 3.5. The levels of a-series G_{M1} and G_{D1a}, and b-series G_{D1b} and G_{T1b} (A, B, C, and D, respectively) in the cortex region of 3- and 6-month-old WT, Neu3-/-, Galgt-/-, and Neu3-/-Galgt-/- mice were indicated. Data is representative of mean ± SEM of measurements. Significant levels in the data were presented by using the two-way ANOVA (*$p<0.05$, ***$p<0.001$ and ****$p<0.0001$). (n=3 for 3- and 6-month old mice)

Moreover, the band intensities of acidic GSLs were measured in the cortex region. In the results, there were no significantly changed G_{M3} levels between Galgt-/- and Neu3-/-Galgt-/- for both ages (Figure 3.6 A). The significant increase in the levels of o-acetyl G_{D3} between 3- and 6-month-old Galgt-/- mice were detected as 1.3-fold (Figure 3.6 B). The 1.3-fold reduction between 3- and 6-month-old Neu3-/-Galgt-/- were shown in the levels of o-acetyl-G_{D3}. Moreover, the decreasing levels in Neu3-/-Galgt-/- mice compared to Galgt-/- in 6-month-old group as 1.7-fold were indicated. There were no significantly changed G_{D3} levels between Galgt-/- and Neu3-/-Galgt-/- for both ages (Figure 3.6 C).

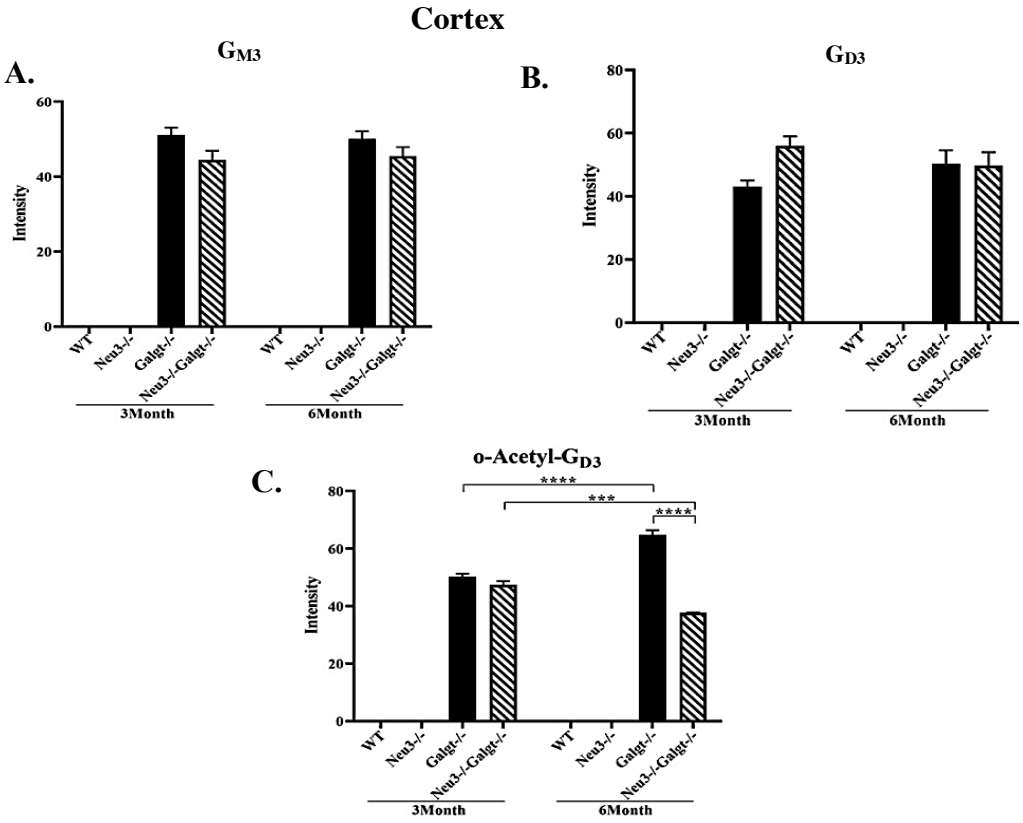

Figure 3.6. The levels of a-series G_{M3}, and b-series G_{D3}, and o-acetyl G_{D3} (A, B, and C, respectively) in the cortex region of 3- and 6-month-old WT, Neu3-/-, Galgt-/-, and Neu3-/-Galgt-/- mice were indicated. Data is representative of mean ± SEM of measurements. Significant levels in the data were presented by using the two-way ANOVA (*p<0.05, ***p<0.001 and ****p<0.0001). (n=3 for 3- and 6-month old mice)

The results of neutral GSLs isolated from the cortex of 3- (Figure 3.7 A) and 6-month-old (Figure 3.7 B) WT, Neu3-/-, Galgt-/-, and Neu3-/-Galgt-/- mice presented changes in LacCer levels in Galgt-/- and Neu3-/-Galgt-/- compared to WT and Neu3-/- mice. Increase in the levels of LacCer in 3-month-old Galgt-/- mice were 1.9-fold and 2.4-fold compared to WT and Neu3-/- mice, respectively (Figure 3.7 C). 1.9-fold increased LacCer levels compared to WT and 2.5-fold increased levels compared to Neu3-/- in 3-month-old Neu3-/-Galgt-/- were shown (Figure 3.7 C). In 6-month-old Galgt-/- mice, LacCer levels were increased compared to WT and Neu3-/- mice as 1.9-fold and 2.0-fold, respectively (Figure 3.7 C). The 1.9-fold and 2.0-fold increased LacCer levels in 6-month-old Neu3-/-Galgt-/- mice to WT and Neu3-/- counterparts were indicated (Figure 3.7 C). Moreover, there were no significantly changed levels of LacCer between age groups among the genotypes (Figure 3.7 C).

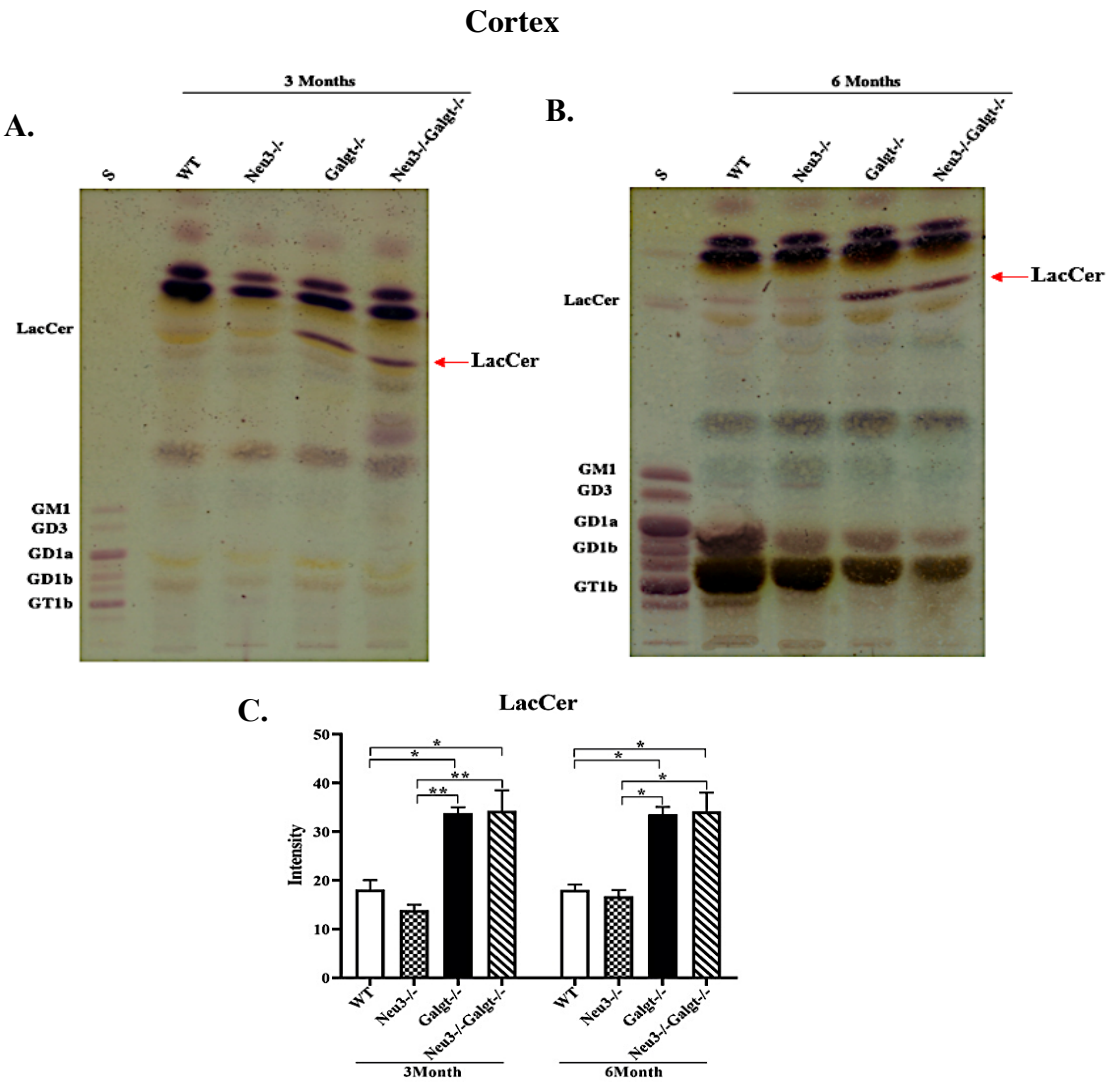

Figure 3.7. TLC plate images for 3- (A) and 6-month-old (B) WT, Neu3-/-, Galgt-/- and Neu3-/-Galgt-/- mice for neutral GSLs of the cortex region. The S shows the ganglioside ladder with indicated gangliosides. The levels of LacCer (C) in the cortex brain region of 3- and 6-month-old WT, Neu3-/-, Galgt-/-, and Neu3-/-Galgt-/- mice were indicated. Data is representative of mean ± SEM of measurements. Significant levels in the data were presented by using the two-way ANOVA (*p<0.05, ***p<0.001 and ****p<0.0001). (n=3 for 3- and 6-month old mice)

Acidic GSLs in cerebellum of 3- (Figure 3.8 A) and 6-month-old (Figure 3.8 B) WT, Neu3-/-, Galgt-/- and Neu3-/-Galgt-/- mice were analyzed. In results, only complex ganglioside series as G_{M1}, G_{D1a}, G_{D1a}, G_{D1b}, and G_{T1b} were detected in WT and Neu3-/- (Figure 3.9) in contrast to only simple gangliosides as G_{M3}, G_{D3}, and G_{D3} isoform called o-acetyl G_{D3} in Galgt-/- and Neu3-/-Galgt-/- (Figure 3.10). Then, neutral GSLs were

analyzed in cerebellum of 3- (Figure 3.11 A) and 6-month-old (Figure 3.11 B) WT, Neu3-/-, Galgt-/- and Neu3-/-Galgt-/- mice.

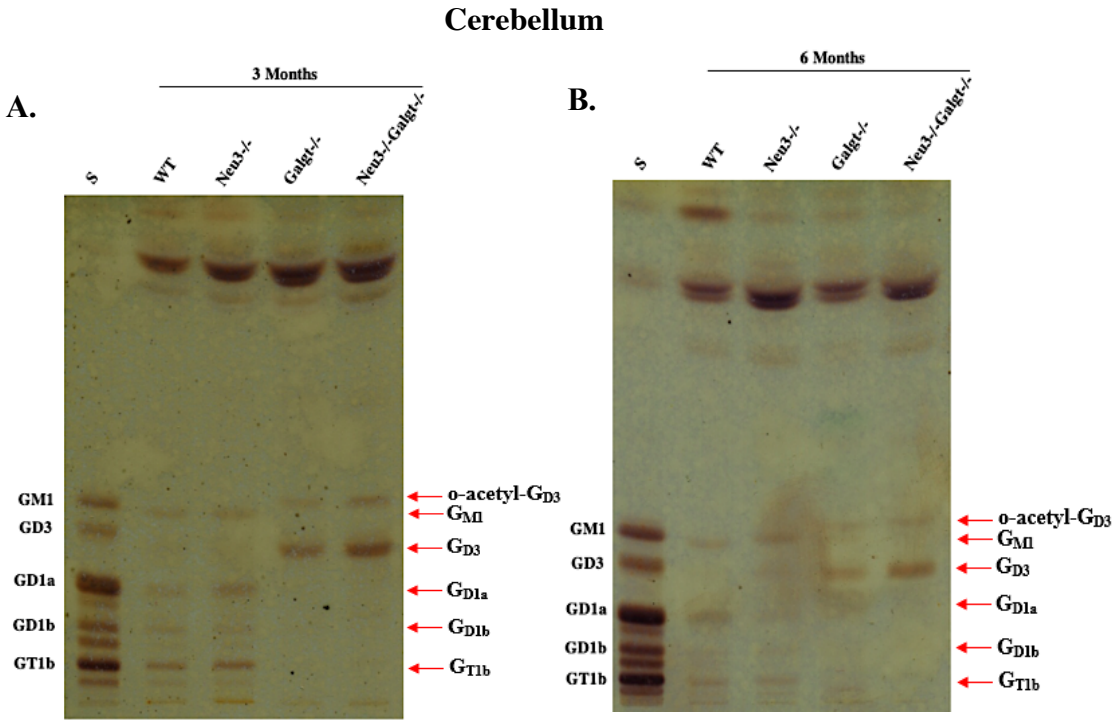

Figure 3.8. TLC plate images for 3-month-old (A) and 6-month-old (B) WT, Neu3-/-, Galgt-/- and Neu3-/-Galgt-/- mice for acidic GSLs of the cerebellum region loaded in 7.5mg amounts. The S shows the ganglioside standards with indicated gangliosides. (n=3 for 3- and 6-month old mice)

According to analyses of band intensities, 1.9-fold increase in G_{M1} levels between 3- and 6-month-old Neu3-/- were shown (Figure 3.9 A). Moreover, 1.9-fold increase in levels of 6-month-old Neu3-/- mice compared to WT counterparts were measured (Figure 3.9 A). Additionally, there were significantly decreased levels of G_{D1a} (2.6-fold) in 6-month-old Neu3-/- mice compared to WT counterpart (Figure 3.9 B). The levels of G_{D1b} revealed that there was an apparent decrease (1.3-fold) in Neu3-/- mice between 3- and 6-month-old (Figure 3.9 C). However, G_{D1b} levels in 6-month-old WT were inclined compared to Neu3-/- mice as 1.2-fold (Figure 3.9 C). There were no indicated differences for G_{T1b} levels (Figure 3.9 D).

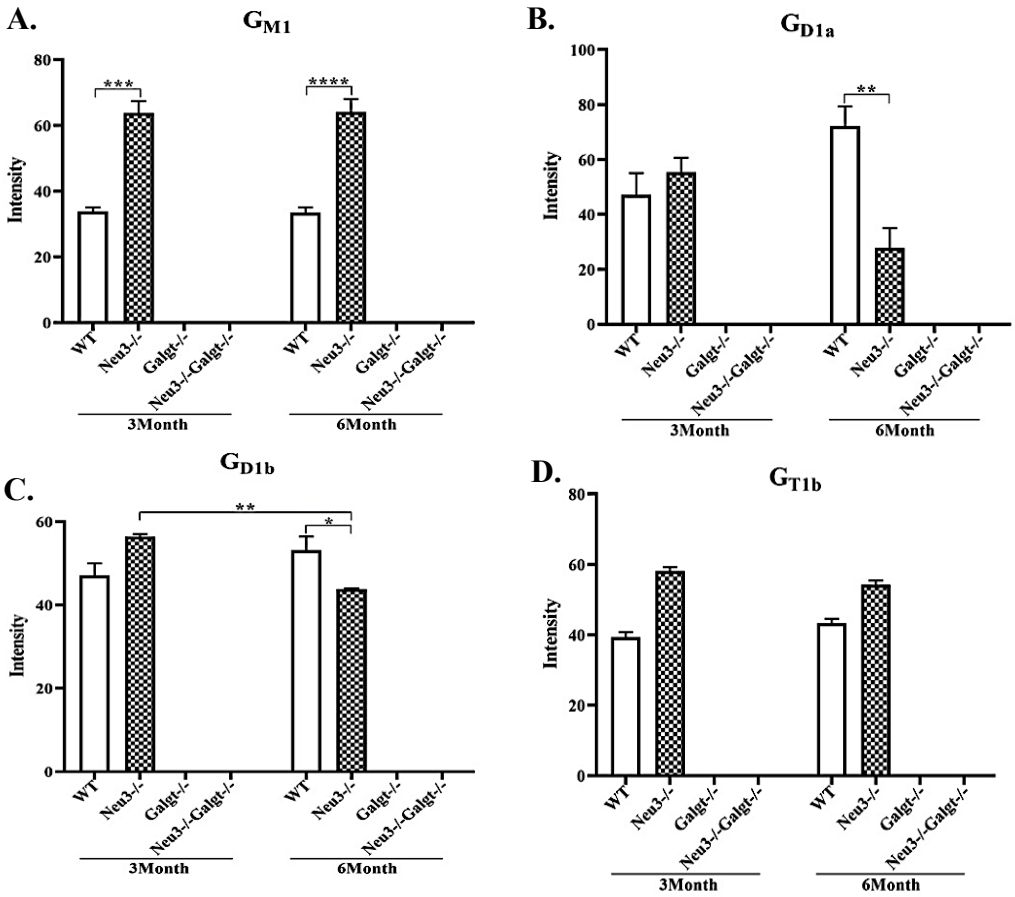

Figure 3.9. The levels of a-series G_{M1} and G_{D1a}, and b-series G_{D1b} and G_{T1b} (A, B, C, and D, respectively) in the cerebellum region of 3- and 6-month-old WT, Neu3-/-, Galgt-/-, and Neu3-/-Galgt-/- mice were indicated. Data represents mean ± SEM of measurements. Significant levels in the data were presented by using the two-way ANOVA (*p<0.05, ***p<0.001 and ****p<0.0001). (n=3 for 3- and 6-month old mice).

Next, the acidic GSLs analyses in cerebellum region showed a significant decrease in the levels of o-acetyl G_{D3}between 3- and 6-month-old Galgt-/- mice as 1.5-fold (Figure 3.10 A). Furthermore, age-related increase in Neu3-/-Galgt-/- mice was shown as 1.2-fold (Figure 3.10 A). In 3- and 6-month-old Galgt-/- mice, there were a decrease in the levels of o-acetyl G_{D3} compared to Neu3-/-Galgt-/- mice as 1.3- and 2.5-fold, respectively (Figure 3.10 A). Moreover, in G_{D3} levels, there was a significant increase as 4.8-fold in Neu3-/-Galgt-/- mice compared to Galgt-/- mice at 6-month-old age (Figure 3.10 B).

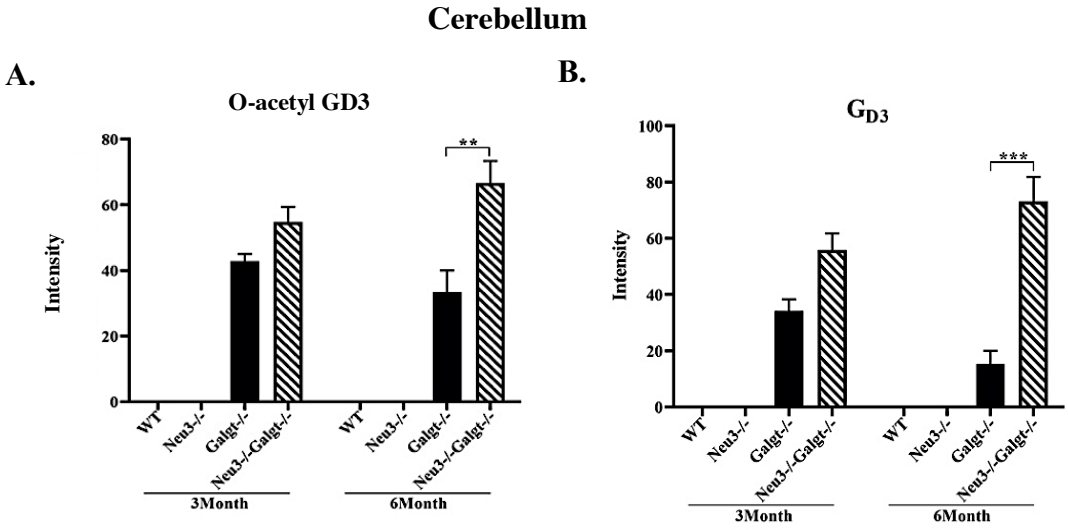

Figure 3.10. The levels of b-series G_{D3} and o-acetyl G_{D3} (A, and B, respectively) in the cerebellum region of 3- and 6-month-old WT, Neu3-/-, Galgt-/-, and Neu3-/-Galgt-/- mice were presented. Data is representative of mean ± SEM of measurements. Significant levels in the data were presented by using the two-way ANOVA (**$p<0.01$ and ***$p<0.001$). (n=3 for 3- and 6-month old mice).

According to the results of neutral GSLs in cerebellum region of 3- (Figure 3.11 A) and 6-month-old (Figure 3.11 B) WT, Neu3-/-, Galgt-/-, and Neu3-/-Galgt-/- mice, LacCer levels were changed in Galgt-/- and Neu3-/-Galgt-/- mice compared to WT and Neu3-/- mice littermates (Figure 3.11 C). Significantly increased levels of LacCer in 3-month-old Galgt-/- mice were indicated compared to WT and Neu3-/- mice (2.7-fold and 3.1-fold, respectively) (Figure 3.11 C). Moreover, the 2.1-fold and 2.4-fold increase in the levels of LacCer compared to WT and Neu3-/- mice, respectively in 3-month-old Neu3-/-Galgt-/- were shown (Figure 3.11 C). In 6-month-old Galgt-/- mice, LacCer levels increased in comparison to WT and Neu3-/- mice groups as 2.7-fold and 2.1-fold, respectively (Figure 3.11 C). The 3.2-fold and 2.5-fold increase in LacCer levels of 6-month-old Neu3-/-Galgt-/- mice compared to WT and Neu3-/- counterparts were shown (Figure 3.11 C). However, there were no significant changes in the levels of LacCer between 3- and 6-month-old groups (Figure 3.11 C).

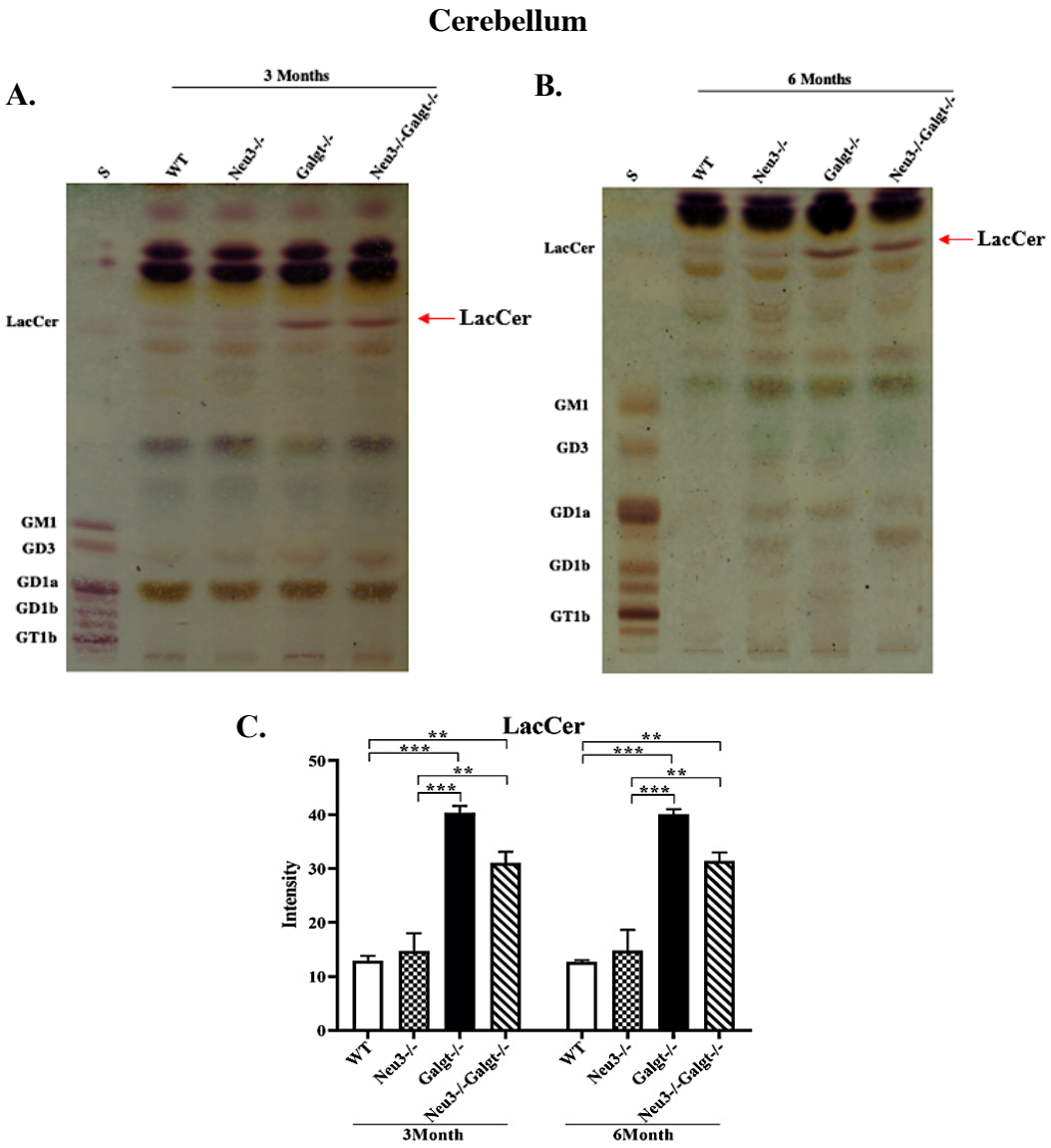

Figure 3.11. TLC plate images for 3-month-old (A) and 6-month-old (B) WT, Neu3-/, Galgt-/- and Neu3-/-Galgt-/- mice for neutral GSLs of the cerebellum region loaded in 7.5mg amounts. The S shows the ganglioside ladder with indicated gangliosides. The levels of LacCer (C) in the cerebellum region of 3- and 6-month-old WT, Neu3-/-, Galgt-/-, and Neu3-/-Galgt-/- mice were indicated. Data is representative of mean ± SEM of measurements. Significant levels in the data were presented by using the two-way ANOVA (**p<0.01 and ***p<0.001). (n=3 for 3- and 6-month old mice)

3.4. Apoptosis Analyses for Cortex Region

For understanding alterations in apoptosis in cortex tissues of 3- and 6-month-old WT, Neu3-/-, Galgt-/- and Neu3-/-Galgt-/- were subjected to DNA fragmentation assay, RT-PCR, and Western Blotting.

3.4.1. DNA Fragmentation Assay

The DNA fragmentation assay is generally used as the classical method to investigate fragmented DNA molecules since in the presence of apoptosis, caspase activated DNase cleaves DNA molecules by resulting in DNA fragments. After performing DNA fragmentation assay to obtain DNA fragments, the samples are loaded to agarose gel. Mostly, this technique gives results as semi-quantitatively (Bortner *et al*. 1995). The results (Figure 3.12) in cortex did not show any additional DNA fragment but there were more intense smears in 6-month-old Galgt-/- mice compared to other groups.

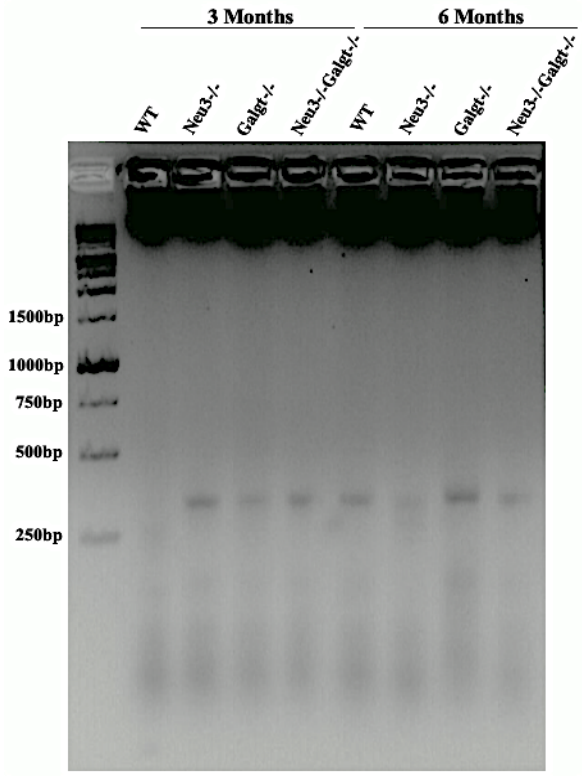

Figure 3.12. DNA fragmentation analyses in the cortex tissues of 3- and 6-month-old WT, Neu3-/-, Galgt-/- and Neu3-/-Galgt-/- mice.

3.4.2. Real Time-PCR Analyses

Since the results of DNA fragmentation were not explanatory for revealing alterations in apoptotic pathway in single- or double-deficiency of Neu3 and Galgt enzymes, the markers of ER-stress, oxidative stress, and apoptosis were used to show the changes in their levels by Real Time-PCR. Initially, the levels were analyzed in cortex (Figure 3.13, 3.14, and 3.15), tissues of 3- and 6-month-old WT, Neu3-/-, Galgt-/- and Neu3-/-Galgt-/- mice by using markers listed in Table 2.2.

Firstly, the ER-stress markers Calnexin (Figure 3.13 A), ATF6 (Figure 3.13 B), and spliced XBP-1 (Figure 3.13 C) were analyzed to present the possible alterations in ER-stress mechanism in cortex tissues of 3- and 6-month-old WT, Neu3-/-, Galgt-/- and Neu3-/-Galgt-/- mice. The protein of interest encoded by ATF6 acts to activate ER-stress responsive elements by translocating into nucleus in the presence of Unfolded Protein Response (UPR). The XBP-1 mRNA is post-transcriptionally modified to act in the activation of ER-stress related genes in the form of spliced XBP-1. Those unfolded protein response elements are mostly prevented by Ca^{2+}-binding ER chaperones like Calnexin. Their concerted action enables the removal of unfolded proteins. Unless the presence of those unfolded proteins is controlled, the cells could be terminated to cell death pathways (Liu *et al*. 2016).

According to results of Calnexin (Figure 3.13 A), the expression levels of 6-month-old Neu3-/- and Neu3-/-Galgt-/- mice significantly elevated compared to their 3-month-old Neu3-/- and Neu3-/-Galgt-/- mice as 1.3-fold and 1.5-fold, respectively. In Galgt-/- mice, there was a slight increase between 3-month-old and 6-month-old. The 6-month-old Neu3-/-Galgt-/- mice showed significantly increased expression levels of ATF6 (Figure 3.13 B) compared to WT (1.5-fold), Neu3-/- (1.5-fold), and Galgt-/- (1.5-fold) counterparts. There were age-related increases in Neu3-/-Galgt-/- (3.0-fold), Galgt-/- (2.0-fold), Neu3-/- (2.0-fold), and WT (2.0-fold) between 3- and 6-month-old counterparts. Finally, double deficient mice compared to Neu3-/- littermates at 6-month-old indicated an increase in XBP-1 gene expression levels (Figure 3.13 C) as 1.5-fold while there was an age-related elevation for Neu3-/-Galgt-/- mice as 1.6-fold.

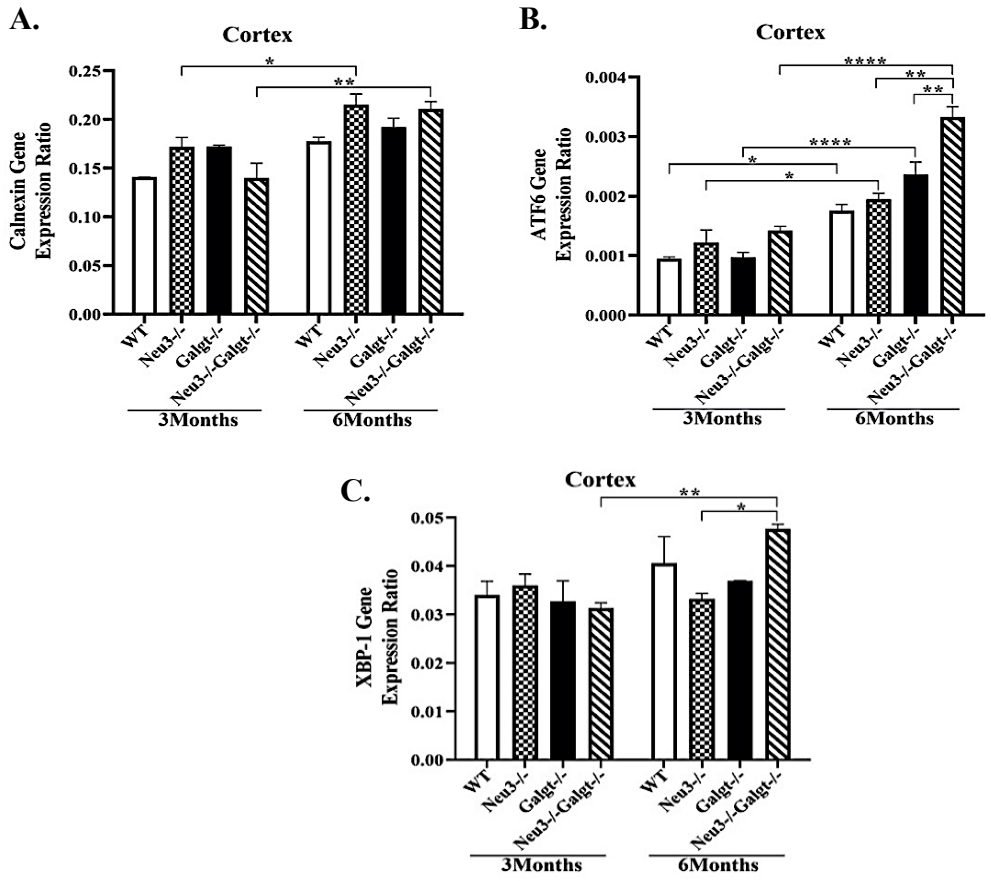

Figure 3.13. The expression levels of ER-stress markers named as Calnexin (A), ATF6 (B), and spliced XBP-1 (C) in cortex tissues of 3- and 6-month-old WT, Neu3-/-, Galgt-/- and Neu3-/-Galgt-/- mice. Expression ratio calculations were performed by ΔCT method. Significant levels in the data were presented by using the two-way ANOVA (*$p<0.05$, **$p<0.01$, ***$p<0.001$, and ****$p<0.0001$). (n=3 for 3- and 6-month old mice)

Secondly, the oxidative stress markers TTase 1 (Figure 3.14 A), SOD2 (Figure 3.14 B), and Catalase (Figure 3.14 C), were used for revealing the possible alterations in the mechanism of oxidative stress in the cortex tissues of 3- and 6-month-old WT, Neu3-/-, Galgt-/- and Neu3-/-Galgt-/- mice. The oxidative stress markers encode the enzymes working in the context of antioxidant defense mechanisms to remove ROS from environment (Storz and Imlayt 1999). According to results of TTase 1 marker (Figure 3.14 A), in 3-month-old Galgt-/-, expression levels were significantly increased as 1.3-fold compared to WT and Neu3-/-Galgt-/- mice. 6-month-old Galgt-/- mice showed significantly elevated levels of TTase 1 marker (Figure 3.14 A), compared to WT and Neu3-/-Galgt-/- as 1.3-fold and 1.2-fold, respectively. 6-month-old Galgt-/- mice indicated an apparent elevation as 1.2-fold compared to 3-month-old Galgt-/-. For the

SOD2 expression (Figure 3.14 B), there were age-dependent increases for Neu3-/- mice as 2.0-fold, Galgt-/- mice as 2.2-fold, and Neu3-/-Galgt-/- mice as 3.1-fold. 6-month-old Neu3-/-Galgt-/- mice increased in SOD2 expression (Figure 3.14 B) compared to WT littermates. Finally, the expression levels of Catalase (Figure 3.14 C) showed a significant increase in 3-month-old Neu3-/- mice compared to 3-month-old Neu3-/-Galgt-/- mice (1.6-fold). In 6-month-old Neu3-/-Galgt-/- mice, there was age-related elevation (1.6-fold). Therefore, it was shown that the levels of oxidative stress were elevated in Galgt-/- mice and Neu3-/-Galgt-/- mice in especially their older ages when the SOD2 and Catalase levels were compared (Figure 3.14 B and 3.14 C).

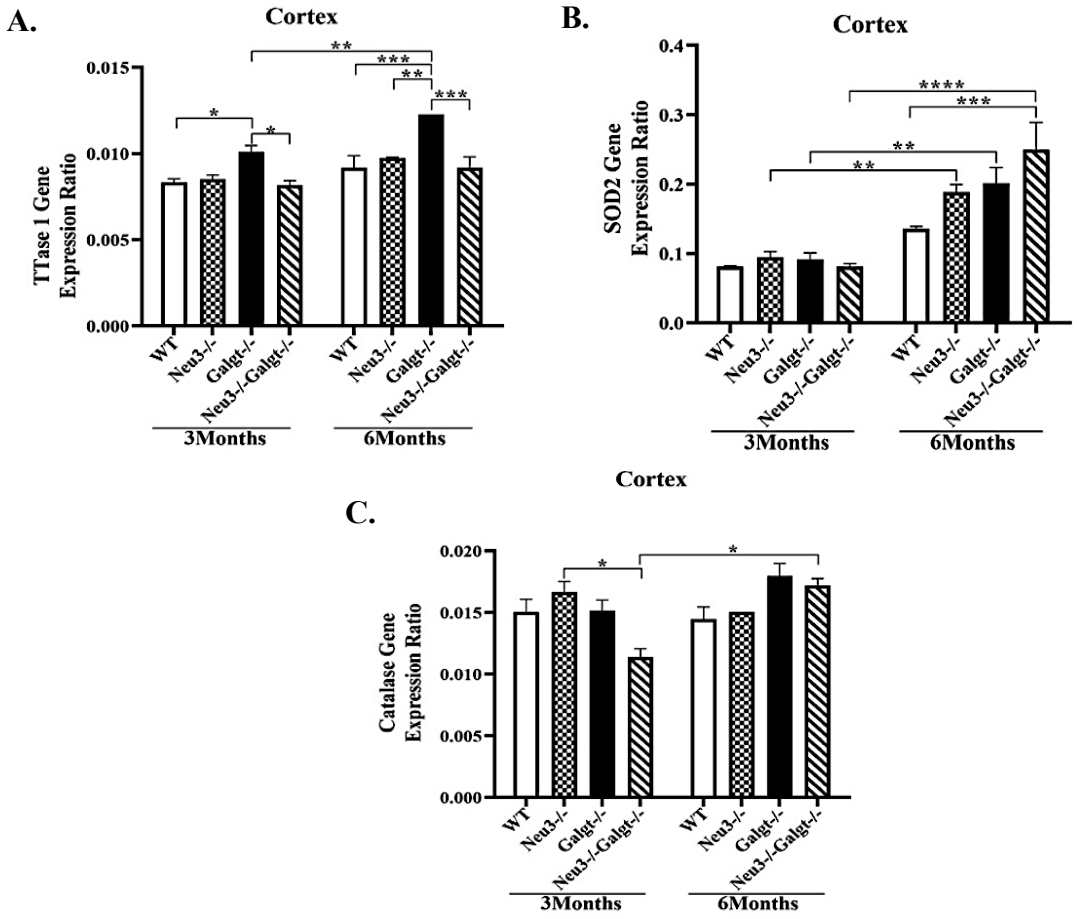

Figure 3.14. The expression levels of oxidative stress markers named as TTase 1 (A), SOD2 (B), and Catalase (C) in cortex tissues of 3- and 6-month-old WT, Neu3-/-, Galgt-/- and Neu3-/-Galgt-/- mice. Expression ratio calculations were performed by ΔCT method. Significant levels in the data were presented by using the two-way ANOVA (*p<0.05, **p<0.01 ***p<0.001, and ****p<0.0001). (n=3 for 3- and 6-month old mice)

Finally, apoptosis markers Bcl-2 (Figure 3.15 A), Bcl-XL (Figure 3.15 B), and Bax (Figure 3.15 C) were used to show possible alterations in the mechanism of apoptosis in the cortex tissues of 3- and 6-month-old WT, Neu3-/-, Galgt-/- and Neu3-/-Galgt-/- mice. The apoptosis related genes are the anti-apoptotic forms of Bcl-2 and Bcl-XL while the pro-apoptotic marker is Bax. The activities of Bax are normally prevented by the actions of Bcl-2 and Bcl-XL encoding proteins of interest. All of those proteins encoded by those markers are associated with mitochondrial membrane in which any alterations regarding the disturbed membrane potential result in the release of certain apoptogenic factors and the activation of pro-apoptotic Bax while anti-apoptotic markers are prevented (Elmore 2007).

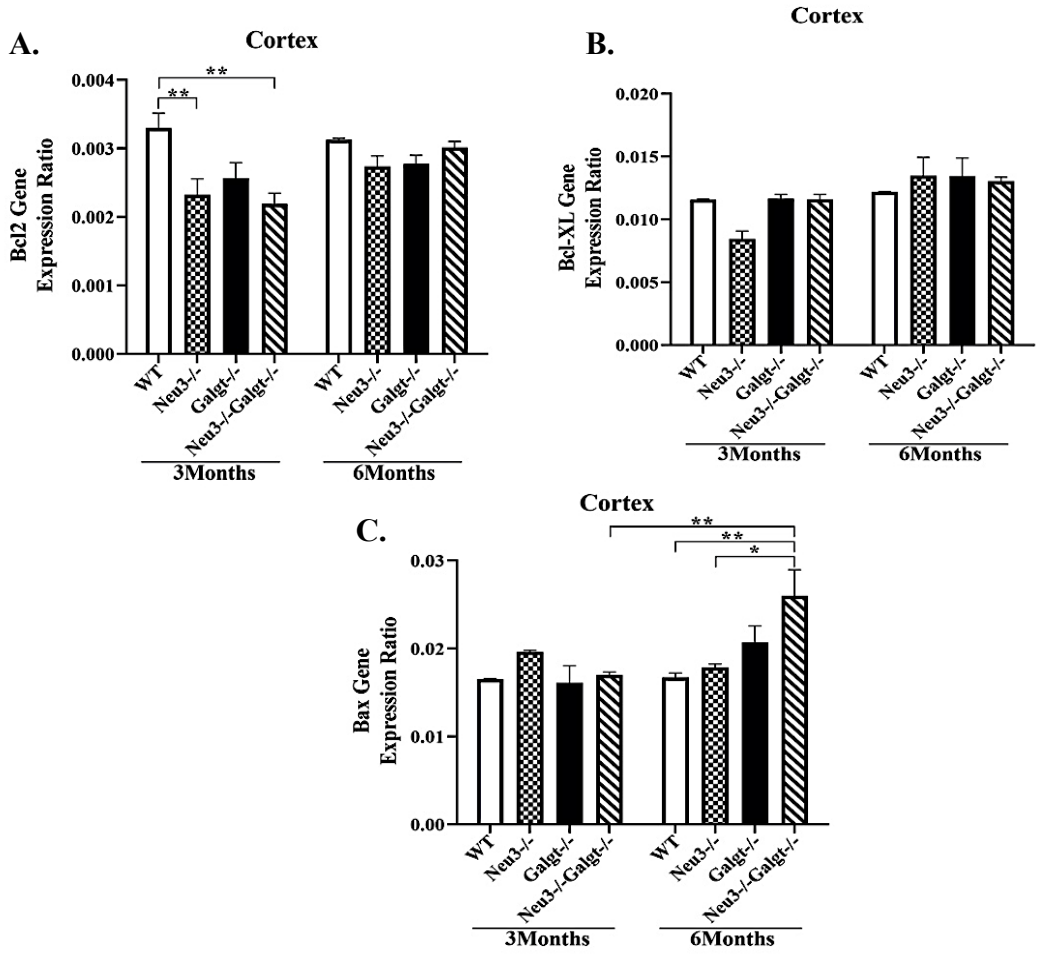

Figure 3.15. The expression levels of apoptosis markers named as Bcl2 (A), Bcl-XL (B), and Bax (C) in cortex tissues of 3- and 6-month-old WT, Neu3-/-, Galgt-/- and Neu3-/-Galgt-/- mice. Expression ratio calculations were performed by ΔCT method. Significant levels in the data were presented by using two-way ANOVA (*$p<0.05$ and **$p<0.01$). (n=3 for 3- and 6-month old mice)

According to expression level analyses of Bcl-2 marker (Figure 3.15 A), significant decreases in Neu3-/- and Neu3-/-Galgt-/- mice compared to WT littermates as 1.5-fold were shown. However, Galgt-/- mice presented a slight reduction (Figure 3.15 A). There were not any significant changes for Bcl-XL expression levels (Figure 3.15 B), for both ages. Finally, Bax expression levels (Figure 3.15 C) were shown to increase as 1.5-fold and 1.4-fold for Neu3-/-Galgt-/- mice compared to WT and Neu3-/- mice, respectively. The age-dependent increase in the Bax expression levels as 1.5-fold was indicated for Neu3-/-Galgt-/- mice. The increase in the Bax activity were not prevented by anti-apoptotic proteins in terms of the sligthly reduced levels of Bcl-2 and unchanged Bcl-XL levels in cortex region.

3.4.3. Western Blot Analyses

The western blot analyses were done for understanding changes in protein expression levels of BiP (Figure 3.16), Caspase 9 (Figure 3.17), Caspase 3 (Figure 3.18), and Fas-Ligand (Figure 3.19) antibodies. The analyses were performed in the cortex tissues of 3- and 6-month-old WT, Neu3-/-, Galgt-/-, and Neu3-/-Galgt-/- mice. The antibodies were chosen to show any potential alterations in apoptosis and ER-stress mechanisms in single- or double-deficiency of Neu3 and Galgt enzymes. Firstly, BiP -ER chaperone- levels were assessed to show ER-stress conditions. According to results of BiP antibody (Figure 3.16 A), there was a slight change among the genotypes. The levels for Neu3-/- and Galgt-/- lowered slightly compared to Neu3-/-Galgt-/- mice in both age-groups. Moreover, there were no age-dependent differences among the genotypes (Figure 3.16 B).

Initiator caspase of apoptosis called as Caspase 9 was also assayed in cortex in its cleaved form from Pro-caspase 9. According to results of the antibody (Figure 3.17 A), there were significant increases in the Neu3-/- mice compared to WT and Neu3-/-Galgt-/- as 1.6-fold and 1.4-fold, respectively at 6-month-old age (Figure 3.17 B).

Next, executioner caspase of apoptosis called Caspase 3 was evaluated for the cortex region in its cleaved form from Pro-caspase 3. According to results (Figure 3.18 A), there was an apparent increase (2.0-fold) in the Galgt-/- mice compared to WT at 3-month-old age while there were slightly increased levels in Galgt-/- mice compared to

Neu3-/- and Neu3-/-Galgt-/- mice at the same ages. The slightly increased levels in 6-month-old were also obtained (Figure 3.18 B).

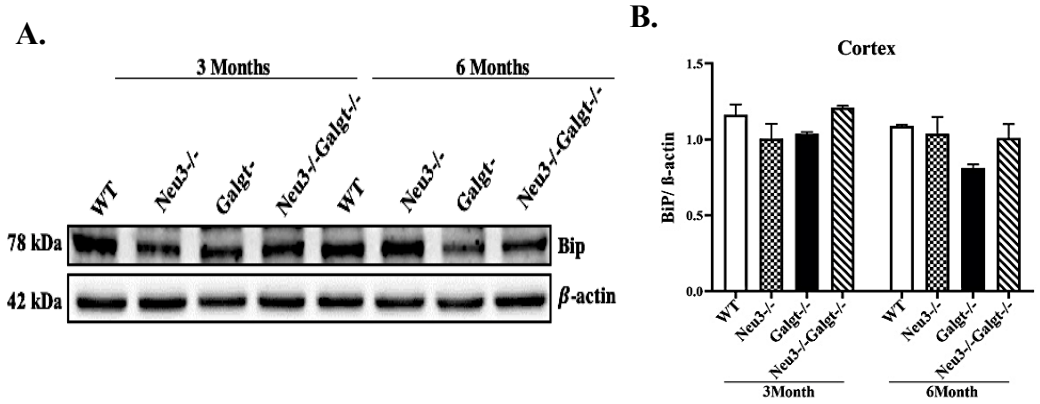

Figure 3.16. Western Blot image of Bip antibody in the cortex region of 3- and 6-month-old WT, Neu3-/-, Galgt-/-, and Neu3-/-Galgt-/- mice (A). β-actin was used as the internal control. The graph (B) shows the ratio of the band intensity of BiP antibody to the band intensity of β-actin. Significant levels in the data were presented by using the two-way ANOVA. (n=3 for 3- and 6-month old mice)

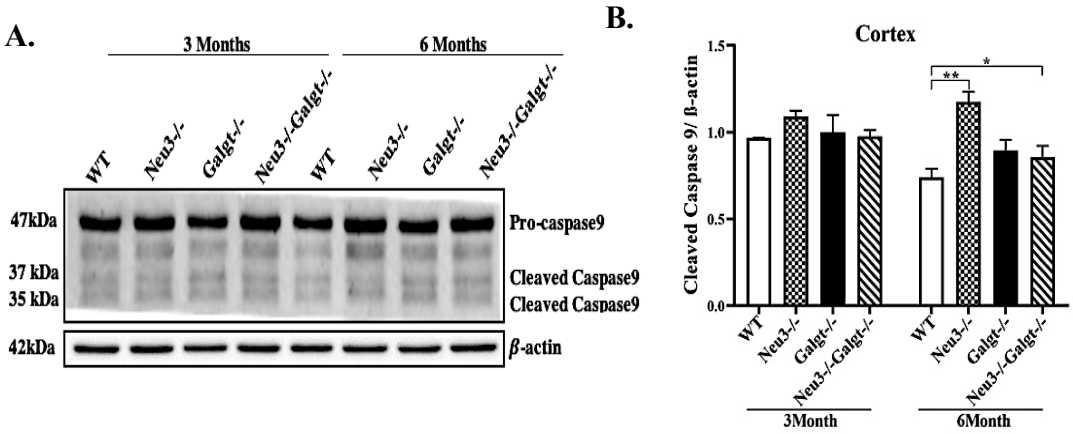

Figure 3.17. Western Blot image of Caspase 9 antibody in the cortex region of 3- and 6-month-old WT, Neu3-/-, Galgt-/-, and Neu3-/-Galgt-/- mice (A). β-actin was used as the internal control. The graph (B) shows the ratio of the band intensity of Cleaved Caspase9 antibody to the band intensity of β-actin. Significant levels in the data were presented by using the two-way ANOVA (*$p<0.05$ and **$p<0.01$). (n=3 for 3- and 6-month old mice)

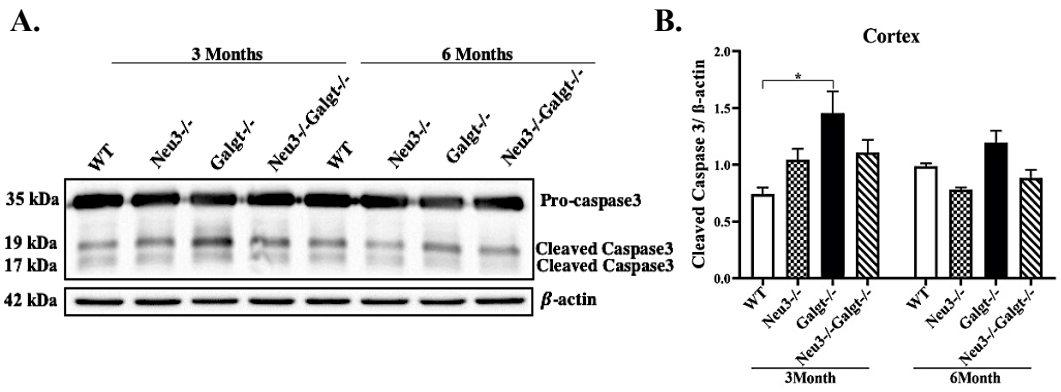

Figure 3.18. Western Blot image of Caspase 3 antibody in the cortex region of 3- and 6-month-old WT, Neu3-/-, Galgt-/-, and Neu3-/-Galgt-/- mice (A). β-actin was used as the internal control. The graph (B) shows the ratio of the band intensity of Cleaved Caspase3 antibody to the band intensity of β-actin. Significant levels in the data were presented by using the two-way ANOVA (*p<0.05). (n=3 for 3- and 6-month old mice)

The extrinsic apoptotic pathway marker called Fas-Ligand that binds to its receptor to induce apoptosis, was also assayed for the cortex region (Figure 3.19 A). According to results (Figure 3.19 B), there were only slightly increased levels in 3-month-old Neu3-/- mice compared to WT and Galgt-/- mice. However, all genotypes of 6-month-old group were reduced slightly compared to their 3-month-old counterparts.

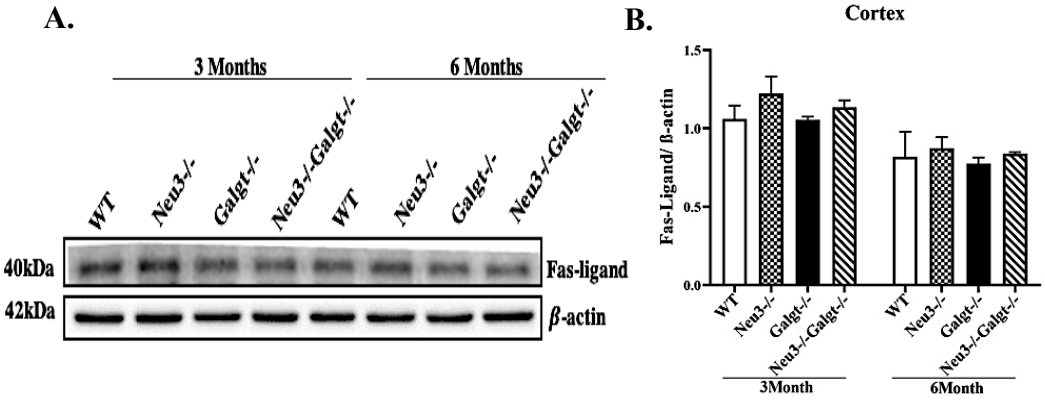

Figure 3.19. Western Blot image of Fas-Ligand antibody in the cortex region of 3- and 6-month-old WT, Neu3-/-, Galgt-/-, and Neu3-/-Galgt-/- mice (A). β-actin was used as the internal control. The graph (B) shows the ratio of the band intensity of Fas-Ligand antibody to the band intensity of β-actin. Significant levels in the data were presented by using the two-way ANOVA. (n=3 for 3- and 6-month old mice)

3.5. Apoptosis Analyses for Cerebellum Region

For understanding alterations in apoptosis in cerebellum tissues of 3- and 6-month-old WT, Neu3-/-, Galgt-/- and Neu3-/-Galgt-/- were subjected to DNA fragmentation assay, RT-PCR, and Western Blotting.

3.5.1. DNA Fragmentation Assay

After performing DNA fragmentation assay to obtain DNA fragments, the samples are loaded to agarose gel. Mostly, this technique gives results as semi-quantitatively (Bortner *et al*. 1995). In the study, in 3-month-old Neu3-/- and 6-month-old Neu3-/-Galgt-/- mice, there were additional DNA fragments in 3-month-old Neu3-/- and 6-month-old Neu3-/-Galgt-/- mice (Figure 3.20).

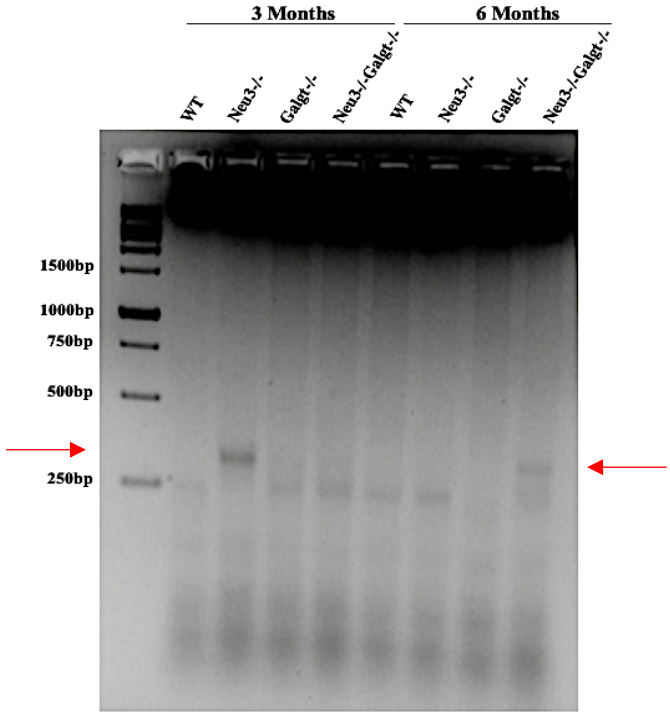

Figure 3.20. DNA fragmentation analyses in the cerebellum tissues of 3- and 6-month-old WT, Neu3-/-, Galgt-/- and Neu3-/-Galgt-/- mice.

3.5.2. Real-Time PCR Analyses

The ER-stress, oxidative stress, and apoptosis markers (Figure 3.21, 3.22, and 3.23, respectively) were evaluated in cerebellum tissues of tissues of 3- and 6-month-old WT, Neu3-/-, Galgt-/- and Neu3-/-Galgt-/- mice by using markers listed in Table 2.2.

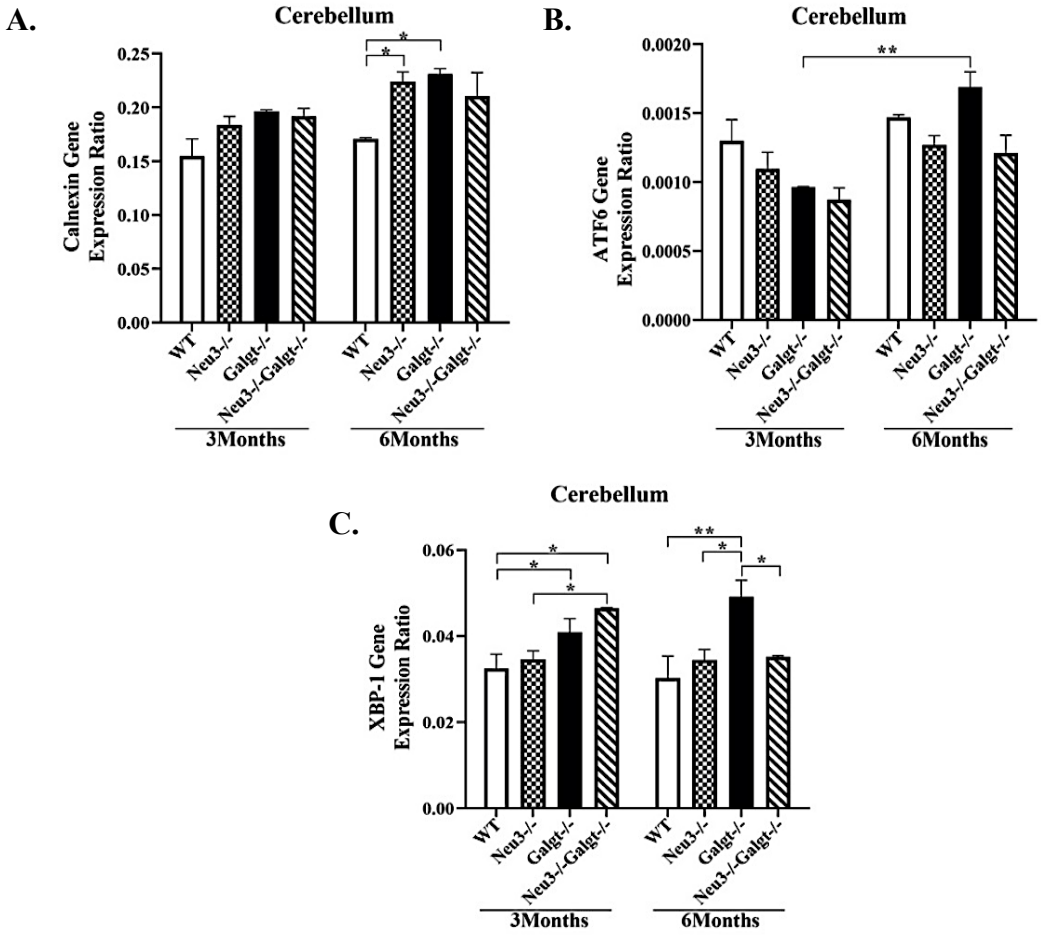

Figure 3.21. The expression levels of ER-stress related markers named as Calnexin (A), ATF6 (B), and spliced XBP-1 (C) in cerebellum tissues of 3- and 6-month-old WT, Neu3-/-, Galgt-/- and Neu3-/-Galgt-/- mice. Expression ratio calculations were performed by ΔCT method. Significant levels in the data were presented by using the two-way ANOVA (*$p<0.05$ and **$p<0.01$). (n=3 for 3- and 6-month old mice)

Firstly, the ER-stress markers Calnexin (Figure 3.21 A), ATF6 (Figure 3.21 B), and spliced XBP-1 (Figure 3.21 C) were used for understanding any alterations in the ER-stress mechanism in the cerebellum tissues of 3- and 6-month-old WT, Neu3-/-, Galgt-/- and Neu3-/-Galgt-/- mice. According to results of Calnexin marker (Figure 3.21 A), the levels in Neu3-/- and Galgt-/- mice were apparently elevated compared to WT mice as 1.3-fold and 1.4-fold, respectively. There were slightly increased Calnexin levels between two age groups for all genotypes. Then, significantly increased expression levels of ATF6 (Figure 3.21 B) were shown in two age groups of Galgt-/- mice as 2.0-fold. Moreover, the age-dependent increases were seen in Neu3-/-Galgt-/- mice but not significantly. Finally, for expression level of XBP-1 (Figure 3.21 C), it was indicated that Galgt-/- and Neu3-/-Galgt-/- mice had higher expression levels compared to WT littermates in 3-month-old as 1.3-fold while 3-month-old Galgt-/- mice XBP-1 expression was elevated as 1.3-fold compared to Neu3-/- counterpart. For older group, the levels of 6-month-old Galgt-/- mice were apparently increased in contrast to WT, Neu3-/-, and Neu3-/-Galgt-/- as 1.6-fold, 1.4-fold, and 1.4-fold, respectively (Figure 3.21 C).

Then, the oxidative stress markers TTase 1 (Figure 3.22 A), SOD2 (Figure 3.22 B), and Catalase (Figure 3.22 C) were used for showing the potential alterations in the mechanism of oxidative stress in cerebellum of 3- and 6-month-old WT, Neu3-/-, Galgt-/- and Neu3-/-Galgt-/- mice. In the gene expression analyses of TTase 1 (Figure 3.22 A), there were not significantly changed levels but the slightly increased expression was shown in age-related manner. Next, SOD2 expression levels (Figure 3.22 B) indicated apparent increases in 3-month-old Galgt-/- and Neu3-/-Galgt-/- mice as 2.1-fold compared to WT littermates. There were age-dependent increases in WT (2.8-fold) and Galgt-/- (1.7-fold) mice while the same pattern was obtained for Neu3-/- and Neu3-/-Galgt-/- mice in a slight manner. Finally, expression levels of Catalase (Figure 3.22 C) indicated increase in the levels of Neu3-/- (1.8-fold), Galgt-/- (1.7-fold), and Neu3-/-Galgt-/- (1.6-fold) mice in 3-month-old group compared to WT counterparts. In the 6-month-old group, the levels were also significantly elevated for Neu3-/- (1.9-fold), Galgt-/- (1.8-fold), and Neu3-/-Galgt-/- (1.7-fold) mice in contrast to WT littermates but there were no age-related changes for Catalase expression (Figure 3.22 C).

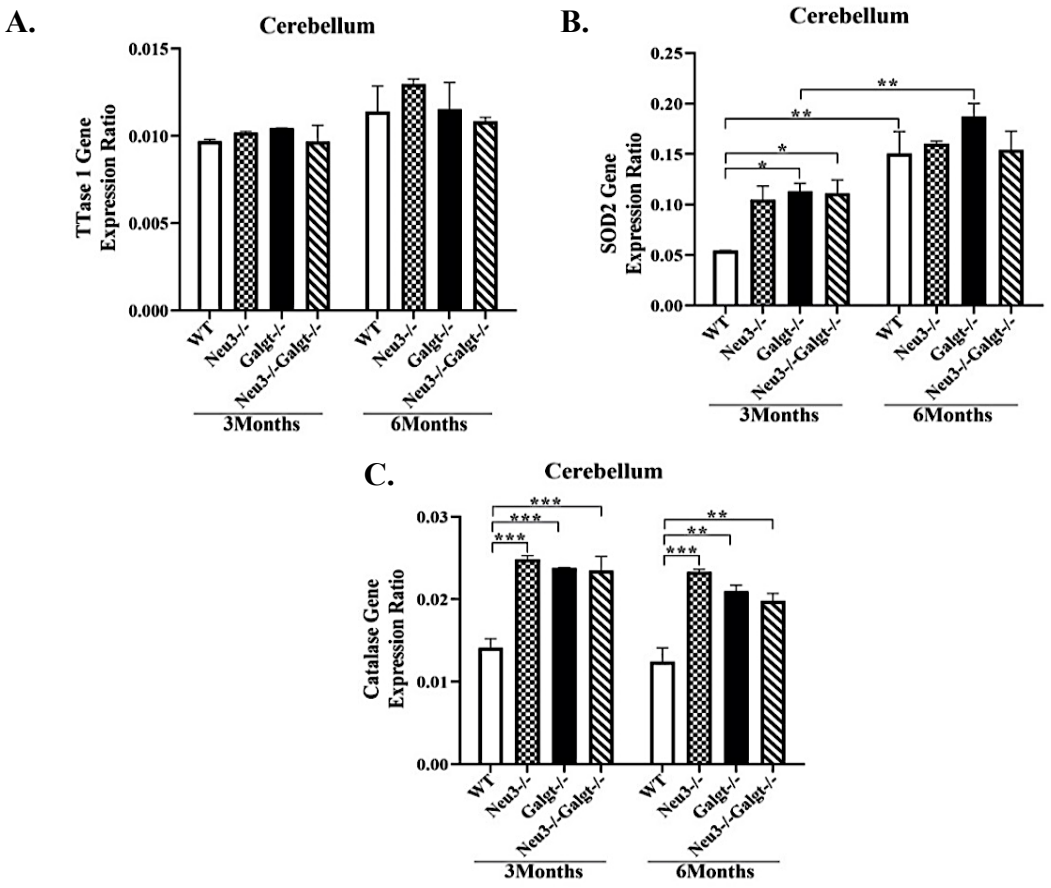

Figure 3.22. The expression levels of oxidative stress markers named as TTase 1 (A), SOD2 (B), and Catalase (C) in cerebellum tissues of 3- and 6-month-old WT, Neu3-/-, Galgt-/- and Neu3-/-Galgt-/- mice. Expression ratio calculations were performed by ΔCT method. Significant levels in the data were presented by using the two-way ANOVA (*p<0.05, **p<0.01, and ***p<0.001). (n=3 for 3- and 6-month old mice)

Next, the apoptosis markers Bcl-2 (Figure 3.23 A), Bcl-XL (Figure 3.23 B), and Bax (Figure 3.23 C) were used for showing the alterations in apoptosis in cerebellum tissues of 3- and 6-month-old WT, Neu3-/-, Galgt-/- and Neu3-/-Galgt-/-. According to the results, expression levels of Bcl-2 (Figure 3.23 A) were significantly decreased for 6-month-old Galgt-/- and Neu3-/- mice as 1.5-fold compared to WT littermates. The expression levels of Bcl-XL (Figure 3.23 B) did not show any significant change. Finally, the expression levels of Bax (Figure 3.23 C) indicated age-dependent increases in Neu3-/- and Galgt-/- mice as 2.4-fold and 2.2-fold, respectively. The levels of Bax in 6-month-old Galgt-/- were apparently elevated compared to WT littermates as 1.7-fold. The 6-month-old Neu3-/- mice indicated 1.6-fold increased levels of Bax marker compared to

WT counterparts (Figure 3.23 C). The 3-month-old Neu3-/-Galgt-/- mice showed increased Bax levels as 2.0-fold compared to WT (Figure 3.23 C).

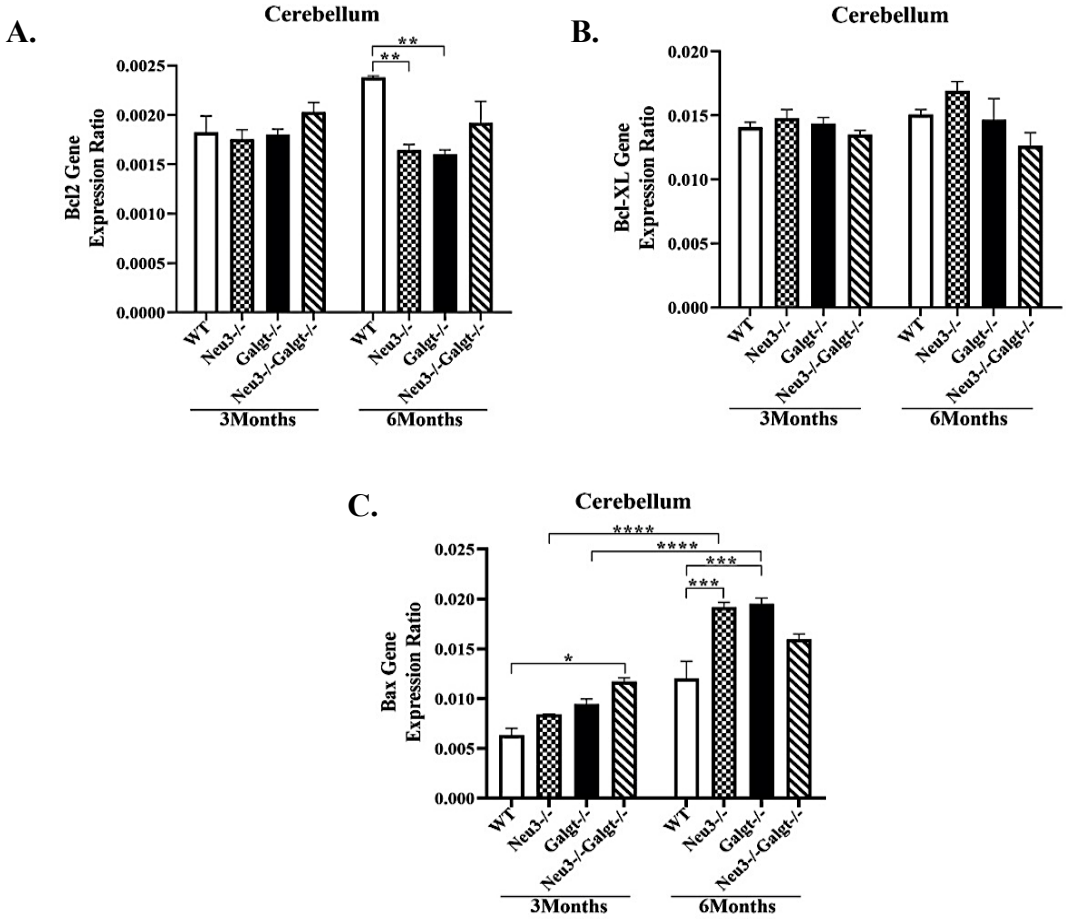

Figure 3.23. The expression levels of apoptosis markers named as Bcl2 (A), Bcl-XL (B), and Bax (C) in cerebellum tissues of 3- and 6-month-old WT, Neu3-/-, Galgt-/- and Neu3-/-Galgt-/- mice. Expression ratio calculations were performed by ΔCT method. Significant levels in the data were presented by using the two-way ANOVA (*p<0.05, **p<0.01 ***p<0.001 and ****p<0.0001). (n=3 for 3- and 6-month old mice)

In conclusion, the decreased levels of Bcl-2 and unchanged Bcl-XL levels while elevated Bax levels in Neu3-/- mice supported the changes in Caspase 9 and Caspase 3. However, for Neu3-/-Galgt-/- mice Bax levels were less than the levels shown in Galgt-/- mice. For Neu3-/-Galgt-/-, the apoptosis could probably be directed by ER stress conditions and changing Ca^{2+} ion content in cytosol. This alteration resulted in the opening of mitochondrial pores and release of apoptogenic factors like Caspase 9. The

elevated Bax levels in Galgt-/- mice would be caused by again the changes in Ca^{2+} levels of cytosol but the changes in Caspase 9 were not detected significantly.

3.5.3. Western Blot Analyses

The western blot was applied to the cerebellum tissues of 3- and 6-month-old WT, Neu3-/-, Galgt-/-, and Neu3-/-Galgt-/- mice as shown in the cortex region for apoptosis and ER-stress. The changes in protein expression levels of BiP (Figure 3.24), Caspase 9 (Figure 3.25), Caspase 3, (Figure 3.26) and Fas-Ligand (Figure 3.27) were evaluated.

According to western blot results of BiP antibody in the cerebellum (Figure 3.24 A), the levels of BiP were shown significantly higher in 6-month-old Galgt-/- mice compared to Neu3-/- counterparts as 2.4-fold (Figure 3.24 B). Moreover, in Neu3-/- mice, the levels were decreased compared to Neu3-/-Galgt-/- mice as 2.4-fold (Figure 3.24 B). For both age groups, the levels were slightly increased in Galgt-/- and Neu3-/-Galgt-/- mice compared to WT and Neu3-/- mice. There were no age dependent differences among the genotypes (Figure 3.24 B).

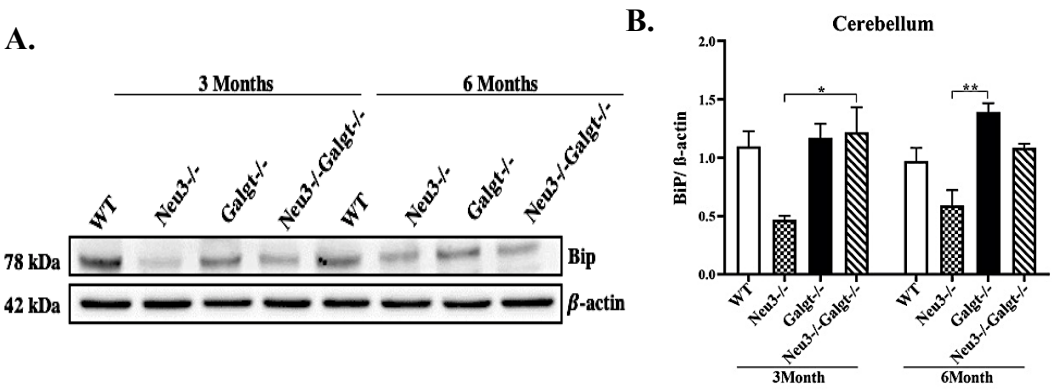

Figure 3.24. Western Blot image of Bip antibody in the cerebellum region of 3- and 6-month-old WT, Neu3-/-, Galgt-/-, and Neu3-/-Galgt-/- mice (A). β-actin was used as the internal control. The graph (B) shows the ratio of the band intensity of BiP antibody to the band intensity of β-actin. Significant levels in the data were presented by using the two-way ANOVA (*$p<0.05$ and **$p<0.01$). (n=3 for 3- and 6-month old mice)

Then, another marker called as initiator Caspase 9 in cleaved form was analyzed in the cerebellum region. According to the results of this antibody (Figure 3.25 A), there

was an apparent increase in the Neu3-/- mice compared to other genotypes at both 3- and 6-month-old of ages (Figure 3.25 B). The Neu3-/- cleaved caspase 9 levels were shown to increase as 2.1-fold compared to Galgt-/- mice in 3-month-old. Moreover, there were increased cleaved caspase 9 levels as 1.8-fold, 2.0-fold, and 1.6-fold compared to the levels in 6-month-old WT, Galgt-/-, and Neu3-/-Galgt-/- mice of ages in 6-month-old Neu3-/- mice (Figure 3.25 B). The slightly elevated cleaved caspase 9 levels were also detected for Neu3-/-Galgt-/- mice compared to Galgt-/- littermates for both age groups (Figure 3.25 B).

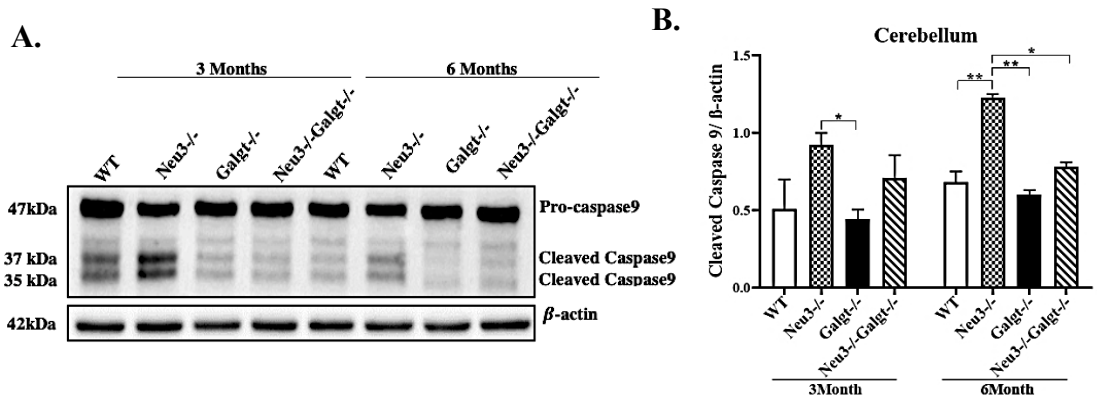

Figure 3.25. Western Blot image of Caspase9 antibody in the cerebellum region of 3- and 6-month-old WT, Neu3-/-, Galgt-/-, and Neu3-/-Galgt-/- mice (A). β-actin was used as the internal control. The graph (B) shows the ratio of the band intensity of Cleaved Caspase9 antibody to the band intensity of β-actin. Significant levels in the data were presented by using the two-way ANOVA (*$p<0.05$ and **$p<0.01$). (n=3 for 3- and 6-month old mice)

Later, Caspase 3 in cleaved form was evaluated in the cerebellum region. According to the results of the antibody (Figure 3.26 A), there was an apparent increase (3.4-fold) in the 3-month-old Neu3-/- mice compared to Galgt-/- counterparts. Furthermore, there were significantly increased levels in Neu3-/-Galgt-/- mice compared to WT (2.4-fold) and Galgt-/- (4.6-fold) littermates. Except slight increase between Neu3-/- and Galgt-/- mice and 2.0-fold elevated levels in Neu3-/-Galgt-/- compared to Galgt-/-, there were not any other differences at 6-month-old of age (Figure 3.26 B). as 0.9-fold in the 6-month-old Neu3-/- mice compared to WT counterparts. The levels were slightly reduced between 3-and 6-month-old Neu3-/-Galgt-/- (Figure 3.27 B). Finally, for the cerebellum region, the extrinsic apoptotic pathway marker, Fas-Ligand was also analyzed. In the results of this antibody (Figure 3.27 A), there was only apparent decrease

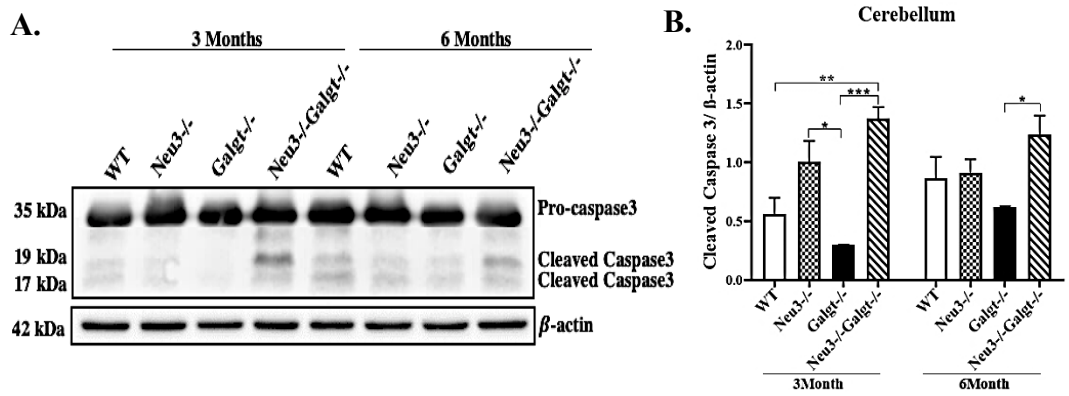

Figure 3.26. Western Blot image of Caspase3 antibody in the cerebellum region of 3- and 6-month-old WT, Neu3-/-, Galgt-/-, and Neu3-/-Galgt-/- mice (A). β-actin was used as the internal control. The graph (B) shows the ratio of the band intensity of Cleaved Caspase3 antibody to the band intensity of β-actin. Significant levels in the data were presented by using the two-way ANOVA (*p<0.05, **p0.01, and ***p<0.001). (n=3 for 3- and 6-month old mice)

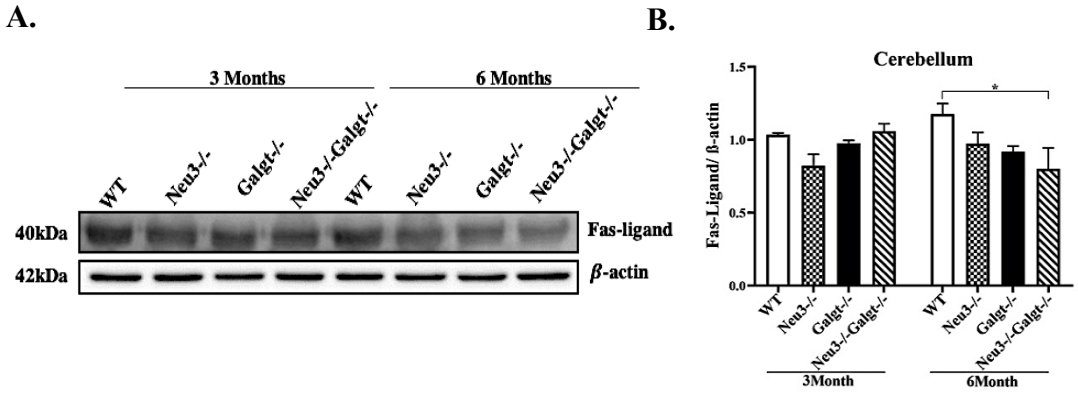

Figure 3.27. Western Blot image of Fas-Ligand antibody in the cerebellum region of 3- and 6-month-old WT, Neu3-/-, Galgt-/-, and Neu3-/-Galgt-/- mice (A). β-actin was used as the internal control. The graph (B) shows the ratio of the band intensity of Fas-Ligand antibody to the band intensity of β-actin. Significant levels in the data were presented by using the two-way ANOVA (*p<0.05). (n=3 for 3- and 6-month old mice)

3.6. Apoptosis Analyses for Thalamus Region

For understanding alterations in apoptosis in thalamus tissues of 3- and 6-month-old WT, Neu3-/-, Galgt-/- and Neu3-/-Galgt-/- were subjected to DNA fragmentation assay, RT-PCR, and Western Blotting.

3.6.1. DNA Fragmentation Assays

After performing DNA fragmentation assay to obtain DNA fragments, the samples are loaded to agarose gel. Mostly, this technique gives results semi-quantitatively (Bortner *et al*. 1995).

Finally, in the thalamus of Neu3-/-, Galgt-/-, and Neu3-/-Galgt-/- mice of 3- and 6-month-old groups, there were more intense smeared fragments in contrast to their WT counterparts (Figure 3.28)

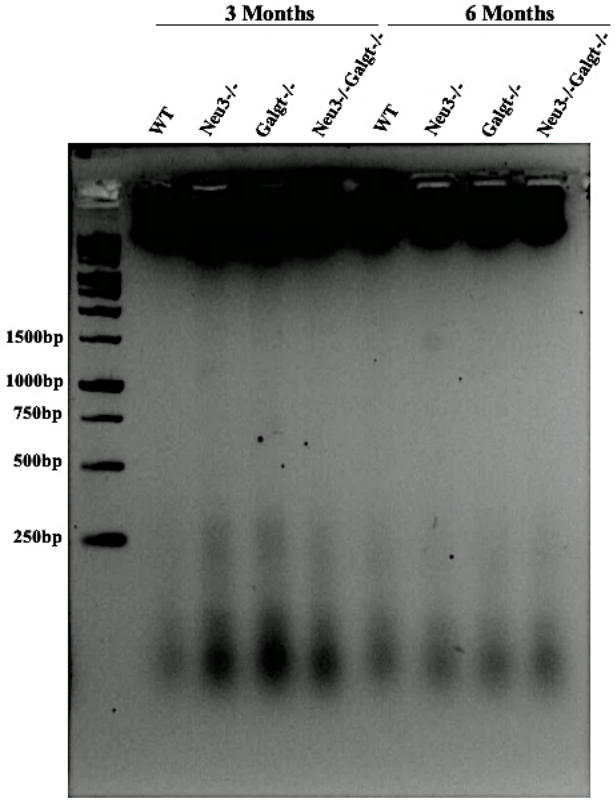

Figure 3.28. DNA fragmentation analyses in the thalamus tissues of 3- and 6-month-old WT, Neu3-/-, Galgt-/- and Neu3-/-Galgt-/- mice.

3.6.2. Real-Time PCR Analyses

The ER-stress, oxidative stress, and apoptosis markers (Figure 3.29, 3.30, and 3.31) were evaluated in thalamus tissues of 3- and 6-month-old WT, Neu3-/-, Galgt-/- and Neu3-/-Galgt-/- mice by using markers listed in Table 2.2.

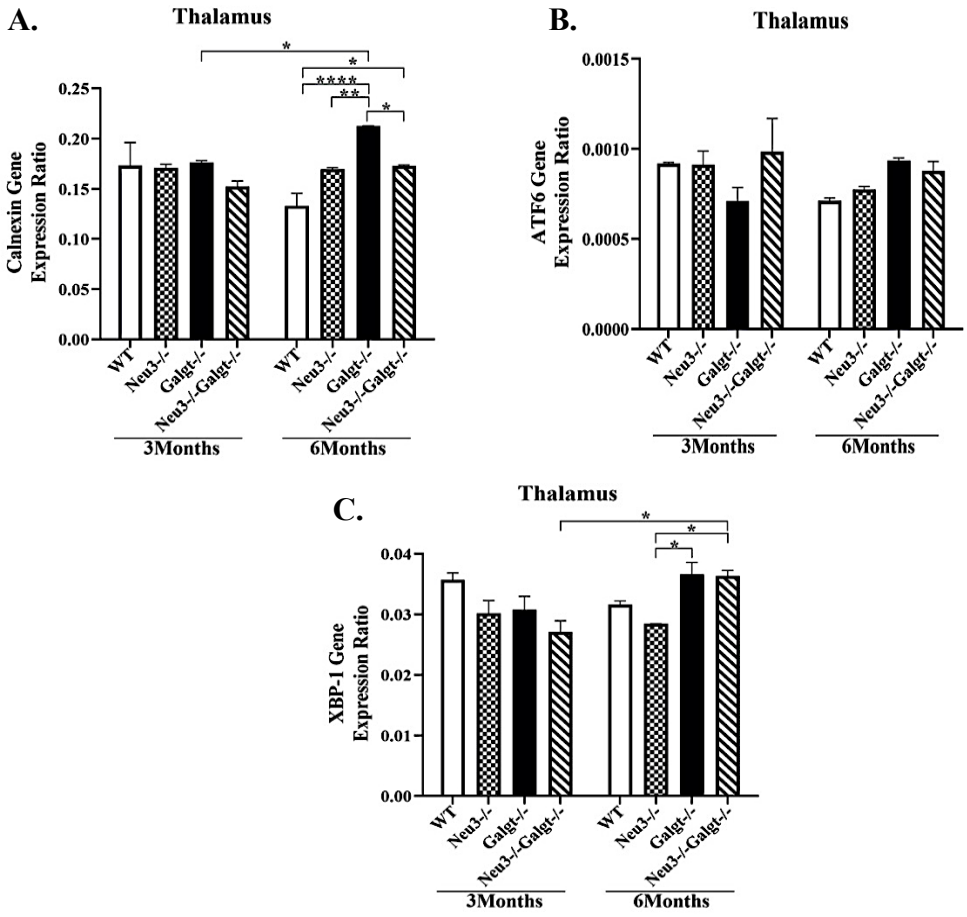

Figure 3.29. The expression levels of ER-stress markers named as Calnexin (A), ATF6 (B), and spliced XBP-1 (C) gene expression levels of thalamus tissues of 3- and 6-month-old WT, Neu3-/-, Galgt-/- and Neu3-/-Galgt-/- mice. Expression ratio calculations were performed by ΔCT method. Significant levels in the data were presented by using the two-way ANOVA (*$p<0.05$, **$p<0.01$ and ****$p<0.0001$). (n=3 for 3- and 6-month old mice)

Firstly, the ER-stress markers Calnexin (Figure 3.29 A), ATF6 (Figure 3.29 B), and spliced XBP-1 (Figure 3.29 C) were used for analyzing potential alterations in the

ER-stress mechanism in the thalamus. The expression levels of Calnexin marker (Figure 3.29 A) were indicated increased levels in Galgt-/- mice compared to WT (1.6-fold), Neu3-/- (1.3-fold), and Neu3-/-Galgt-/- (1.2-fold) littermates. The levels of Calnexin gene (Figure 3.29 A) in 6-month-old Neu3-/-Galgt-/- mice were elevated as 1.3-fold compared to WT counterparts. Moreover, the age-related increase was observed in Galgt-/- mice as 1.2-fold. According to the results of ATF6 marker (Figure 3.29 B), there were not significant changes among the genotypes but the 6-month-old Galgt-/- and Neu3-/-Galgt-/- mice showed a slight increase compared to WT mice. Finally, the expression levels of spliced XBP-1 (Figure 3.29 C) revealed an increase in 6-month-old Galgt-/- and Neu3-/-Galgt-/- mice compared to Neu3-/- mice as 1.3-fold. The age-related elevation in Neu3-/-Galgt-/- mice was observed as 1.3-fold (Figure 3.29 C). In line with the results of TTase 1 and Catalase markers, the changes in the levels of oxidative stress could not be detected significantly. The significantly elevated SOD2 levels were observed in the 6-month-old Galgt-/- mice indicating the elevation of superoxide radical that was terminally converted into oxygen and hydrogen peroxide. The removal of H_2O_2 was generated by the slightly increased levels of Catalase in especially 6-month-old Galgt-/- mice.

In addition to the analyses in ER stress mechanisms in thalamus tissue, the oxidative stress markers TTase 1 (Figure 3.30 A), SOD2 (Figure 3.30 B), and Catalase (Figure 3.30 C) were analyzed in 3- and 6-month-old WT, Neu3-/-, Galgt-/- and Neu3-/-Galgt-/- mice. In levels of TTase 1 gene (Figure 3.30 A), there were not any significant changes but the levels of TTase 1 in 6-month-old Galgt-/- and Neu3-/-Galgt-/- mice were slightly increased (Figure 3.30 A). Next, the levels of SOD2 (Figure 3.30 B) were shown to increase in 6-month-old Galgt-/- mice compared to WT and Neu3-/- as 1.3-fold. However, decrease was indicated in Neu3-/- between 3- and 6-month-old groups. Finally, the gene expression levels of ATF6 (Figure 3.30 C) were evaluated. There were only slightly increased levels for single and double deficient mice models compared to WT littermates at 6-month-old (Figure 3.30 C).

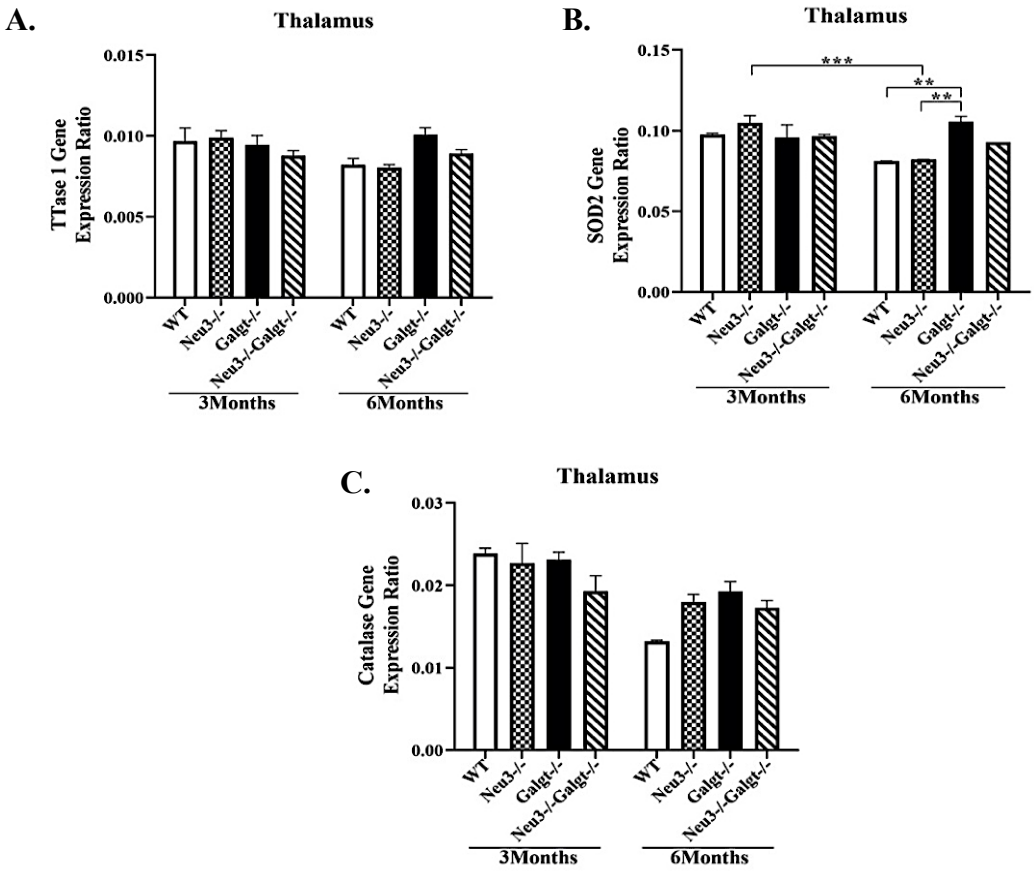

Figure 3.30. The expression levels of TTase 1 (A), SOD2 (B), and Catalase (C) in thalamus tissues of 3- and 6-month-old WT, Neu3-/-, Galgt-/- and Neu3-/-Galgt-/- mice. Expression ratio calculations were performed by ΔCT method. Significant levels in the data were presented by using the two-way ANOVA (**p<0.01 and ***p<0.001). (n=3 for 3- and 6-month old mice)

Finally, the apoptosis markers Bcl-2 (Figure 3.31 A), Bcl-XL (Figure 3.31 B), and Bax (Figure 3.31 C) were analyzed to indicate possible alterations in apoptotic mechanism in the cerebellum tissues of 3- and 6-month-old WT, Neu3-/-, Galgt-/- and Neu3-/-Galgt-/- mice. The results were evaluated and showed that the levels of Bcl-2 (Figure 3.31 A), Bcl-XL (Figure 3.31 B), and Bax (Figure 3.31 C) were not changed significantly. However, the levels of Bax marker were slightly increased in 6-month-old Neu3-/-, Galgt-/-, and Neu3-/-Galgt-/- compared to WT littermates (Figure 3.31 C). The RT-PCR analysis of apoptotic markers were not conclusive in thalamus tissue so further studies were performed to understand whether apoptosis existed in this region or not.

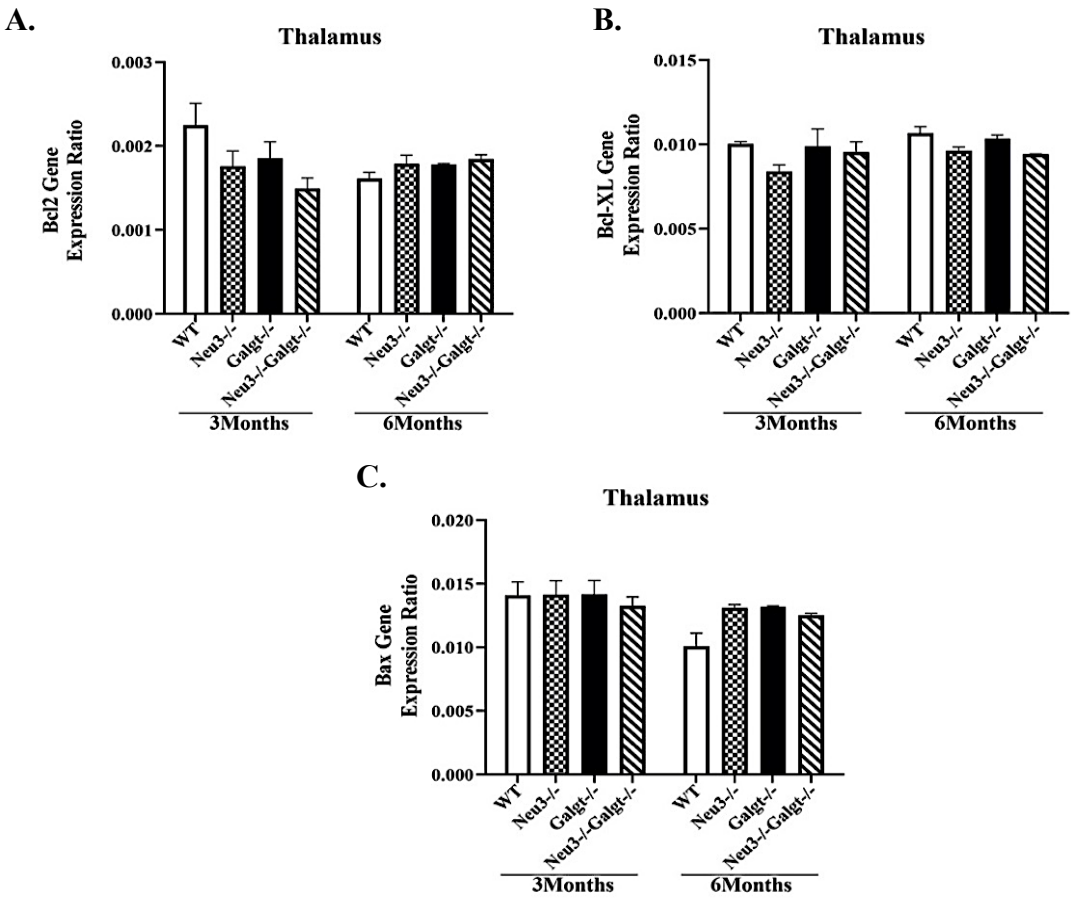

Figure 3.31. The expression levels of Bcl2 (A), Bcl-XL (B), and Bax (C) in thalamus tissues of 3- and 6-month-old WT, Neu3-/-, Galgt-/- and Neu3-/-Galgt-/- mice. Expression ratio calculations were performed by ΔCT method. Significant levels in the data were presented by using the two-way ANOVA. (n=3 for 3- and 6-month old mice)

3.6.3. Western Blot Analyses

Western blot analyses were generated in thalamus tissue of 3- and 6-month-old WT, Neu3-/-, Galgt-/-, and Neu3-/-Galgt-/- mice, as well. The investigation of the effects of single- or double-deficiencies of Neu3 and Galgt enzymes in apoptosis in thalamus tissue were analyzed by using BiP (Figure 3.32), Caspase 9 (Figure 3.33), Caspase 3 (Figure 3.34), and Fas-Ligand (Figure 3.35) antibodies.

According to the results of BiP antibody (Figure 3.32 A), it was assessed that 1.4-fold and 1.5-fold increased levels in 3-month-old Galgt-/- mice compared to WT and Neu3-/-Galgt-/- mice were indicated, respectively. Although it was not significant, the

levels in 6-month-old Galgt-/- mice were also higher compared to WT and Neu3-/-Galgt-/- counterparts. The levels of Neu3-/- were slightly elevated compared to Neu3-/-Galgt-/- littermates for both age groups (Figure 3.32 B).

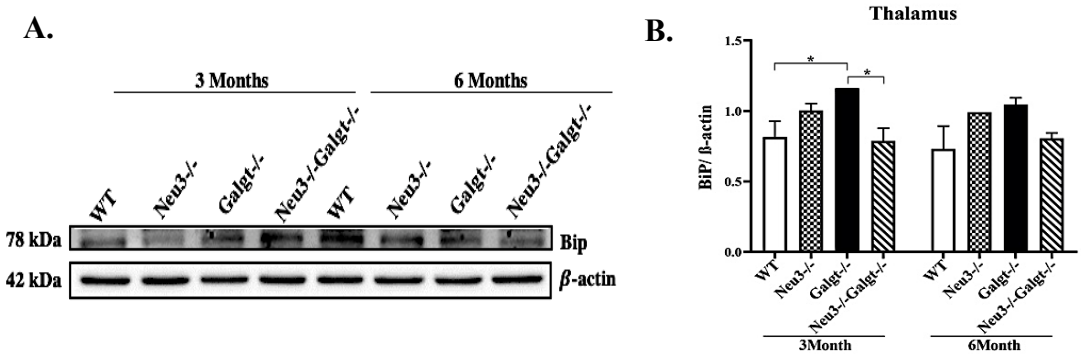

Figure 3.32. Western Blot image of Bip antibody in the thalamus region of 3- and 6-month-old WT, Neu3-/-, Galgt-/-, and Neu3-/-Galgt-/- mice (A). β-actin was used as the internal control. The graph (B) shows the ratio of the band intensity of BiP antibody to the band intensity of β-actin. Significant levels in the data were presented by using the two-way ANOVA (*p<0.05). (n=3 for 3- and 6-month old mice)

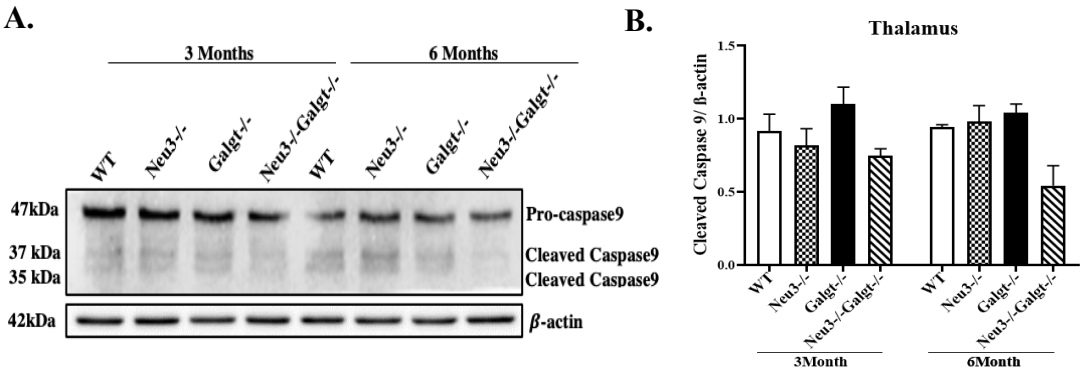

Figure 3.33. Western Blot image of Caspase9 antibody in the thalamus region of 3- and 6-month-old WT, Neu3-/-, Galgt-/-, and Neu3-/-Galgt-/- mice (A). β-actin was used as the internal control. The graph (B) shows the ratio of the band intensity of Cleaved Caspase9 antibody to the band intensity of β-actin. Significant levels in the data were presented by using the two-way ANOVA. (n=3 for 3- and 6-month old mice)

The levels of initiator Caspase 9 of apoptosis were also assessed in thalamus. According to the results of the antibody (Figure 3.33 A), there was a slight increase in the

Galgt-/- mice compared to other genotypes at 3-month-old age. Additionally, there were slightly increased levels in 6-month-old Galgt-/- mice compared to Neu3-/-Galgt-/- counterparts (Figure 3.33 B). The age-dependent increase was detected in Neu3-/- mice in a slight manner (Figure 3.33 B).

Later, executioner Caspase 3 of apoptosis in cleaved form from Pro Caspase was evaluated in thalamus, as well. According to results of the antibody (Figure 3.34 A), there was an apparent increase (1.7-fold) in the Galgt-/- mice compared to WT mice. Moreover, 3-month-old Galgt-/- mice indicated 1.7-fold increase compared to Neu3-/-Galgt-/-. There were significantly decreased levels in 6-month-old Galgt-/- compared to 3-month-old Galgt-/- mice as 3.7-fold. 6-month-old Galgt-/- mice compared to WT counterpart (2.7-fold) indicated a decreased level of Cleaved caspase 3. Although it was not significant, the levels in Neu3-/-Galgt-/- compared to Galgt-/- increased in 6-month-old of age (Figure 3.34 B).

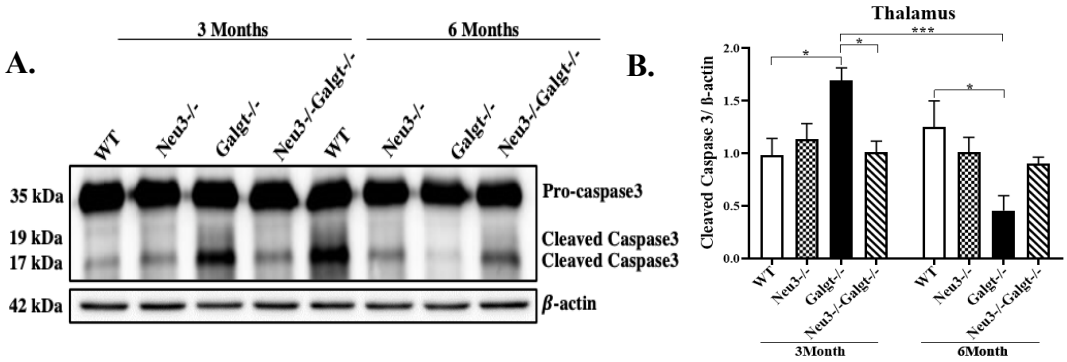

Figure 3.34. Western Blot image of Caspase 3 antibody in the thalamus region of 3- and 6-month-old WT, Neu3-/-, Galgt-/-, and Neu3-/-Galgt-/- mice (A). β-actin was used as the internal control. The graph (B) shows the ratio of the band intensity of Cleaved Caspase3 antibody to the band intensity of β-actin. Significant levels in the data were presented by using the two-way ANOVA (*$p<0.05$ and ***$p<0.001$). (n=3 for 3- and 6-month old mice)

Finally, extrinsic apoptotic pathway marker called Fas-Ligand was also evaluated. In the western blot results of this antibody (Figure 3.35 A), there was no apparent or slight changes were detected (Figure 3.35 B). Moreover, there were no any other age-dependent changes among the genotypes (Figure 3.35 B).

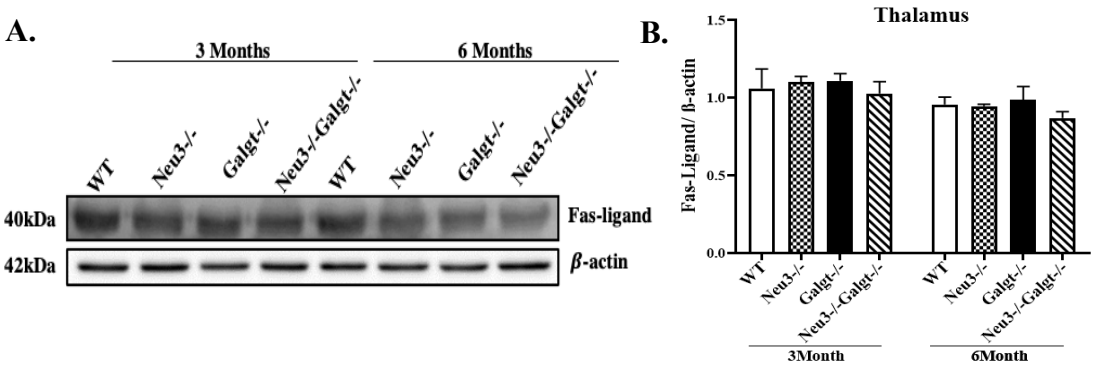

Figure 3.35. Western Blot image of Fas-Ligand antibody in the thalamus region of 3- and 6-month-old WT, Neu3-/-, Galgt-/-, and Neu3-/-Galgt-/- mice (A). β-actin was used as the internal control. The graph (B) shows the ratio of the band intensity of Fas-Ligand antibody to the band intensity of β-actin. Significant levels in the data were presented by using the two-way ANOVA. (n=3 for 3- and 6-month old mice)

3.7. TUNEL Assay

In order to investigate how apoptosis mechanism is altered in the single or double absence of Neu3 and Galgt enzymes, Terminal deoxynucleotidyl transferase (TdT) dUTP nick-end labeling abbreviated as TUNEL assay (DeadEnd™ Fluorometric TUNEL System) were performed. In the instructions given by the manufacturer of the TUNEL assay kit, the apoptotic cells were detected by labelling the free 3'OH ends at the DNA break regions by enzymatic addition of modified nucleotides. Then, through presence of DNA fragments in cells, the DNA strand breaks as either single or double could possibly be detected. The analyses were performed in 6-month-old WT, Neu3-/-, Galgt-/- and Neu3-/-Galgt-/- mice (Figure 3.36 and 3.37). The result of TUNEL staining for cortex (Figure 3.36 A), cerebellum (Figure 3.36 B), thalamus (Figure 3.37 A), and hippocampus (Figure 3.37 B) showed that the apoptotic cells were appeared in green while red nucleus were visible via Propidium Iodide. Green signals were correlated with the existence of apoptotic nuclei. When the merge images of green colored apoptotic cells and red stained nuclei were analyzed in 6-month-old WT, Neu3-/-, Galgt-/- and Neu3-/-Galgt-/- mice, the levels of the yellow colored TUNEL positive cells could be investigated.

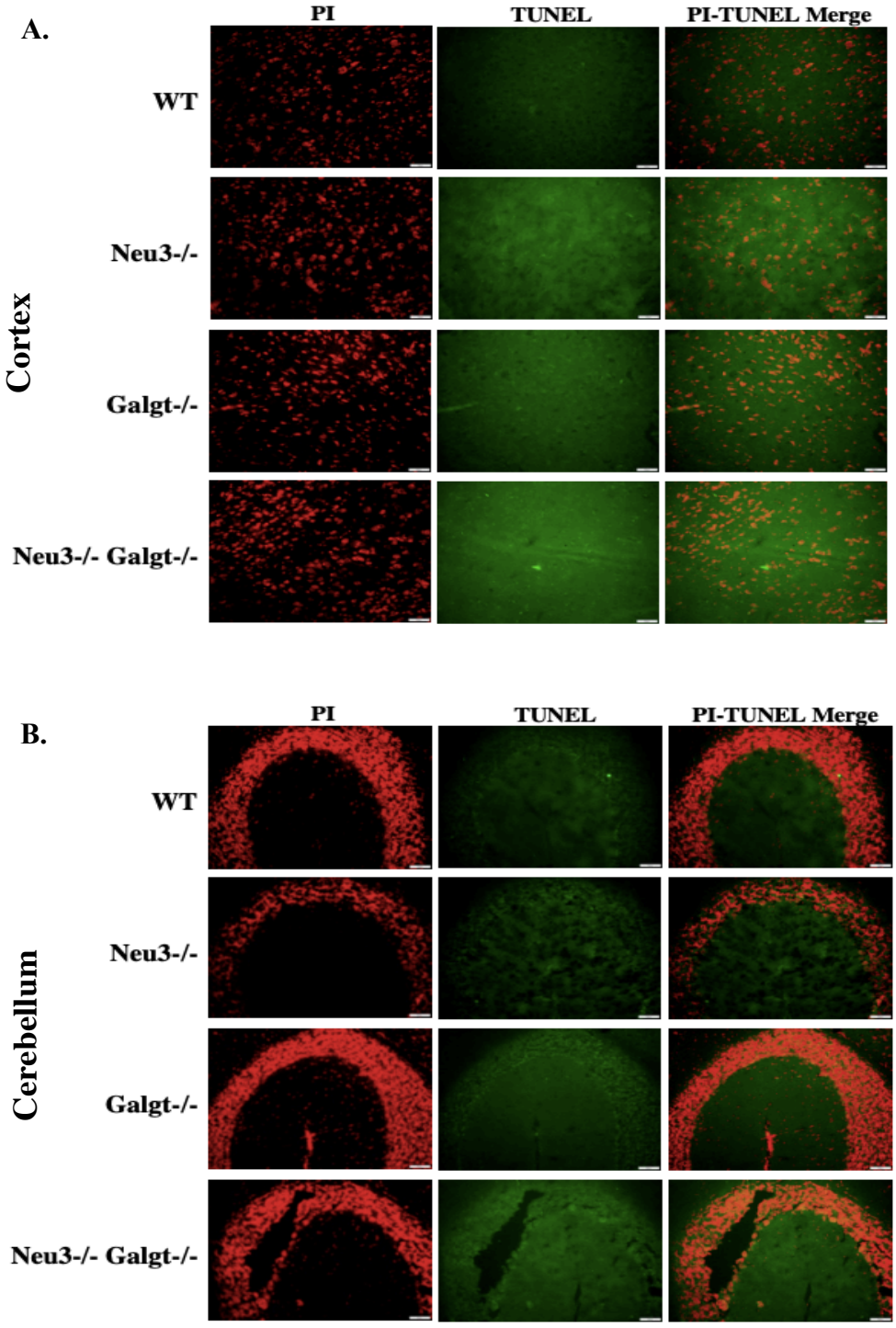

Figure 3.36. TUNEL assay for cortex (A) and cerebellum (B) regions of 6-month-old WT, Neu3-/-, Galgt-/- and Neu3-/-Galgt-/- mice. The 20μm coronal sections were stained in green (TUNEL) while nuclei were in red by Propidium iodide (PI). In merges, yellow TUNEL positive cells were visualized. They were quantified by NIH Image J program and normalized to WT for cortex (C) and cerebellum (D). Data is representative of mean ± SEM of measurements. Significant levels in the data were presented by using the one-way ANOVA (**p<0.025, ***p<0.001, and ****p<0.0001). (n=3 for 6-month old mice)

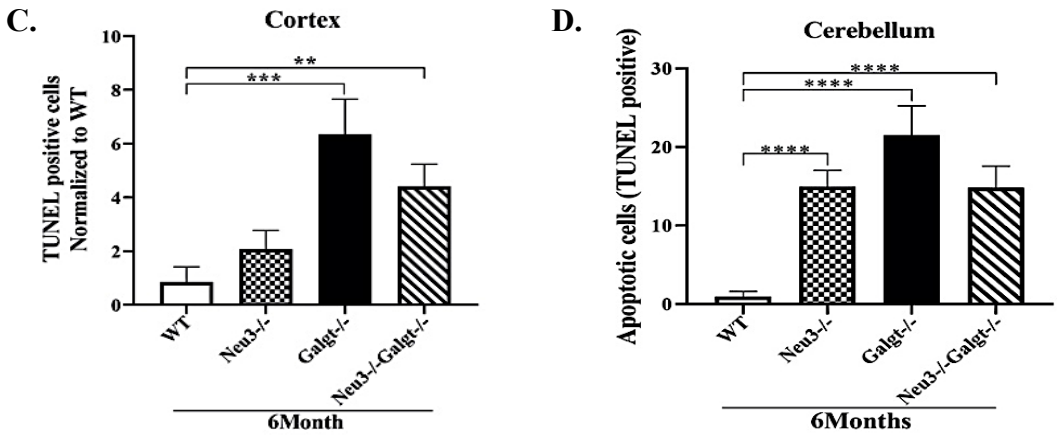

Figure 3.36 (cont.)

According to colocalization analyses, Galgt-/- mice had significantly higher levels of TUNEL positive cells in cortex (Figure 3.36 C) and cerebellum (Figure 3.36 D) in contrast to WT (7.4-fold) and Neu3-/- mice (3.2-fold). The levels of TUNEL positive cells were increased as 5.1-fold in Neu3-/-Galgt-/- mice compared to WT in cortex (Figure 3.36 C). Moreover, 15.0-fold increased apoptotic nuclei were shown in Neu3-/- mice compared to WT in cerebellum (Figure 3.36 D) whereas TUNEL positive cells were elevated in Neu3-/-Galgt-/- mice as 14.8-fold of the levels in WT mice. Moreover, the levels in Galgt-/- were also elevated in 21.5-fold compared to WT levels in cerebellum region (Figure 3.36 D).Evaluation of TUNEL positive cells in thalamus (Figure 3.37 C) and hippocampus (Figure 3.37 D) regions revealed that the levels were significantly increased (10.8-fold, and 3.3-fold, respectively) in Neu3-/- mice compared to WT mice. The levels in Galgt-/- mice were also elevated in thalamus as 12.7-fold and 2.3-fold (Figure 3.37 C) compared to WT and Neu3-/-Galgt-/- mice, respectively. Additionally, 3.9-fold increase in hippocampus of Galgt-/- mice (Figure 3.37 D) compared to WT mice was shown. Neu3-/-Galgt-/- mice showed the increased TUNEL positive cells in both thalamus (5.4-fold) and hippocampus (3.1-fold) regions compared to WT littermates (Figure 3.37 C and D, respectively).

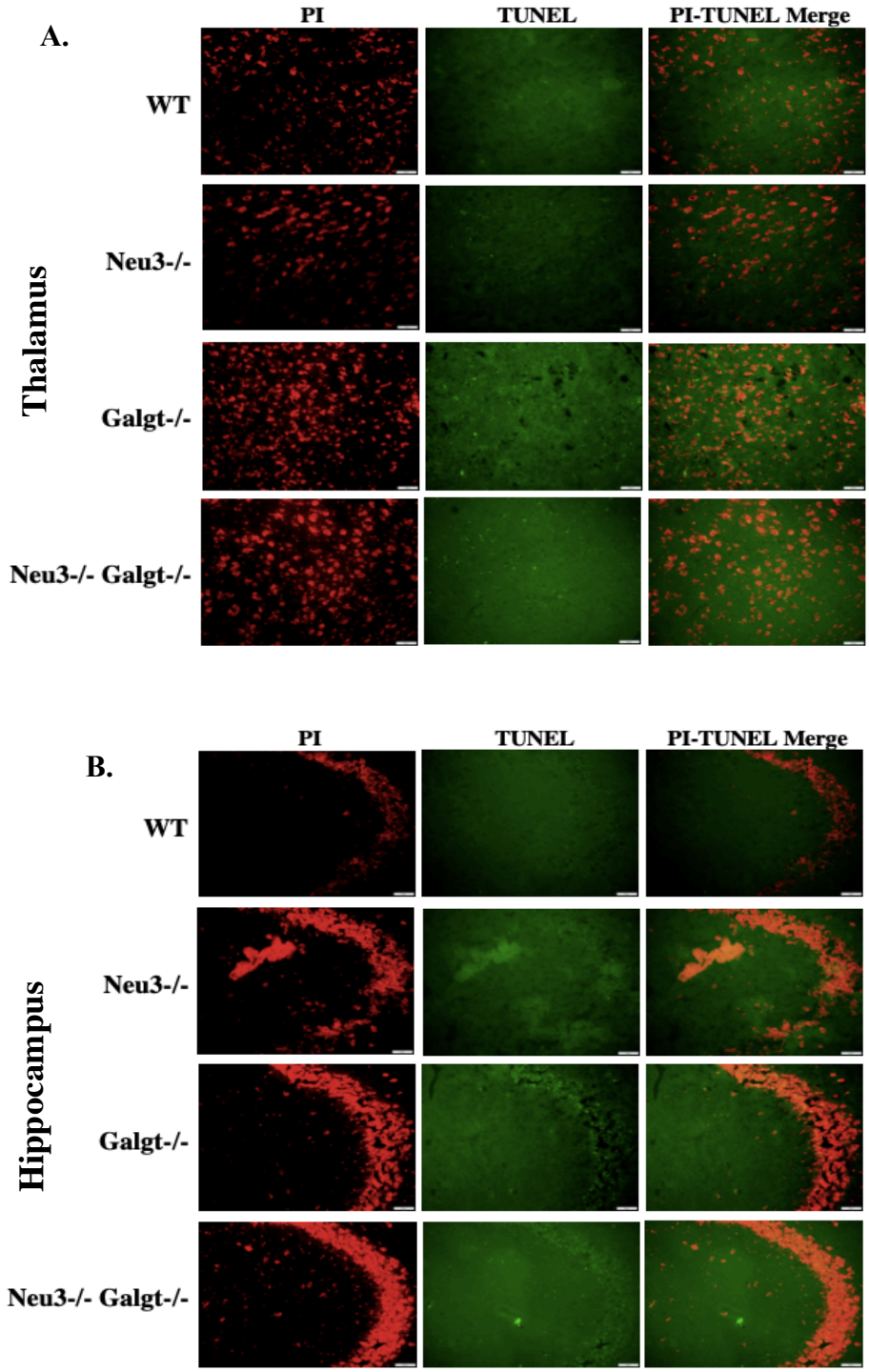

Figure 3.37. TUNEL assay for thalamus (A) and hippocampus (B) regions of 6-month-old WT, Neu3-/-, Galgt-/- and Neu3-/-Galgt-/- mice. The 20μm coronal sections were stained in green (TUNEL) while nuclei were in red by Propidium iodide (PI). In merges, yellow TUNEL positive cells were visualized. They were quantified by NIH Image J program and normalized to WT for thalamus (C) and hippocampus (D). Data is representative of mean ± SEM of measurements. Significant levels in the data were presented by using the one-way ANOVA (*$p<0.05$ and **$p<0.025$). (n=3 6-month old mice)

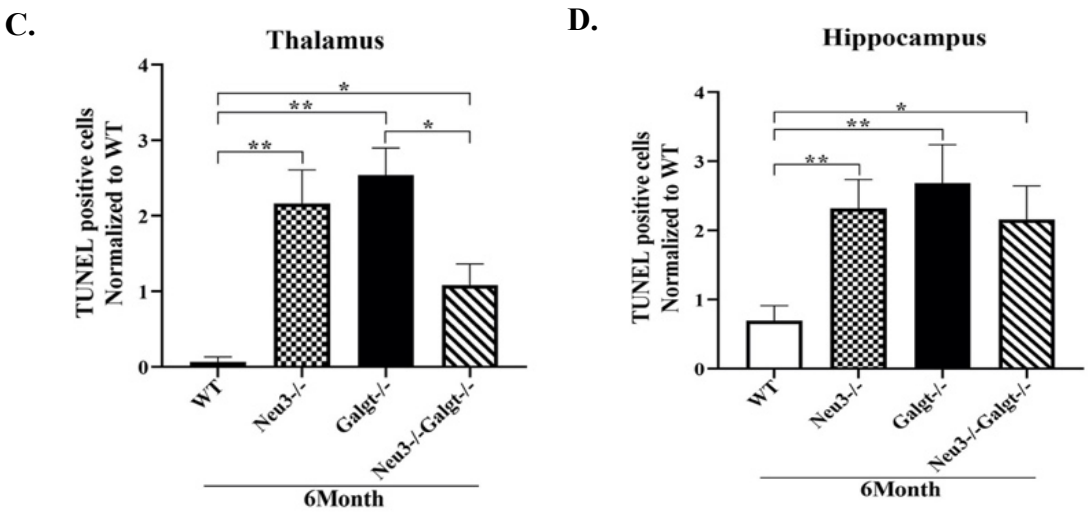

Figure 3.37 (cont.)

3.8. Histopathology Analyses

The coronal sections from fixed brains of 6-month-old WT, Neu3-/-, Galgt-/-, and Neu3-/-Galgt-/- mice were subjected to histopathological analyses by using s such as Cresyl Echt Violet, Hematoxylin-Eosin, Periodic acid-Schiff, and Luxol Fast Blue.

3.8.1. Cresyl Echt Violet Staining

The Cresyl Echt Violet staining was performed to investigate the nerve cell morphology and number. By acting on the Nissl substance in nerve cells and their nuclei, the dye made apparent the neurons in the coronal brain slices. According to results of Cresyl Echt Violet staining performed on 6-month-old cortex (Figure 3.38 A, B, C, and D), hippocampus (Figure 3.38 E, F, G, and H), thalamus (Figure 3.38 I, J, K, and L), and cerebellum (Figure 3.38 M, N, O, and P) of WT, Neu3-/-, Galgt-/-, and Neu3-/-Galgt-/- mice, there were not degenerating neurons or abnormal distribution of Nissl substance in WT mice while Galgt-/- and Neu3-/-Galgt-/- mice in the cortex tissue were shown to decrease in neuron number compared to WT and Neu3-/- littermates. The cortex tissue of Galgt-/- and Neu3-/-Galgt-/- mice indicated karyolysis, unevenly distributed Nissl substance, and degenerating neurons compared to Neu3-/- and WT littermates (Figure 3.38 C and D, respectively). In hippocampus, thalamus, and cerebellum regions, the

degenerating neurons and karyolysis were detected in Galgt-/- and Neu3-/-Galgt-/- mice compared to WT littermates (Figure 3.38 G, H, K, L, O, and P, respectively).

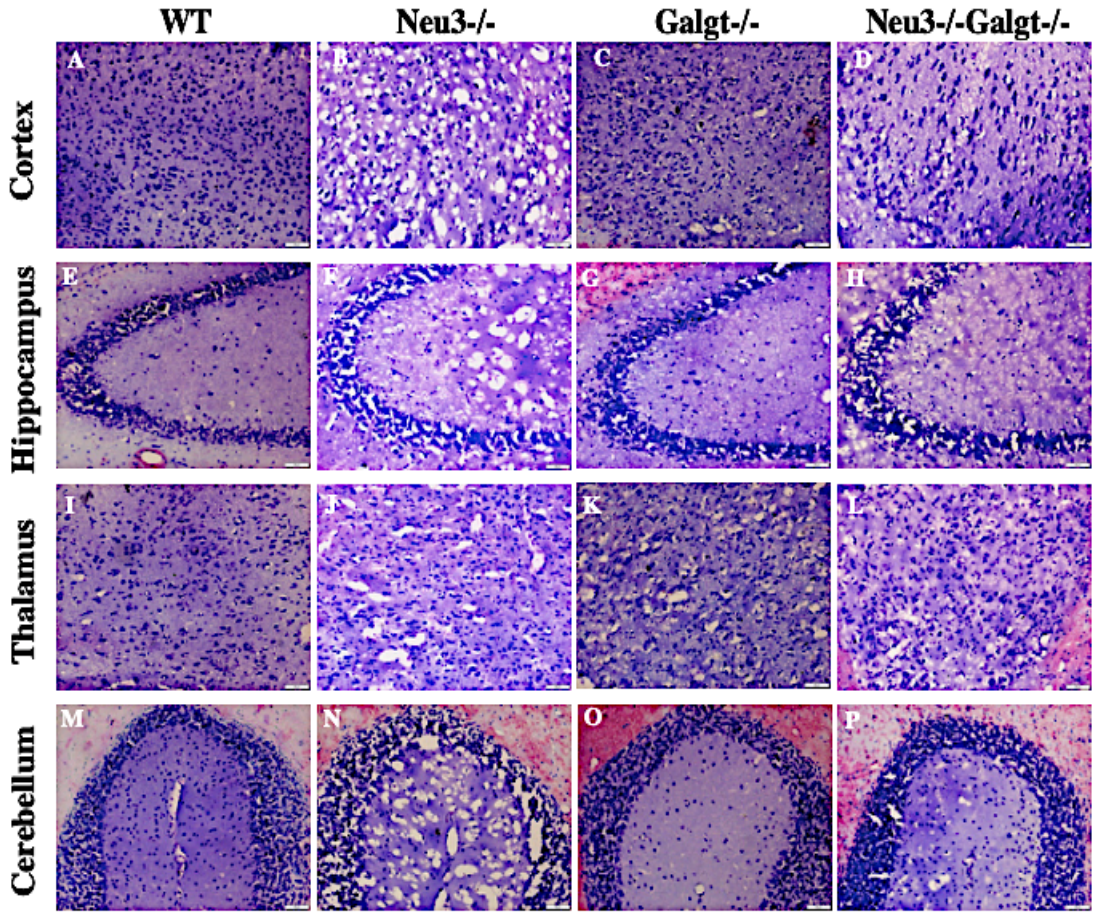

Figure 3.38. Cresyl Echt Violet staining n the cortex (A, B, C, and D), hippocampus (E, F, G, and H), thalamus (I, J, K, and L), and cerebellum (M, N, O, and P) regions of 6-month-old WT, Neu3-/-, Galgt-/- and Neu3-/-Galgt-/- mice. 20x images were taken with the Olympus Light Microscope. (n=3 for 6-month old mice)

3.8.2. Hematoxylin-Eosin Staining

The Hematoxylin-Eosin staining was performed to understand the nerve cell morphology in the cortex (Figure 3.39 A, B, C, and D), hippocampus (Figure 3.39 E, F, G, and H), thalamus (Figure 3.39 I, J, K, and L), and cerebellum (Figure 3.39 M, N, O, and P) of 6-month-old WT, Neu3-/-, Galgt-/-, Neu3-/-Galgt-/- mice.

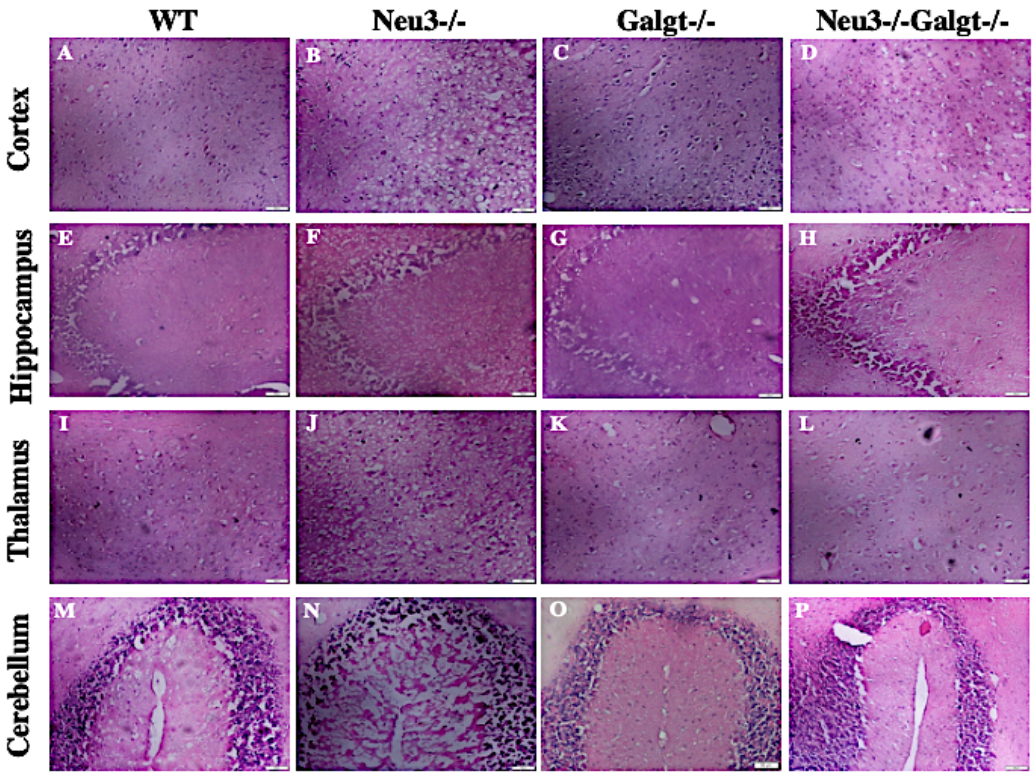

Figure 3.39. Hematoxylin-Eosin staining in the cortex (A, B, C, and D), hippocampus (E, F, G, and H), thalamus (I, J, K, and L), and cerebellum (M, N, O, and P) of 6-month-old WT, Neu3-/-, Galgt-/- and Neu3-/-Galgt-/- mice. 20x images were taken with the Olympus Light Microscope. (n=3 for 6-month old mice)

In the WT mice, the cortex, hippocampus, thalamus, and cerebellum regions were shown to be normal (Figure 3.39 A, E, I, and M) in terms of normal nerve cell structure and evenly distributed Purkinje cell layers. However, higher levels of blood vessel dilation, edema, degenerating neurons and glial cells were detected in Galgt-/- and Neu3-/-Galgt-/- mice compared to Neu3-/- counterparts (Figure 3.39 C, G, K, and O; Figure 3.39 D, H, L, and P, respectively). In hippocampus of Galgt-/- and Neu3-/-Galgt-/- mice, there were apparent karyolysis, and neuronal degeneration. Moreover, presence of edema was indicated in this region and the thalamus of Galgt-/- and Neu3-/-Galgt-/- mice (Figure 3.39 G and H; Figure 3.39 K and L, respectively). The Neu3-/- mice hippocampus region was not as altered as Galgt-/- and Neu3-/-Galgt-/- mice but there were small amounts of edema and decrease in neuron number in this region (Figure 3.39 F). In the cerebellum of Neu3-/- mice (Figure 3.39 M), less degeneration in Purkinje cell layer was revealed compared to intensively occurring edema and loss in Galgt-/- and Neu3-/-Galgt-/- mice (Figure 3.39 O and P, respectively).

3.8.3. Periodic Acid-Schiff Staining

The Periodic acid-Schiff (PAS) staining was generated for the cortex, hippocampus, thalamus, and cerebellum regions of 6-month-old WT, Neu3-/-, Galgt-/- and Neu3-/-Galgt-/- in order to investigate the accumulation or presence of glycolipids, glycoproteins, or mucins in higher levels. In the WT mice, there was not the presence of glycosphingolipid accumulation in any of those brain regions. In the Galgt-/-and Neu3-/-Galgt-/- mice, the glycosphingolipid accumulating cells were more apparent than Neu3-/- mice in the cortex (Figure 3.40 C and D; Figure 3.40 G and H; Figure 3.40 K and L; Figure 3.40 O and P). The accumulating G_{D3} and G_{M3} were detected in Galgt-/- and Neu3-/-Galgt-/- mice models.

3.8.4. Luxol Fast Blue Staining

In order for evaluating the possible alterations in the myelin contents of cortex, hippocampus, and thalamus regions of and 6-month-old WT, Neu3-/-, Galgt-/- and Neu3-/-Galgt-/-, the Luxol Fast Blue Staining was done. In the results, there were not any loss of myelin content of WT and Neu3-/- mice groups in 3- and 6-month-old in cortex (Figure 3.41 A and B), hippocampus (Figure 3.41 E and F), and thalamus (Figure 3.41 I and J) regions. The higher levels of myelin loss were observed in Galgt-/- and Neu3-/-Galgt-/- mice in the cortex (Figure 3.41 C and D), hippocampus (Figure 3.41 G and H), thalamus (Figure 3.41 K and L). In order to further understand those changes in myelin content, the anti-CNPase antibody staining was also performed.

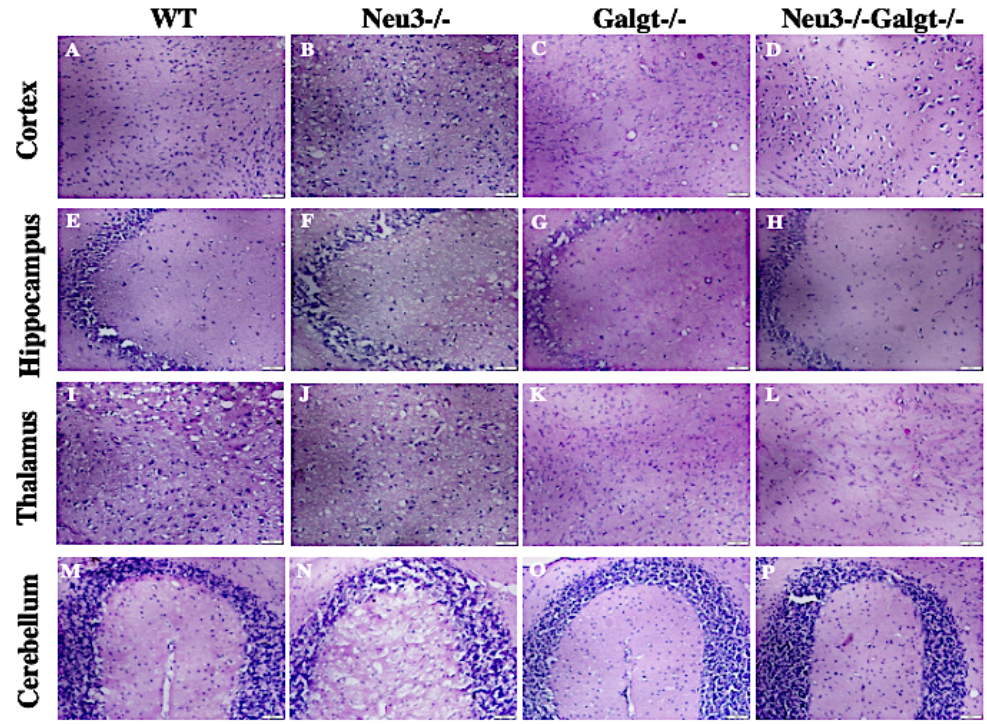

Figure 3.40. Periodic acid-Schiff staining in the in the cortex (A, B, C, and D), hippocampus (E, F, G, and H), thalamus (I, J, K, and L), and cerebellum (M, N, O, and P) regions of 6-month-old WT, Neu3-/-, Galgt-/- and Neu3-/-Galgt-/- mice. 20x images were taken with the Olympus Light Microscope. (n=3 for 6-month old mice)

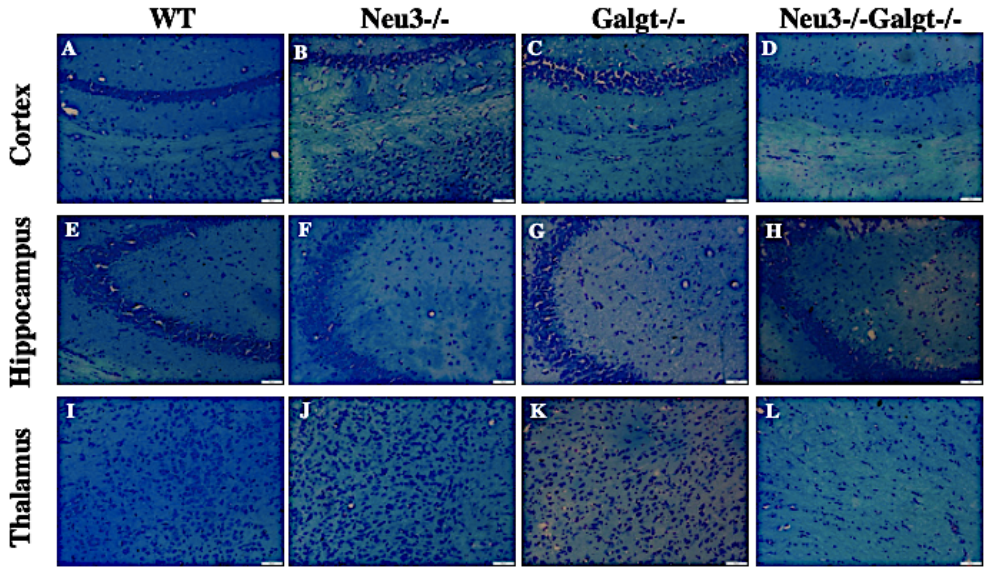

Figure 3.41. Luxol Fast Blue staining in the cortex (A, B, C, and D), hippocampus (E, F, G, and H), and thalamus (I, J, K, and L) regions of 6-month-old WT, Neu3-/-, Galgt-/- and Neu3-/-Galgt-/- mice. 20x images were taken with the Olympus Light Microscope. (n=3 for 6-month old mice)

3.9. Neuronal Staining for Neuron Number Analyses

To evaluate the alterations in neuron number in single- or double-deficiency of *Neu3* and *Galgt*, Anti-NeuN immuno-staining was performed in four brain regions as cortex (Figure 3.42 A, B, C, and D), hippocampus (Figure 3.42 E, F, G, and H), thalamus (Figure 3.42 I, J, K, and L), and cerebellum (Figure 3.42 M, N, O, and P) of 3-month-old WT, Neu3-/-, Galgt-/-, and Neu3-/-Galgt-/- mice. In the cortex region of 3-month-old group, there were 46%, 41%, and 39% reduction in the neuron number of Neu3-/-Galgt-/- mice (Figure 3.42 R) compared to WT, Neu3-/-, and Galgt-/- mice, respectively. However, in the hippocampus of the 3-month-old group (Figure 3.42 S), there were not any alterations. For the thalamus region, the neuron number in Galgt-/- mice (Figure 3.42 T) was reduced (36%) in contrast to its WT counterpart. Finally, the cerebellum regions of 3-month-old mice were compared to show reduced neuron number in Galgt-/- mice (Figure 3.42 U) as 37%, 38%, and 27% compared to WT, Neu3-/-, and Neu3-/-Galgt-/- mice, respectively.

Secondly, anti-NeuN immuno-staining was performed in cortex (Figure 3.43 A, B, C, and D), hippocampus (Figure 3.43 E, F, G, and H), thalamus (Figure 3.43 I, J, K, and L), and cerebellum (Figure 3.43 M, N, O, and P) of 6-month-old WT, Neu3-/-, Galgt-/-, and Neu3-/-Galgt-/- mice. The 48%, 45%, and 36% neuron loss were identified in cortex of Galgt-/- mice (Figure 3.43 R) compared with WT, Neu3-/-, and Neu3-/-Galgt-/-, respectively. Additionally, the neuronal loss as 19% in double deficient mice in cortex compared to its WT counterpart was detected. In hippocampus (Figure 3.43 S) of Galgt-/- mice, there were significant reductions in neuron number compared to WT, Neu3-/-, and Neu3-/-Galgt-/- mice as 48%, 33%, and 36%, respectively. In thalamus (Figure 3.43 T) of Neu3-/- (60%), Galgt-/- (36%), and Neu3-/-Galgt-/- (34%) mice, there were significantly reduced levels of nerve cells compared to the age-matched WT mice. The 36% neuronal loss was also investigated between Neu3-/- and Galgt-/- mice in the thalamus region (Figure 3.43 T). Finally, cerebellum region (Figure 3.43 U) was quantified for the alterations in neuron number that there was 51% and 33% neuronal loss in Neu3-/-Galgt-/- mice compared to WT and Neu3-/- mice, respectively. Reduction in neuron number in cerebellum of Neu3-/- and Galgt-/- mice compared to WT was 17% and 38% was shown, respectively (Figure 3.43 T).

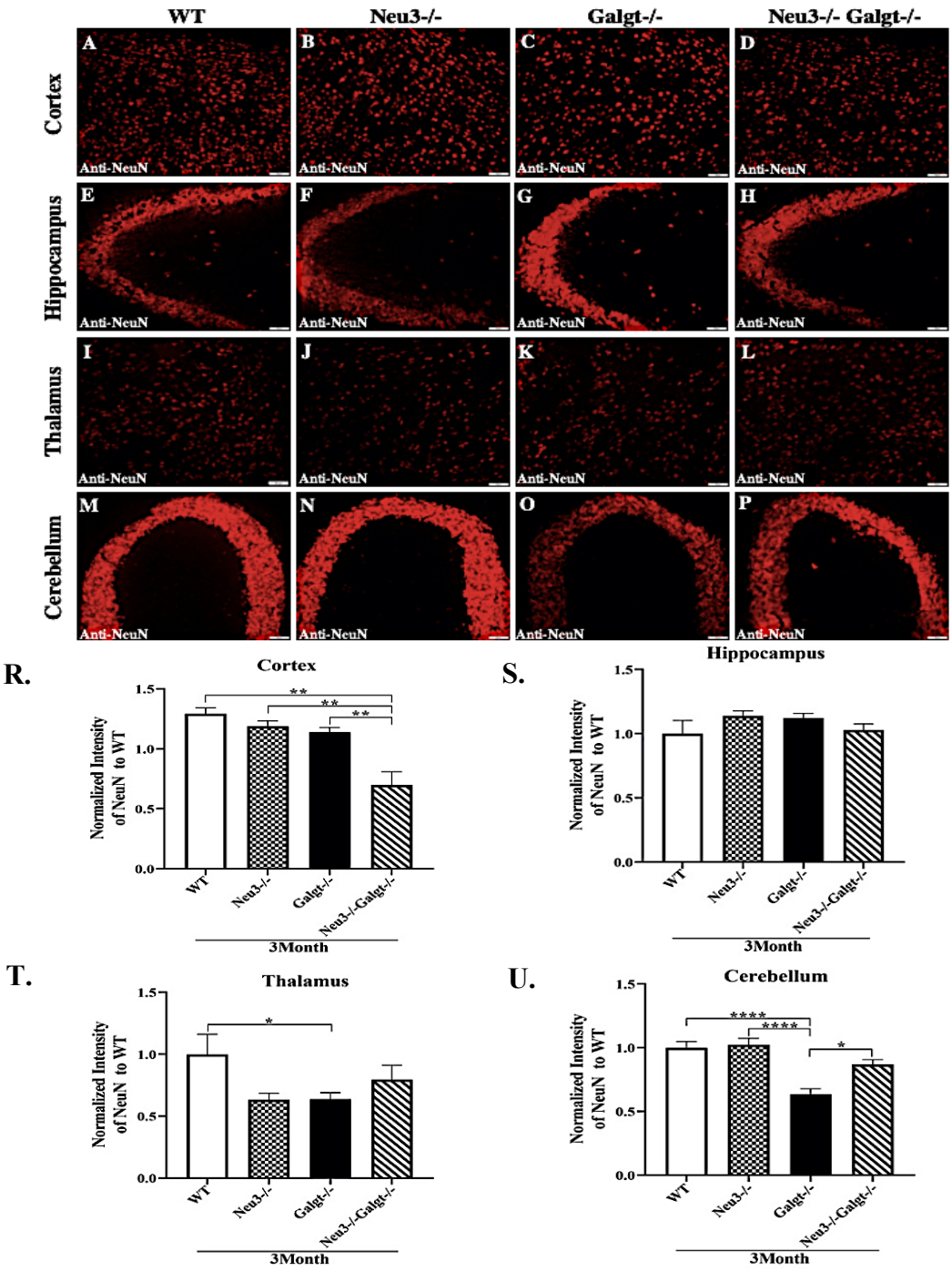

Figure 3.42. Anti-NeuN staining for cortex (A, B, C, and D), hippocampus (E, F, G, and H), thalamus (I, J, K, and L), and cerebellum (M, N, O, and P) of 3-month-old WT, Neu3-/-, Galgt-/- and Neu3-/-Galgt-/- mice. 20μm coronal sections were stained in red by Anti-NeuN antibody. Density analyses by NIH Image J program and normalized to WT for cortex (R), hippocampus (S), thalamus (T), and cerebellum (U) were shown. Scale bar indicates 50μm of cortex, hippocampus, thalamus, and cerebellum. Data is representative of mean ± SEM of measurements. Significant levels in the data were presented by the one-way ANOVA (*p<0.05, **p<0.025, and ****p<0.0001). (n=3 for 3-month old mice)

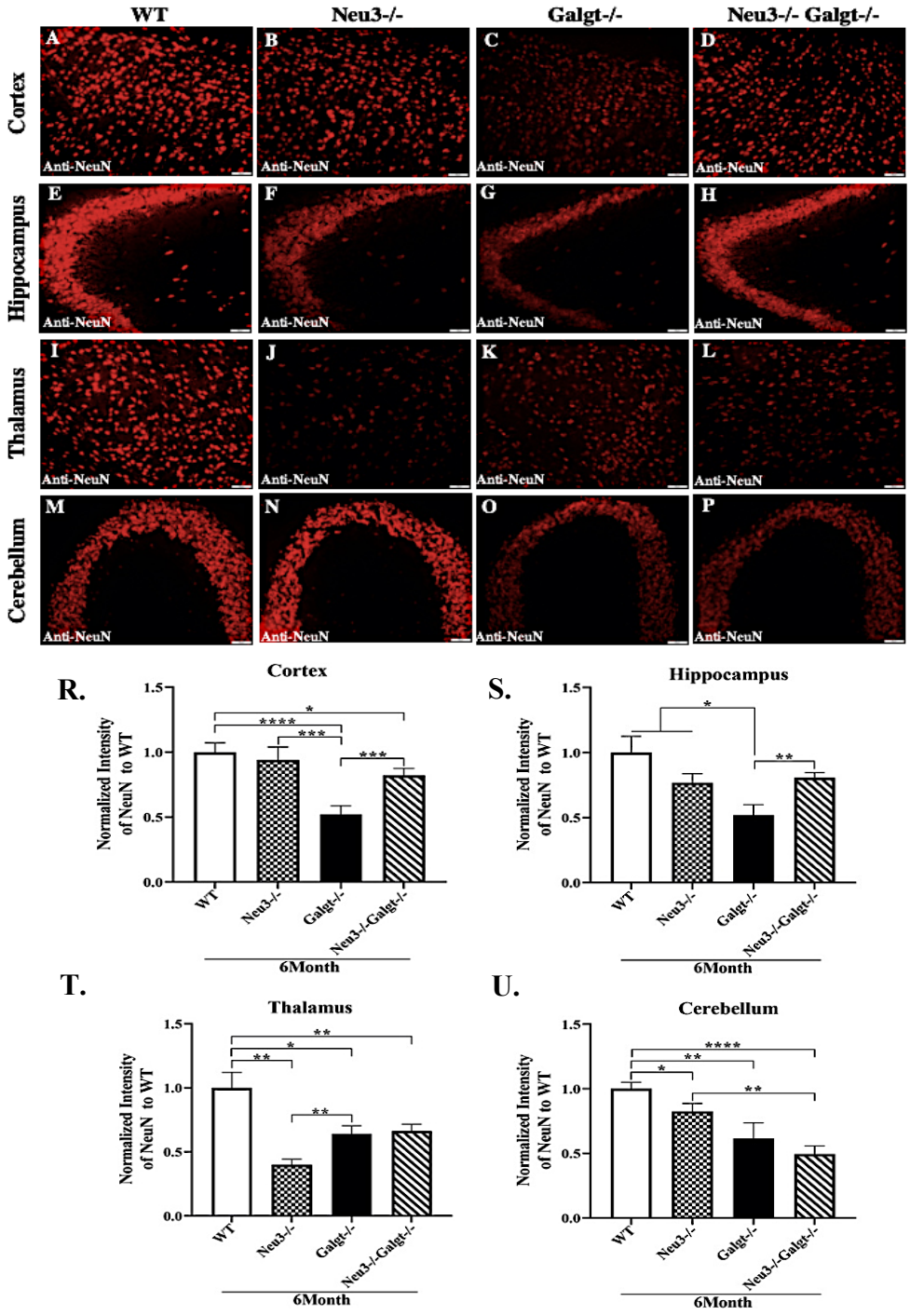

Figure 3.43. Anti-NeuN staining for cortex (A, B, C, and D), hippocampus (E, F, G, and H), thalamus (I, J, K, and L), and cerebellum (M, N, O, and P) of 6-month-old WT, Neu3-/-, Galgt-/- and Neu3-/-Galgt-/- mice. 20μm coronal sections were stained in red by Anti-NeuN antibody. Neuronal density analyses performed by NIH Image J program and normalized to WT for cortex (R), hippocampus (S), thalamus (T), and cerebellum (U) were shown. Scale bar indicates 50μm of cortex, hippocampus, thalamus, and cerebellum. Data is representative of mean ± SEM of measurements. Significant levels in the data were presented by the one-way ANOVA (*p<0.05, **p<0.025, ***p<0.001 and ****p<0.0001). (n=3 for 6-month old mice)

3.10. Oligodendrocyte Analyses

In oligodendrocyte analyses, cortex (Figure 3.44 A and 3.44 C), thalamus (Figure 3.44 B and 3.44 D), cerebellum (Figure 3.45 A and 3.45 C), and pons (Figure 3.45 B and 3.45 D) of 3-month-old WT, Neu3-/-, Galgt-/-, and Neu3-/-Galgt-/- mice were stained with Anti-CNPase antibody. Since this antibody specifically stains oligodendrocytes -a type of glial cells for myelin formation, the green stained regions were detected as oligodendrocyte areas.

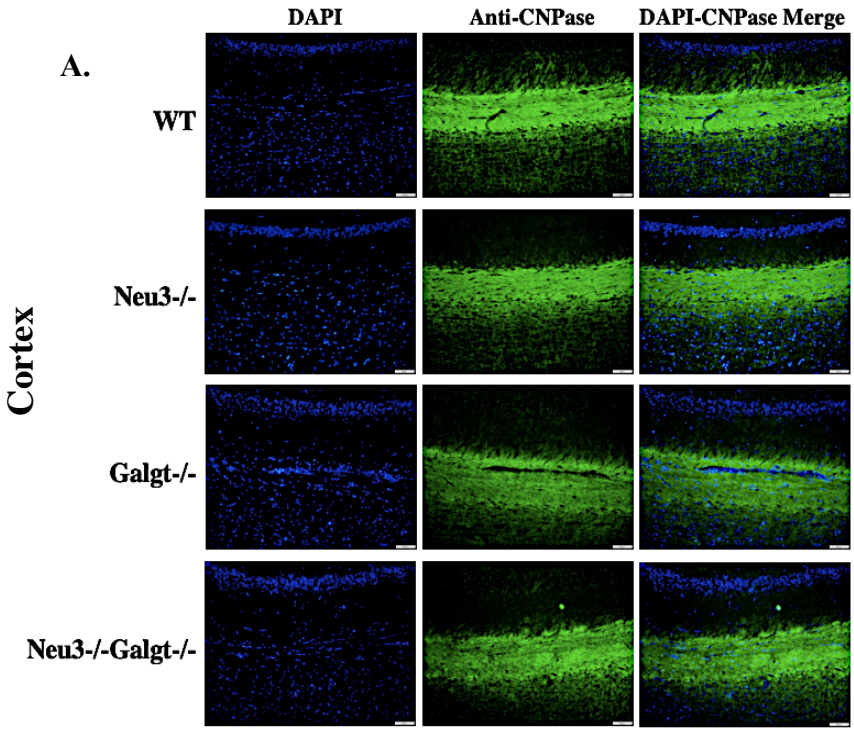

Figure 3.44. Anti-CNPase staining for cortex (A) and thalamus (C) regions of 3-month-old WT, Neu3-/-, Galgt-/- and Neu3-/-Galgt-/- mice for oligodendrocyte detection. The 20μm coronal sections were stained in green by Anti-CNPase antibody (oligodendrocyte marker) and in blue by DAPI (nucleus). Oligodendrocyte intensity analyses performed by NIH Image J program and normalized to WT for cortex (B), and thalamus (D) were shown. Scale bar indicates 50μm of cortex, and thalamus. Data is representative of mean ± SEM of measurements. Significant levels in the data were presented by using the one-way ANOVA (*$p<0.05$ and **$p<0.025$). (n=3 for 3-month old mice)

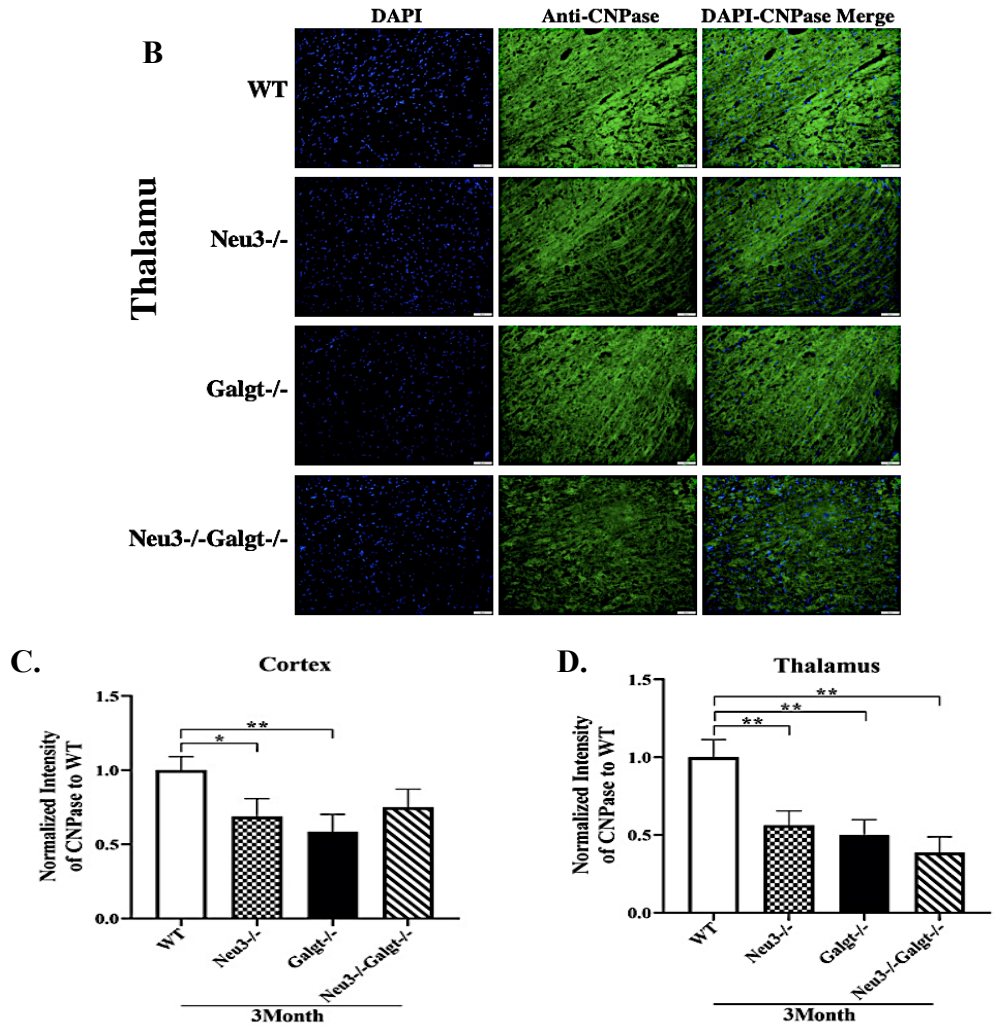

Figure 3.44 (cont.)

First of all, the levels of CNPase were shown in the cortex (Figure 3.44 C) and thalamus (Figure 3.44 D) region of 3-month-old WT, Neu3-/-, Galgt-/-, and Neu3-/-Galgt-/- mice. In the cortex region (Figure 3.44 C) 39% and 52% reductions in oligodendrocyte content and thus in myelination were observed in Neu3-/- and Galgt-/- mice, respectively when compared to WT counterparts. In thalamus region (Figure 3.44 D), oligodendrocyte loss was identified in Neu3-/-, Galgt-/- and Neu3-/-Galgt-/- mice compared to WT counterparts as 44%, 50%, and 61%, respectively. The oligodendrocyte levels in the cerebellum (Figure 3.45 C) of Galgt-/- mice compared to WT (46%) and Neu3-/- (55%) were reduced significantly. Moreover, the levels in Neu3-/-Galgt-/- mice compared to WT (29%) and Neu3-/- (42%) were decreased significantly. Finally, in the pons region (Figure 3.45 D) of Galgt-/- mice, there was a significant loss in the

oligodendrocyte levels when it was compared to WT, Neu3-/-, and Neu3-/-Galgt-/- mice (33%, 27%, and 29%, respectively).

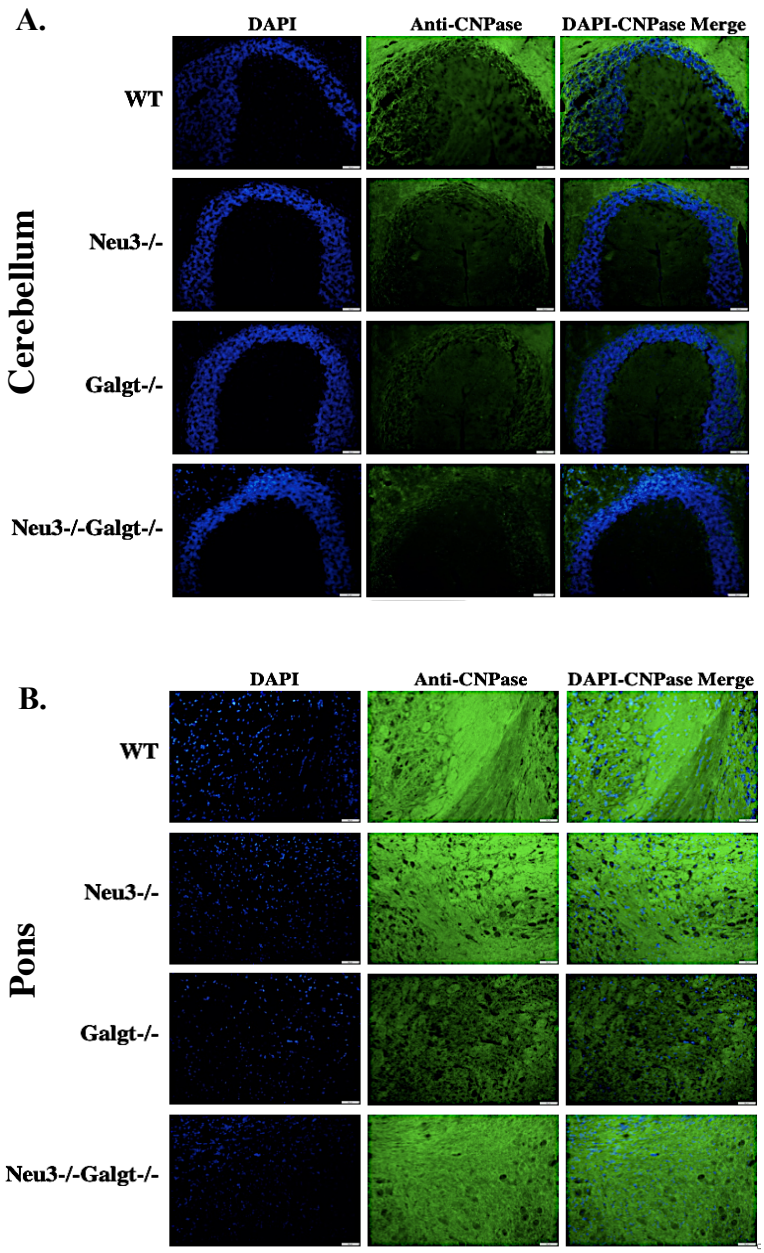

Figure 3.45. Anti-CNPase staining for cerebellum (A) and pons (B) regions of 3-month-old WT, Neu3-/-, Galgt-/- and Neu3-/-Galgt-/- mice for oligodendrocyte detection. The 20μm coronal sections were stained in green by Anti-CNPase antibody (oligodendrocyte marker) and in blue by DAPI (nucleus). Oligodendrocyte intensity analyses performed by NIH Image J program and normalized to WT for cerebellum (C), and pons (D) were shown. Scale bar indicates 50μm of cerebellum, and pons. Data is representative of mean ± SEM of measurements. Significant levels in the data were presented by using the one-way ANOVA (*$p<0.05$, **$p<0.025$, and ***$p<0.001$). (n=3 for 3-month old mice)

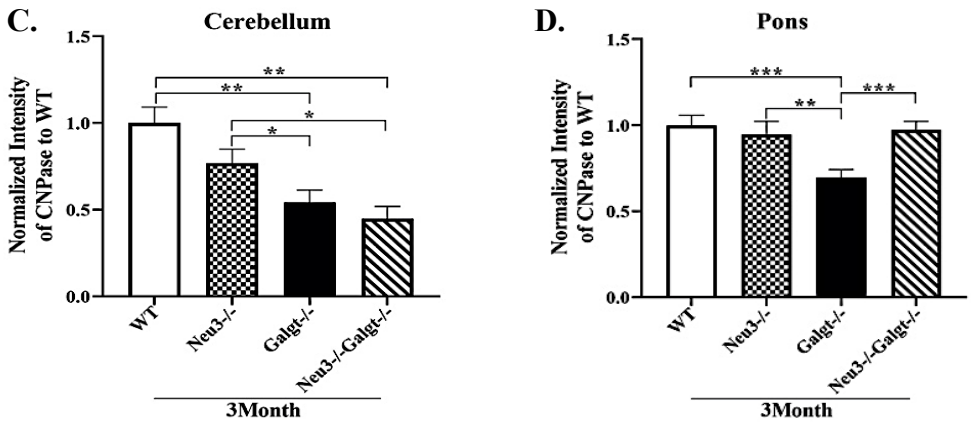

Figure 3.45 (cont.)

In oligodendrocyte analyses, cortex (Figure 3.46 A and C), thalamus (Figure 3.46 B and D), cerebellum (Figure 3.47 A and C), and pons (Figure 3.47 B and D) regions of 6-month-old WT, Neu3-/-, Galgt-/-, and Neu3-/-Galgt-/- mice were stained with Anti-CNPase antibody. In the analyses, the green stained regions were detected as oligodendrocyte including areas. According to results, the 28% and 20% loss in oligodendrocyte content in the cortex of Galgt-/- mice compared to WT and Neu3-/- mice were identified, respectively. Furthermore, the significant loss in Neu3-/-Galgt-/- mice compared to WT (23%) and Neu3-/- (15%) mice (Figure 3.46 C) was shown. In thalamus region (Figure 3.46 D) of Neu3-/- and Galgt-/- mice, there were 35% and 13% reduction in oligodendrocytes compared to WT mice.

In cerebellum (Figure 3.47 C), oligodendrocyte loss was observed in Neu3-/-Galgt-/- compared to WT (54%), Neu3-/- (39%), and Galgt-/- (28%) counterparts. Moreover, in the cerebellum of Neu3-/- and Galgt-/- mice, 25% and 36% reduction in oligodendrocyte contents were shown compared to WT littermates (Figure 3.47 C). Finally, in pons region (Figure 3.47 D) only Galgt-/- mice oligodendrocyte levels were negatively affected compared to WT (26%), and Neu3-/- (18%) mice.

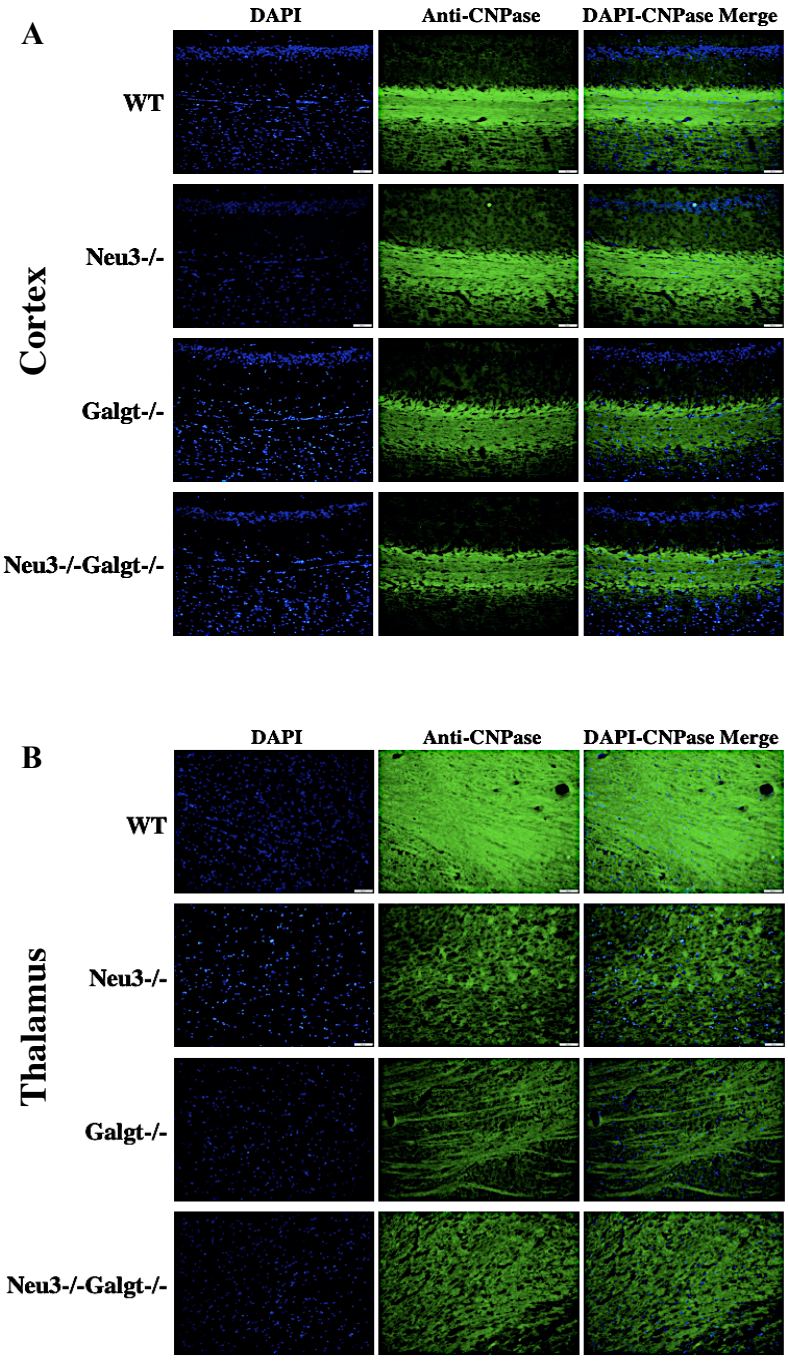

Figure 3.46. Anti-CNPase staining for cortex (A) and thalamus (B) regions of 6-month-old WT, Neu3-/-, Galgt-/- and Neu3-/-Galgt-/- mice for oligodendrocyte detection. The 20μm coronal sections were stained in green by Anti-CNPase antibody (oligodendrocyte marker) and in blue by DAPI (nucleus). Oligodendrocyte intensity analyses performed by NIH Image J program and normalized to WT for cortex (C), and thalamus (D) were shown. Scale bar indicates 50μm of cortex, and thalamus. Data is representative of mean ± SEM of measurements. Significant levels in the data were presented by using the one-way ANOVA (*$p<0.05$). (n=3 for 6-month old mice)

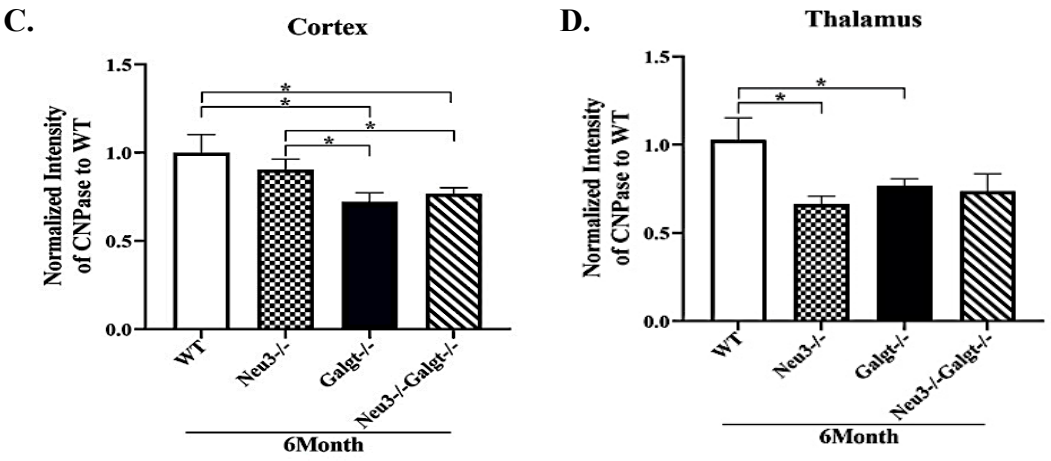

Figure 3.46 (cont.)

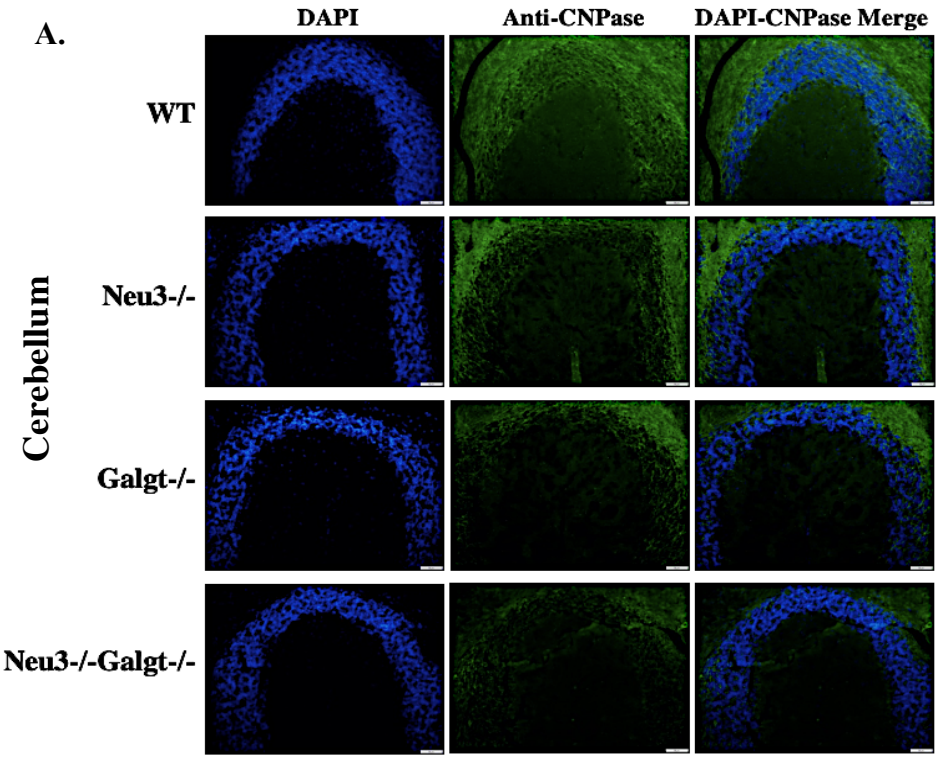

Figure 3.47. Anti-CNPase staining for cerebellum (A) and pons (B) regions of 6-month-old WT, Neu3-/-, Galgt-/- and Neu3-/-Galgt-/- mice for oligodendrocyte detection. The 20μm coronal sections were stained in green by Anti-CNPase antibody (oligodendrocyte marker) and in blue by DAPI (nucleus). Oligodendrocyte intensity analyses performed by NIH Image J program and normalized to WT for cerebellum (C), and pons (D) were shown. Scale bar indicates 50μm of cerebellum, and pons. Data is representative of mean ± SEM of measurements. Significant levels in the data were presented by using the one-way ANOVA (*p<0.05, **p<0.025, ***p<0.001 and ****p<0.0001). (n=3 for 6-month old mice)

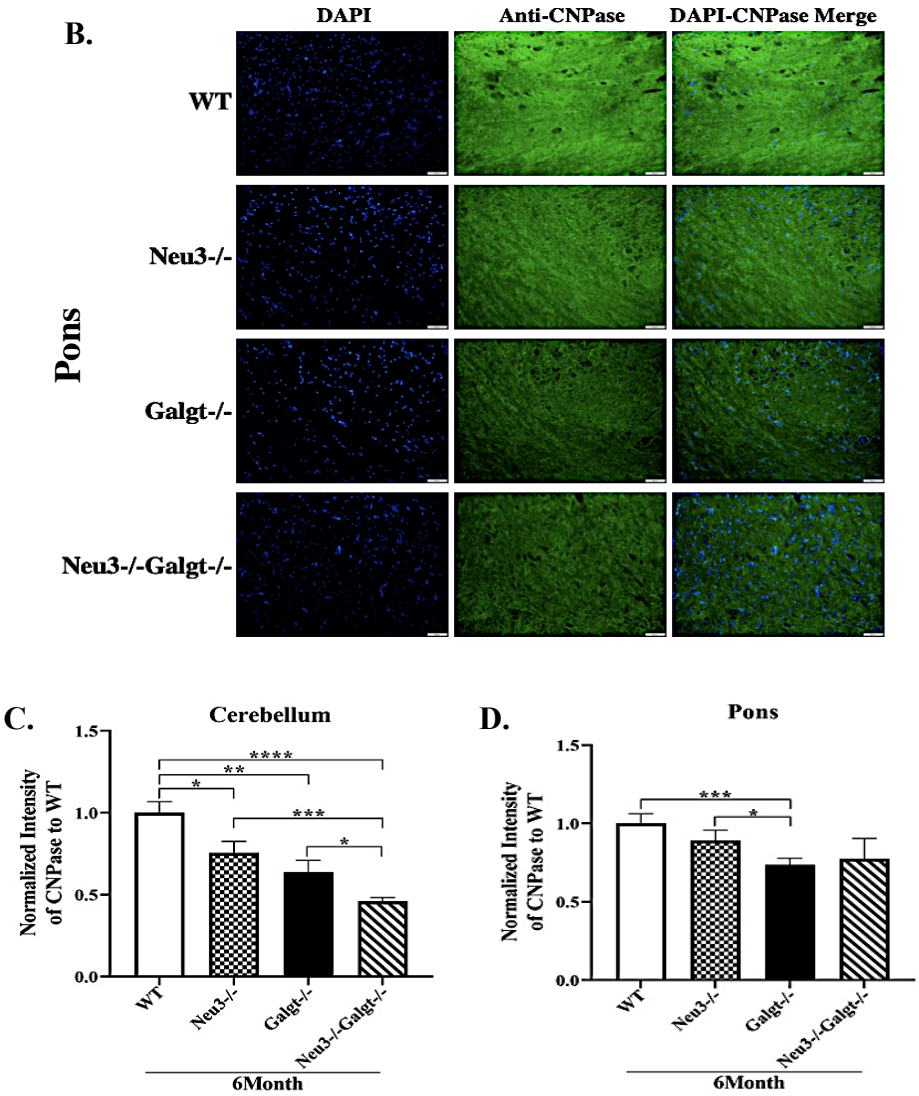

Figure 3.47 (cont.)

3.11. Behavioral Analyses

For showing alterations in behavior of 3- and 6-month-old WT, Neu3-/-, Galgt-/- and Neu3-/-Galgt-/-, Rotarod test Passive avoidance test, Open Field test were applied.

3.11.1. Rotarod Test

The rotarod test in which the animals were trained and tested on a rotating rod was used to evaluate balance and motor coordination of the mice strains (Hamm *et al*. 1994). For this purpose, 3- and 6-month-old WT, Neu3-/-, Galgt-/- and Neu3-/-Galgt-/-

mice were studied and the time of staying on rod were recorded for each group (Figure 3.48). According to results, there was not an age-dependent alteration among two age groups of each genotype. However, the reduction in time over the rod was observed in Neu3-/-Galgt-/- mice compared to WT and Neu3-/- littermates as 73% and 2%, respectively. Moreover, the reduced levels in 6-month-old Galgt-/- compared to WT counterpart as 65% were detected. For 3-month-old Neu3-/-Galgt-/-, the levels were reduced as 47% when they were compared with the WT littermates (Figure 3.48).

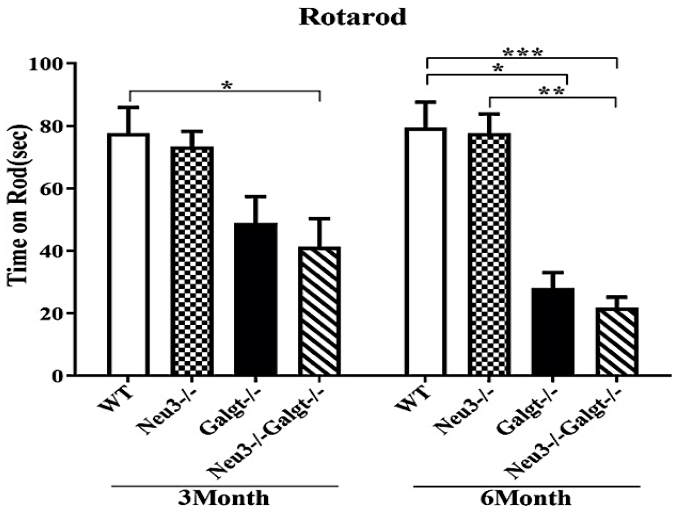

Figure 3.48. Rotarod analyses of 3- and 6-month-old WT, Neu3-/-, Galgt-/- and Neu3-/-Galgt-/- mice with accelerating speed of rod from 4 rpm to 40 rpm over a 5 minutes period. Data is representative of mean ± SEM of measurements. Significant levels in the data were presented by using the two-way ANOVA (*$p<0.05$, **$p<0.025$, and ***$p<0.001$). (n=6 for 3- and 6-month old mice)

3.11.2. Passive Avoidance Task

The passive avoidance task was applied to investigate fear-controlled learning and memory by using a two-box-system and the results were shown escape latency time (Figure 3.49). The habituation, training and testing procedures were performed on 3- and 6-month-old WT, Neu3-/-, Galgt-/- and Neu3-/-Galgt-/- mice. The results showed that in both age groups, Neu3-/-Galgt-/- mice could not be able to escape as quickly as their WT counterpart (Figure 3.49). The escape latencies for WT, Neu3-/-, Galgt-/-, and Neu3-/-Galgt-/- were 102.200±17.023 s, 61.350±15.151 s, 43.000±3.500 s, and 26.300±6.864

s, respectively for 3-month-old group. The escape latencies were 98.333±13.750 s, 76.250±13.750 s, 53.667±7.535 s, and 17.833±6.119 s for 6-month-old WT, Neu3-/-, Galgt-/- and Neu3-/-Galgt-/- mice, respectively (Figure 3.49). Thus, for both ages, Neu3-/-Galgt-/- mice had the lowest learning and memory forming capacity (Figure 3.49).

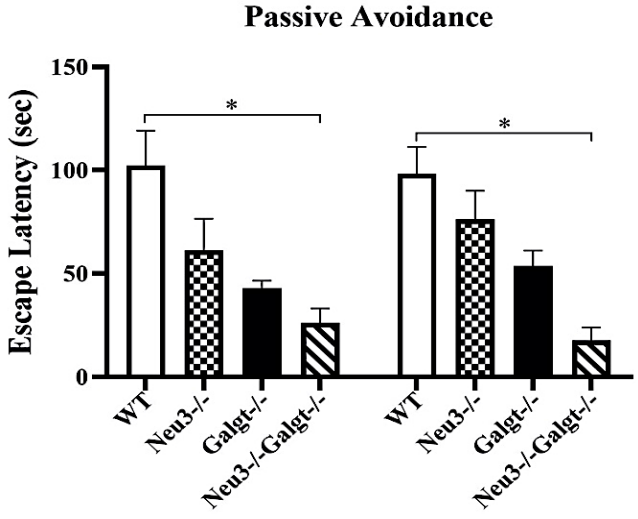

Figure 3.49. Passive avoidance analyses of 3- and 6-month-old WT, Neu3-/-, Galgt-/- and Neu3-/-Galgt-/- mice for testing of the latencies to enter the dark compartment were shown. Data is representative of mean ± SEM of measurements. Significant levels in the data were presented by using the two-way ANOVA (*$p<0.05$, ***$p<0.001$ and ****$p<0.0001$). (n=6 for 3- and 6-month old mice)

3.11.3. Open Field Task

The anxiety levels of 3- and 6-month-old WT, Neu3-/-, Galgt-/- and Neu3-/-Galgt-/- mice were tested by performing 5-minute open field task. The evaluations were done by recording the time spent in center (Figure 3.50 A) and periphery (Figure 3.50 B). of open field box. In the resulting graph of the time spent in center (Figure 3.50 A), there was an apparent reduction for Neu3-/-, Galgt-/-, and Neu3-/-Galgt-/- mice compared to WT littermates as 40%, 63%, and 60% ($p<0.001$), respectively at 3-month-old age (Figure 3.50 A). Although there was no age-dependent change, in the 6-month-old group, Galgt-/- and Neu3-/-Galgt-/- anxiety levels were increased as 73% and 86% compared to WT littermates, respectively (Figure 3.50 A). The time spent in periphery (Figure 3.50

B) was increased in Neu3-/-, Galgt-/-, and Neu3-/-Galgt-/- mice as 1.0-fold compared to WT mice at 3-month-old. In the older group, Neu3-/-, Galgt-/-, and Neu3-/-Galgt-/- were all increased in time spent in periphery as 1.0-, 1.1-, and 1.1-fold compared to WT littermates, respectively while Galgt-/- mice showed increased time in periphery as 0.8-fold compared to Neu3-/- counterparts (Figure 3.50 B).,

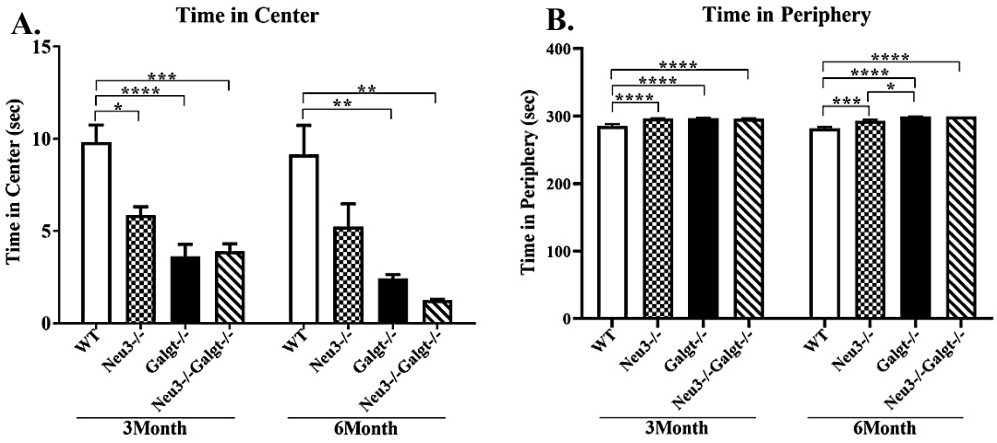

Figure 3.50. Open field analyses of 3- and 6-month-old WT, Neu3-/-, Galgt-/- and Neu3-/-Galgt-/- mice were performed. Time spent in center (A) and periphery (B) of the open field box for 5minutes were indicated. Data is representative of mean ± SEM of measurements. Significant levels in the data were presented by using the two-way ANOVA (*p<0.05, **p<0.01, ***p<0.001 and ****p<0.0001). (n=6 for 3- and 6-month old mice)

CHAPTER 4

DISCUSSION

The mice models were preferentially used for characterizing human diseases and their pathophysiology because of the physiological and genetic similarities among those organisms. In accordance with this study, the importance of complex ganglioside synthesizing enzyme Galgt and plasma membrane associated sialidase Neu3 and their potential cooperation in the ganglioside metabolism was aimed to investigate by benefitting from readily available single enzyme deficient models as Neu3-/- and Galgt-/- which were crossed to obtain double deficient mice named as Neu3-/-Galgt-/-. Through the proper breedings for WT, Neu3-/-, Galgt-/- and Neu3-/-Galgt-/-, the mice groups were obtained from the F2 generations. At the ages of 3-month-old and 6-month-old, the samples were collected to show age-dependent differentiations in the molecular or biochemical mechanisms among the animal models.

After the collection of required samples, the soft brain tissues for biochemical experiments like TLC analysis of acidic or neutral gangliosides, RT-PCR with specific markers, Western blot with distinct antibodies, and DNA fragmentation assays and urine samples for oligosaccharide analyses were all used. Furthermore, PFA fixed brain samples were subjected to immunohistochemical, histopathological analyses or TUNEL assay with special antibodies, dyes or kit reagents. Finally, the animals were assayed in three different behavioral tests such as rotarod, open field, and passive avoidance for evaluating balance, coordination, memory or anxiety levels of animals in the presence of ganglioside alterations.

First of all, the changes in the weight of animals (Figure 3.3 A and 3.3 B) and their gross appearance (Figure 3.3 C) were monitored. The weight measurements were performed by starting from 6 weeks to 24 weeks. According to weight measurement graph (Figure 3.3 A and 3.3 B) there were not any significant changes among the genotypes but the slight reduction in the weight of male and female mice at around 20 weeks of their ages were detected. In the studies of Chiavegatto *et al*., there were apparently lost body weight starting from the 32 weeks of the animal's age (Chiavegatto *et al*. 2000).

Therefore, the slight reduction in this study could continue with a significant reduction as the animals were aging.

Initially, TLC analyses were assayed for evaluating brain gangliosides according to their chromatographic mobility and reactivity toward the staining. The gangliosides change their composition in cell type- or tissue type-specific manner in order to locally regulate signaling pathways like apoptosis. Thus, the importance of brain gangliosides in the induction of apoptotic pathways through altering ER Ca^{2+} content and oxidative status in cells would be initially evaluated through TLC analyses (Malisan and Testi 2002). Especially, elevated levels of the acidic GSLs like G_{M1} through ER-stress response and G_{D3} via both ER-stress response and oxidative stress in mammalian cells were correlated with the release of apoptogenic factors from mitochondrial pores through the changes in their content on those organelles. (Malisan and Testi 2002; Sano *et al*. 2009). The resulting ganglioside bands from the cortex, and cerebellum tissues were compared to the specific standard. According to cortex (Figure 3.4) and cerebellum (Figure 3.8) results, the expected bands for WT and Neu3-/- as complex gangliosides and Galgt-/- and Neu3-/-Galgt-/- as the simplest ones in acidic plate were detected for both age groups (Kappagantula *et al*. 2014; Takamiya *et al*.1996).

In the cortex region, the decrease in G_{M1} in Neu3-/- at 6 months compared to WT and its younger counterpart was seen (Figure 3.5 A). Normally, the Neu3 sialidase has higher desialylation activity toward LacCer, G_{M3}, G_{D3}, G_{D1a}, G_{D1b}, and G_{T1b} whereas it has lower activity toward G_{M1} and G_{M2} having a sialic acid in branching part according to sialidase activity analyses of Neu3 isolated from human brain tissue and to *in vitro* studies toward the ganglioside substrates (Oehler *et* al. 2002). Therefore, the reduction in G_{M1} substrate would be correlated with the compensatory effects of other sialidases like Neu4 to degrade G_{M1} substrate into downstream gangliosides in the absence of Neu3 sialidase. In the studies of Pan *et al.* in 2017, it was shown that the progressively accumulating G_{M3} in contrast to the reduced levels of G_{M1} ganglioside. Therefore, once both of those sialidases were removed, it would probably reduce the G_{M1} ganglioside levels showing the compensatory actions of sialidases to degrade this ganglioside (Pan *et al*. 2017). The G_{D1a} levels (Figure 3.5 B) were not changed despite being a good substrate for Neu3 sialidase so there would be a control mechanism of other sialidases like Neu4 to compensate its levels. The reduction in G_{D1b} and G_{T1b} levels (Figure 3.5 C and 3.5 D) in Neu3-/- for both ages could be related with the other enzymes to degrade by removing

their galactose and sialic acid residues. The downstream molecules and enzymes would be further evaluated.

Then, the simple gangliosides G_{M3}, G_{D3}, and G_{D3} isoform o-acetyl-G_{D3} were observed in only Galgt-/- and Neu3-/-Galgt-/- mice at elevated levels (Figure 3.6). According to studies, it was shown that Galgt gene disruption prevented the formation of complex gangliosides and elevated the levels of simple gangliosides for compensatory actions of them. By this way, the animal would develop normally with the limited severity in the phenotype (Ngamukote *et al*. 2007; Furukawa *et al*. 2008). The G_{D3} ganglioside but not G_{M3} was investigated to induce apoptotic pathways through perturbation of Ca^{2+} content of ER and the effects of those calcium ions to mitochondrial membrane while its acetylated form prevented its proapoptotic activity in cells. In line with these observations, the levels of G_{D3} and o-acetyl G_{D3} were shown to change in the cortex region (Figure 3.6 B and 3.6 C). For Galgt-/- mice G_{M3} levels (Figure 3.6 A) would be balanced by the activity of Neu3 sialidase but in double deficient mice this would be performed by compensatory actions of other enzymes or sialidases as the explanation for absence of the differences among the genotypes. The G_{D3} levels were not changed significantly while its acetylated form was elevated in Galgt-/- mice at 6 months compared to its younger counterpart and Neu3-/-Galgt-/- mice. The levels in Neu3-/-Galgt-/- mice were also reduced among two ages (Figure 3.6 B). This change could be correlated with the lower affinity of Neu3 sialidase toward the acetylated gangliosides. Moreover, the isoform of G_{D3} (Figure 3.6 C) were shown to increase because one-fourth of G_{D3} ganglioside is normally found in the form of o-acetyl-G_{D3} in the brain (Matsuda *et al*. 2006).

For the cerebellum tissues, G_{M1} levels (Figure 3.9 A) were significantly increased between WT and Neu3-/- at 6-month-old, respectively, indicating the cell-type specific G_{M1} ganglioside composition and the enzymatic activity of Neu3. The age-dependent increase was also detected in G_{M1} levels of Neu3-/- mice indicating lower compensatory enzymatic activity in this region. The increase in G_{M1} in this region could be an indicator of ER stress conditions that would be checked in the latter stages (Figure 3.9 A). The reduction in G_{D1a} levels (Figure 3.9 B) in *Neu3* deficient mice at older ages could be an evidence for compensatory actions of certain enzymes in an age-dependent manner or the age-related accumulation of this ganglioside in brain. The G_{D1b} levels were evaluated to show the compensation of Neu3 sialidase in older ages through the reduction compared to WT and to Neu3-/- at 3-month-old (Figure 3.9 C). In the G_{T1b} levels, there were

significant or slight increase in 3- or 6-month-old Neu3-/- showing the activity of Neu3 sialidase in normal conditions to this ganglioside or the absence of compensating enzymes in cerebellum (Figure 3.9 D). All those observations should be assayed by controlling the changes in the levels of downstream gangliosides or enzymes in the ganglioside degradation.

Then, simple gangliosides except the G_{M3} were detected at elevated levels in the cerebellum of Galgt-/- and Neu3-/-Galgt-/- mice at both ages (Figure 3.10). The absence of G_{M3} ganglioside in the cerebellum tissue would be related to the cell-type specific alterations in the composition of gangliosides. The significant increase in G_{D3} levels (Figure 3.10 B) were observed in 6-month-old double deficient mice while o-acetyl-G_{D3} levels (Figure 3.10 A) were also elevated in 6-month-old Neu3-/-Galgt-/- mice. Since this sialidase has high affinity for desialylation of G_{D3}, the increase in levels would be explained by region specific action of the enzyme. This would indicate the presence of the one-fourth of the G_{D3} enzyme in the form of o-acetyl-G_{D3} in *Galgt* deficient mice models or the lack of compensatory enzymes to degrade this ganglioside in the cerebellum region. The increased G_{D3} and o-acetyl-G_{D3} gangliosides were further evaluated in terms of whether the proapoptotic activity of G_{D3} was prevented by the o-acetyl-G_{D3} in a cell type-specific manner within the cerebellum tissue (Figure 3.10 A).

Later, the neutral gangliosides found in cortex (Figure 3.7) and cerebellum (Figure 3.11) tissues were evaluated by TLC. There were increasing amounts of the Lactosyl Ceramide in the brain tissues of Galgt-/- and Neu3-/-Galgt-/- mice compared to basal levels found in WT and Neu3-/- mice for both age groups (Figure 3.7 C and 3.11 C). This would probably be explained by the enzymatic activity of N-acetylgalactosaminyltransferase for converting LacCer -a simple GSL- into G_{A2}. In the neutral ganglioside plates, the increased LacCer ganglioside was shown by the absence of N-acetylgalactosaminyltransferase enzyme. Moreover, there were no significant changes in the levels of LacCer in double deficient mice since Neu3 sialidase is not compensated by any other sialidases like Neu4 that has no activity toward this GSL lacking sialic acid residues. There were no age-dependent changes in the levels of this neutral GSL for cortex and cerebellum.

For the next part of the study, the possible disturbances in intrinsic or extrinsic apoptotic mechanisms in single- or double-deficiency of Neu3 and Galgt enzymes in cortex, cerebellum, and thalamus tissues of 3- and 6-month-old WT, Neu3-/-, Galgt-/- and Neu3-/-Galgt-/- mice by performing DNA fragmentation assays, Western Blot

analyses, and Real-Time PCR. Since the locally changing compositions or quantities of gangliosides in either cell membrane or subcellular membranes as a response to a stress intrinsically or extrinsically, the cells were directed to apoptotic cell death. Some of the gangliosides were related to induction of ER stress response leading terminally to apoptosis while others acted to elevate oxidative stress causing apoptosis. Their interactions with other membrane proteins enabled them to modify cell fate decisions.

The western blot assays and RT-PCR analyses were performed by applying apoptosis, ER-stress, and oxidative stress related markers. The BiP antibody in Western Blot and Calnexin, ATF6, and XBP-1 markers related to Endoplasmic reticulum were used to assess ER-stress associated apoptosis mechanisms. Moreover, the expression levels of genes encoding the antioxidant defense mechanism enzymes as SOD2, TTase 1, and Catalase to detect ROS leading to oxidative stress were evaluated. Finally, Caspase 9, and Caspase 3 antibodies of intrinsic apoptosis and Fas-Ligand of extrinsic apoptosis in western blot in addition to the apoptosis markers as Bcl-2, Bcl-XL, and Bax in RT-PCR were analyzed in the context of this study. Because the changes in ganglioside pattern like G_{D3} resulted in damages to mitochondrial membranes that could then release reactive oxygen species, cytochrome c and caspase-9 whereas the other gangliosides like G_{D1a} and G_{M3} did not show any effects were indicated in the previous studies, these markers and proteins were used in the study (Rippo *et al*. 2000). In another study, the accumulation of G_{M1} ganglioside in GSL enriched domains of mitochondria associated ER membranes (MAMs) caused alterations in Ca^{2+} regulation so G_{M1} functions like the inducer of ER stress-related and mitochondria regulated apoptosis in nerve cells (Sano *et al*. 2009). The other gangliosides were not as effective as the gangliosides G_{D3} and G_{M1} for inducing apoptosis (Rippo *et al*. 2000; Malisan and Testi 2002; Sano *et al*. 2009).

In line with these investigations, the studies were started with DNA fragmentation assay in order to visualize apoptosis mediated DNA fragmentation but in the cortex region (Figure 3.12), there were not any observable changes except the intensely smeared regions were shown in the 6-month-old Galgt-/- mice compared to other mice groups. However, this study could not clarify the existence or absence of apoptosis in the protein or mRNA expression levels so further studies with Western Blotting and RT-PCR were conducted for the cortex region. The elevated levels of G_{D3} ganglioside in cells either due to endogenous or exogenous effects was shown to cause the deterioration in mitochondrial membrane and release of apoptogenic factors (Malisan and Testi 2002) so Galgt-/- and Neu3-/-Galgt-/- mice were analysed in terms of apoptosis related factors in

the cortex. The expression levels of other ER-stress related proteins encoded by Calnexin, ATF6, and XBP-1 levels were measured (Figure 3.13 A, 3.13 B, and 3.13 C). The results of Calnexin -ER-chaperone- was increased in Neu3-/- and Neu3-/-Galgt-/- significantly. For Neu3-/- mice, the effects of G_{M1} ganglioside was observable to induce ER stress and then apoptosis (Figure 3.13A). The ATF6 (Figure 3.13 B) and spliced XBP-1 (Figure 3.13 C) levels were all increased in Neu3-Galgt-/- mice showing the G_{D3} elevation induced release of Ca^{2+} ions and disturbed mitochondrial membrane permeability (Sano *et al*. 2009). The Neu3-/- and Galgt-/- mice showed an age-dependent increase indicating a progressively accumulating effects of gangliosides. Next, BiP levels (Figure 3.16) were assessed for Galgt-/- and Neu3-/-Galgt-/- without a change so G_{D3} would not perform its action by activating ER stress pathways.

The next part was the evaluation of oxidative stress since through mitochondrial membrane damage, the ROS levels were shown to increase in the previous studies. SOD2, and Catalase levels (Figure 3.14 B and 3.14 C, respectively) were all increased in Galgt-/- and Neu3-/-Galgt-/- mice while TTase 1 levels (Figure 3.14 A) were the highest in Galgt-/- mice. The increase in oxidative stress was tried to be overcome by the action of those antioxidant defence enzymes. In line with this analysis, the single- or double-deficiency of Neu3 and Galgt enzymes led to alterations in the brain functioning of the animals. Moreover, in addition to western blot data, while there were no changes in Bcl-2 and Bcl-XL markers (Figure 3.15 A and 3.15 B), the levels of proapoptotic Bax (Figure 3.15 C) were elevated in Galgt-/- and Neu3-/-Galgt-/- mice. The increasing expression levels of Bax would be associated with the disturbed membrane permeability of mitochondria due to G_{D3} ganglioside, subsequently leading to caspase activation. Since the levels of Bcl-2 or Bcl-XL were not altered, they could not perform their anti-apoptotic effects. For the G_{D3} ganglioside, its acetylated form called o-acetyl G_{D3} was deduced to act in an anti-apoptotic manner. In the TLC results, there was apparently increased levels in 6-month-old Galgt-/- mice. However, the pro-apoptotic effect of G_{D3} was not prevented by the actions of o-acetyl G_{D3} so there would be a certain threshold for this function. This would possibly be related to endogenous not exogenous effects of G_{D3} ganglioside. The apoptosis pathways were activated through either induction of ER-stress or mitochondrial membrane disruption due to changes in the levels of certain gangliosides. Moreover, the absence of Neu3 sialidase was probably the cause of apoptosis that would be further assessed (Sano *et al*. 2009). Slightly increased Caspase 9 levels (Figure 3.17) in addition to the significantly elevated Caspase 3 levels (Figure 3.18) were all detected in Galgt-/-

mice in the older ages. The Neu3-/- mice revealed a significant increase at 6-month-old despite the relatively low levels of Caspase 3 in the same age. The apoptosis was expected to be active in Neu3 sialidase deficient mice because the over-expression of this enzyme was related to the prevention of apoptosis in cancer tumorigenesis like colon cancer. The Caspase 9 in this animal would activate other executioner caspases like Caspase 6 or 7 that would be further assessed. The Fas -Ligand mediated activation of apoptosis was not detected in cortex tissue (Figure 3.19).

The cerebellum tissue was analysed by DNA fragmentation assay (Figure 3.20) showing the additional DNA fragments in 3-month-old Neu3-/- and 6-month-old Neu3-/-Galgt-/- mice. However, these results were not as explanatory as expected since the DNA fragments resulted from caspase activated DNase had smaller sizes to detect clearly or to protect from degradation (Bortner *et al*. 1995). Next, the changes in ER-stress markers as Calnexin, ATF6, spliced XBP-1, and BiP revealed apparently increased levels in Galgt-/- and Neu3-/-Galgt-/- mice showing the ER-stress inducing actions of increased G_{D3} ganglioside (Figure 3.21 and 3.24). The changing Ca^{2+} levels in the cytosol would lead to release of ROS according to increased levels of SOD2 (Figure 3.22 B) and Catalase (Figure 3.22 C) but not TTase 1 (Figure 3.22 A) in these animal groups. The G_{M1} mediated Ca^{2+} level changes were also found in Neu3-/- mice due to the relatively increased levels of SOD2 and Catalase. For further understanding of apoptosis, TUNEL assay was also performed for the older aged mice models since the highest alterations were detected in this group. The antiapoptotic Bcl-2 (Figure 3.22 A) was reduced in Neu3-/- and Galgt-/- mice compared to WT littermates but Bcl-XL (Figure 3.22 B) was not changed. RT-PCR results of Bax (Figure 3.23 C) showed increased levels in Neu3-/- and Galgt-/- compared to WT littermates and their respective 3-month-old groups. Therefore, it was thought that Bax activity was not altered by anti-apoptotic proteins. The pore forming G_{D3} and G_{M1} gangliosides activated Bax led to release of apoptogenic factors and activation of Caspase 9. However, the apparently increased Bax levels but no change in Caspase 9 and Caspase 3 levels (Figure 3.25 and 3.26, respectively) of Galgt-/- mice would be related to the binding and oligomerization pattern of Bax to Bak so the levels of Bak would be further analyzed in order to overcome this confusion. The resulting apoptosis in Neu3-/- mice was associated with the increased levels of G_{M1} that could accumulate in cerebellum. In the studies with a neurodegenerative disorder, G_{M1} gangliosidosis, the accumulating G_{M1} caused apoptotic cell death. However, another reason of the apoptosis in Neu3-/- that was the similar reason for the double deficient

model was the absence of Neu3-/- sialidase normally acting as anti-apoptotic molecule in cancer cells. western blot analyses of Caspase 9 and Caspase 3 revealed increased apoptosis in Neu3-/- and Neu3-/-Galgt-/- mice (Figure 3.25 and 3.26, respectively). There were not significant changes in Fas-Ligand except a reduction in 6-month-old Neu3-/-Galgt-/- mice compared to WT counterparts (Figure 3.27).

Finally, in thalamus region, DNA fragmentation (Figure 3.28) results indicated that there were more intense smeared fragments in 3- and 6-month-old Neu3-/-, Galgt-/-, and Neu3-/-Galgt-/- mice compared to their WT counterparts. Since these results were not as explanatory as expected, the RT-PCR assay was performed. The levels of Bcl-2 and Bcl-XL (Figure 3.31 A and 3.31 B) did not change its function as anti-apoptotic molecules while the slightly increased levels in 6-month-old Neu3-/-, Galgt-/-, and Neu3-/-Galgt-/- were detected for Bax expression (Figure 3.31 C) compared to their WT littermates. For the thalamus region, apoptosis could not be concluded according to those results so further analyses were performed by TUNEL assay. The ER stress levels were higher in Galgt-/- in terms of BiP significantly in 3 months and slightly in 6 months (Figure 3.32 B). The levels of Calnexin and spliced XBP-1 (Figure 3.29 A and 3.29 C) supported the results of BiP, a chaperone. Therefore, in Galgt-/- and Neu3-/-Galgt-/-, there were apparently increased levels of ER-stress. Finally, oxidative stress levels were analysed. Although there was no change for TTase1 marker (Figure 3.30 A), the significantly increasing SOD2 (Figure 3.30 B) and slightly changing Catalase (Figure 3.30 C) were indicated in Galgt-/- and Neu3-/-Galgt-/- mice groups. Caspase 3 and Caspase 9 levels were analysed (Figure 3.33 and 3.34, respectively). The Caspase 3 levels of Neu3-/- and Neu3-/-Galgt-/- in the older group was the higher than Galgt-/- mice while in 3-month-old group, Galgt-/- mice was the highest. The Caspase 9 levels were changed significantly for Neu3-/- and Galgt-/- mice. Moreover, there were no changes for Fas-Ligand (Figure 3.35) which was presented to be important for G_{D3}/Fas-Ligand mediated extrinsic apoptotic pathway. In conclusion, the apoptosis levels were not detectable in thalamus region for all mice groups while observable ER-stress and oxidative stress in Galgt-/- and Neu3-/-Galgt-/- mice were shown. For the further evaluation of apoptosis, the TUNEL assay was performed.

The study was continued for region-specific investigations of the apoptosis levels by applying TUNEL assay to frozen brain slides. The TUNEL assay was performed for understanding the apoptotic cells in cortex (Figure 3.36 A), cerebellum (Figure 3.36 B), thalamus (Figure 3.37 A), and hippocampus (Figure 3.37 B) of 6-month-old WT, Neu3-

/-, Galgt-/- and Neu3-/-Galgt-/- mice through detecting DNA breaks in the cells. When colocalizations of PI stained nuclei with apoptotic cells in green were generated, yellow colored TUNEL positive cells were obtained to show the presence of apoptosis. The results for all brain regions showed that the levels in Galgt-/- were the highest compared to other regions. In cerebellum, thalamus, and hippocampus, the levels for Neu3-/- was also higher compared to WT counterparts (Figure 3.36 D, 3.37 C, and 3.37 D, respectively). Finally, for each brain region, Neu3-/-Galgt-/- mice apoptosis levels were elevated compared to WT littermates. For the cortex region, the levels in Galgt-/- were correlated with caspase levels either significantly or slightly, especially with the Caspase 3 levels (Figure 3.18) but the extrinsic pathway was not altered in terms of the Fas-Ligand levels (Figure 3.16). This was correlated with the elevated G_{D3} levels acting as pro-apoptotic molecule in nerve cells but the Fas-Ligand induced by G_{D3} levels was not detected in this mouse model despite the studies with lymphocytes showing CD95 or Fas-Ligand directed G_{D3} elevation (De Maria 1997). In the cortex, G_{M1} ganglioside acting as pro-apoptotic in Neu3-/- mice did not result in apoptosis induction so further degradation by other enzymes would prevent increase in its level to a threshold for apoptosis induction. In cerebellum region, the levels of Caspase 3 in Neu3-/-Galgt-/- mice and of Caspase 9 (Figure 3.25 and 3.26, respectively) in Neu3-/- mice were the highest while the TUNEL positive cells were slightly elevated in those mice groups. Their levels were significantly increased when they were compared with WT littermates. The highest levels in Galgt-/- mice was related with elevated G_{D3} levels but the slightly lower levels of apoptosis in double deficient mice would be correlated with the absence of Neu3 sialidase. The highest levels in Galgt-/- mice would be further assayed with anti-CNPase staining since the oligodendrocytes were negatively affected by the elevation of G_{D3} levels directing those cells to apoptosis. These conclusions were correlated with a more region-specific investigation of TUNEL assay compared to western blotting since TUNEL assay revealed only apoptotic nuclei in this specific region. In thalamus region, except Caspase 3 and Fas-Ligand levels, other western blotting results indicated a similarity to TUNEL assay results. Therefore, in this region G_{D3} directed apoptosis induction but not Fas-Ligand induced G_{D3} increase occurred in Galgt-/- mice. Moreover, region specific G_{M1} directed apoptotic induction in Neu3-/- mice was also seen. However, the levels in double deficient mice were not as expected so G_{D3} levels or G_{D3} activity toward mitochondria in thalamus would be altered in a region-specific manner. Finally, in hippocampus region, all genotypes revealed increased levels of TUNEL-positive cells

showing the most affected region from the apoptosis. Both the G_{D3} and G_{M1} levels and their pro-apoptotic activity were correlated with the increasing apoptosis levels in this region. Therefore, TUNEL assay showed the levels of apoptotic cells in a detailed manner by specifically showing cortex, cerebellum, thalamus and hippocampus regions in contrast to western blotting and DNA fragmentation studies (Figure 3.36 C, 3.36 D, 3.37 C, and 3.37 D, respectively).

Since apoptosis resulted in cellular loss, the analyses to detect neuron numbers could also be performed. In this study, the apoptotic cell death and resulting neuronal loss were compared by staining nuclei in the cortex, hippocampus, thalamus and cerebellum of 3 and 6-month-old WT, Neu3-/-, Galgt-/-, and Neu3-/-Galgt-/- mice with anti-NeuN antibody. The NeuN protein localized to the nuclei in CNS of mammalian cells could be detected by the recognition of this antibody. According to results of 3-month-old group, the cortex of Neu3-/-Galgt-/- mice (Figure 3.42 R) was the most affected one that could indicate presence of higher levels of apoptotic cell death. The lack of both enzyme activities was resulted in the neuronal loss in Neu3-/-Galgt-/- mice. There was no effect in hippocampus (Figure 3.42 S) neuron number but 6-month-old mice would be studied to show age-related defects. In thalamus, only Galgt-/- mice presented significant reduction compared to WT in addition slight changes of Neu3-/- and Galgt-/- compared to double deficient mice (Figure 3.42 T). The deficiency of those enzymes resulted in increased G_{M1} and G_{D3} levels and accompanying apoptosis levels resulting in neuronal loss. However, Neu3-/-Galgt-/- did not indicate such an expected result that would be checked in 6-month-old group to deduce age-related neuronal loss. In anti-NeuN analyses of 6-month-old mice in the cortex region (3.43 R), neuron number supported increased apoptotic nuclei levels in this region. For the Neu3-/-Galgt-/-, the absence of Neu3 sialidase preserved the alterations in this region. The absence of this sialidase enabled the recovery of neuronal loss occurred in deficiency of Galgt enzyme. This was also correlated with the slightly changed apoptotic nuclei levels in those mice groups. For the hippocampus region (Figure 3.43 S), there was an aging related neuronal loss that would be related to apoptosis levels shown by TUNEL assay, especially for Galgt-/- mice. For Neu3-/-, neuron number changes were slightly correlated with the apoptotic cell number in TUNEL assay. This was resulted from the compensating activity of other sialidases or gangliosides to prevent G_{M1} and G_{D3} induced apoptosis. Moreover, other pathways causing the highest neuronal loss in Galgt-/- mice would be altered in this brain region. In thalamus region (Figure 3.43 T), all genotypes showed significantly reduced neuron

number compared to WT littermates while Neu3-/- mice indicated the highest neuronal loss levels. These results slightly resembled to TUNEL assay results with higher apoptosis levels in Neu3-/- and Galgt-/- mice while Neu3 sialidase loss led to reducing cell number in contrast to apoptosis levels. The reason for this difference could be the absence of Neu3 sialidase in thalamus with region-specific activity in this brain region, normally. Apart from TUNEL assay results, Caspase 3 levels would be correlated with this change. Finally, the cerebellum region (Figure 3.43 U) with the highest levels of neuronal loss in Neu3-/-Galgt-/- mice was detected. However, the levels of apoptosis were the highest in Galgt-/- mice. In this case, the double deficiency of both enzymes would result in the highest levels of neuron loss despite the low levels of apoptosis.

The frozen sections of mice brains were also analysed by applying histopathological staining like Hematoxylin-Eosin staining for showing histological abnormalities, Cresyl Echt Violet staining for indicating neuron number changes, Periodic acid-Schiff staining for assessing glycolipid contents in cells and Luxol Fast Blue staining for evaluating myelin content in distinct brain regions. From those staining techniques, Cresyl Echt violet staining and Luxol Fast Blue staining were histopathologic forms of anti-NeuN and anti-CNPase antibody staining, respectively. According to Cresyl Echt violet staining that stained Nissl substances in nuclei and made apparent the neuron morphology and number, the results were resembled to the results of 6-month-old anti-NeuN antibody staining. The cerebellum, cortex, hippocampus, and thalamus regions were negatively affected due to neuronal degeneration and karyolyis in the 6-month-old Galgt-/- and Neu3-/-Galgt-/- mice compared to Neu3-/- littermates while WT mice were the healthiest group in this study (Figure 3.38).

The potential morphological alterations in the brain regions of mice groups at 6 months of age were analyzed by Hematoxylin-Eosin staining. It showed that the healthiest mouse strain was WT mice that were used to compare other mice groups. According to results of cortex tissue, the blood vessel dilation and edema were detected in higher levels in 6-month-old Galgt-/- and Neu3-/-Galgt-/- mice compared to Neu3-/- littermates. The hippocampus and thalamus tissues of Galgt-/- and Neu3-/-Galgt-/- mice compared to Neu3-/- littermates were more negatively affected due to neuronal degeneration. In the cerebellum of Galgt-/- and Neu3-/-Galgt-/- mice, the Purkinje cell layer deterioration and cell loss in addition to intensive edema were detected at most compared to Neu3-/- littermates. The problems in the cerebellum region of Galgt-/- and Neu3-/-Galgt-/- mice

were behaviorally evaluated in rotarod due to the importance of the signal transmission in these cell types (Figure 3.39).

Next, Periodic acid-Schiff staining was performed to show the accumulating glycosphingolipids in brain tissues of the animal models. According to results, the accumulating GSLs were detected in the cortex, thalamus, hippocampus, and cerebellum regions of Galgt-/- and Neu3-/-Galgt-/- since the elevated levels of G_{D3} ganglioside were detected in those animals as a compensatory mechanism for the absence of other gangliosides. The GSL levels in the brain tissues of those animals were higher than Neu3-/- while the healthiest mouse strain was WT mice in this study. Since there was not much accumulating gangliosides in Neu3-/- mice and the elevated levels of G_{D3} in Galgt-/- and Neu3-/-Galgt-/-, the results of this study were shown as expected (Figure 3.40).

Finally, the Luxol Fast Blue staining procedure was applied to brain slices of animal groups in 6-month-old of ages in order to evaluate the changes in the levels of myelin sheath. In the studies of Sheikh *et al*., it was shown that a demyelination in PNS and decreased myelin content in CNS of Galgt-/- mice were present (Sheikh *et al*. 1999). The reason for this demyelination or the decrease in myelination would be correlated with the G_{D3} mediated apoptosis in oligodendrocytes which were affected in the presence of a stress exposure like elevated levels of G_{D3}. The increase in apoptosis in those glial cells would probably lead to demyelination. The results were shown as expected with a decrease in myelin content of Galgt-/- and Neu3-/-Galgt-/- compared to their Neu3-/- littermates while the most normal animal group was WT mice in this study, as well. These results would be further assessed by performing anti-CNPase antibody staining showing the region-specific changes in the levels of oligodendrocytes (Figure 3.41).

In CNS, apart from the nerve cells, there were glia cells that would also be affected by the apoptotic cell death with reduction in their contents. For this reason, oligodendrocyte for detecting myelin volume was assayed in this study. In addition to the alterations in oligodendrocyte number and so myelin volume due to apoptotic cell death, the *Galgt* disrupted mice models were detected to have demyelination and decreased myelination in PNS and CNS so that a reduction in myelin volume would be presented in these mice models (Yao *et al*. 2014; Sheikh *et al*. 1999). Moreover, since Neu3 sialidase activated axonal regeneration after axotomy by several ways. From those ways, the one was correlated with G_{D1a} being a substrate of inhibitory molecule MAG (myelin-associated glycoprotein) found on CNS and PNS myelinating cells for supporting axonal myelination. G_{D1a} to G_{M1} conversion of Neu3 sialidase enabled axon-myelin integrity

(Kappagantula *et al*. 2014; Collins *et al*. 1997; Vyas *et al*. 2002). Therefore, both of those enzymes were required for normal myelin production from oligodendrocytes or Schwann cells in CNS and PNS either directly as in Galgt-/- mice or indirectly like in Neu3-/- mice. Therefore, for indicating the potential alterations in myelin volume and demyelination of 3- and 6-month-old WT, Neu3-/-, Galgt-/-, and Neu3-/-Galgt-/- mice, the cortex, thalamus, cerebellum, and pons regions of were stained with anti-CNPase antibody showing myelin containing regions in green. According to results of cortex region (Figure 3.44 A), there were the expected reductions in Galgt-/- mice that showed reduction in myelin volume while Neu3-/- anti-CNPase levels were also reduced compared to WT mice. The Neu3-/-Galgt-/- mice were expected to show the lowest myelin volume but there would be region specific and age-dependent effects shown in this model. Then, for showing any region specificity, thalamus region (Figure 3.44 B) was analysed to indicate reduction in myelin volume in double deficient mice in addition to decreasing levels in Neu3-/- and Galgt-/- mice compared to WT littermates. The similar pattern was observed in cerebellum (Figure 3.45 A) showing the importance of region-specific production and alteration of myelin contents. However, pons region (Figure 3.45 B) of Galgt-/- mice was only affected showing the importance of complex gangliosides in myelin volume. The absence of Neu3 sialidase turned the pattern in Neu3-/-Galgt-/- mice back so there would be compensating actions of other sialidases like Neu4 to cleave G_{D3} in this region of brain. In the cortex (Figure 3.46 A) of 6-month-old mice, there were an apparent reduction in myelin contents of Galgt-/- and Neu3-/-Galgt-/- mice but there was no effect of the absence of Neu3 sialidase for Neu3-/- mice. For *Galgt* absent mice models, the importance of complex gangliosides was observed but for Neu3-/- mice, the possible compensation of sialidases like Neu4 would be deduced. In thalamus (Figure 3.46 B), even though there were no genotypic differences, the myelin volume reduction was observed for each genotype as expected. The cerebellum and pons (Figure 3.47 A and 3.47 B) presented the similar pattern to younger aged group showing the importance of region-specific production and alteration of myelin contents. As a conclusion, the complex gangliosides were required for central myelination together with their effects on axon-myelin integrity. These gangliosides were functional when interacted with MAG so the presence of Galgt and Neu3 was important for myelin content of nervous system.

In addition to the biochemical and histological analyses on either soft tissue samples or frozen brain sections, the animals were also subjected to behavioural studies in their respective ages. The 3- and 6-month-old WT, Neu3-/-, Galgt-/-, and Neu3-/-

Galgt-/- mice groups were assessed in terms of locomotor activity, balance, strength, anxiety-like behaviours, and fear-motivated memory by Rotarod test, Open Field assay, and Passive avoidance Test. According to previous studies of Chiavegatto *et al*., it was shown that the complex ganglioside deficient mice expressing only G_{M3} and G_{D3} gangliosides were unable to control strength, reflexes, coordination, and balance due to developing behavioural neuropathies (Chiavegatto *et al*. 2000). Therefore, in the studies of *Galgt* defective model at its older ages, there were an apparent reduction in motor abilities evaluated by Rotarod test in comparison to WT littermates (Figure 3.48). The results of this study deduced the importance of complex gangliosides in long-term stability of neurons since this model showed a reduction in myelin volume and axonal regeneration resulting in an apparent nerve cell degeneration (Chiavegatto *et al*. 2000). The reduction in myelin volume and neuron number in especially cerebellum -balance center- and thalamus relaying signals to cerebellum of Galgt-/- mice at both ages were detected in this study, as well. Moreover, by considering signal relaying roles of Purkinje cells in cerebellum, the defective patterns of them were shown in 6-month-old Galgt-/- mice. These results were then correlated with a reduction in motor balance and coordination of this model through a decrease in latency to fall from a rotating rod (Figure 3.48). The results in this study also supported the importance of complex gangliosides in normal neuron stability (Figure 3.48). As a conclusion, the defective motor coordination and balance in this model could be thought. For investigating the potential role of Neu3 sialidase in the absence of complex gangliosides, the double deficient model was also assessed by Rotarod analyses. However, the absent of Neu3 sialidase did not reverse the phenotype despite behaving similar to WT counterparts. The cerebellum for balance control indicated a reduction in myelin volume and neuron number in especially aged group. Furthermore, purkinje cell layer alterations were seen in the cerebellum of this model. Therefore, for both cases the importance of complex gangliosides was investigated while the absence of Neu3 sialidase did not change the latency to fall (Figure 3.48) (Lee *et al*. 2018).

Next, the anxiety like behaviours of the animals were tested by subjecting them to open field test and measuring the time spent at the center of open box and comparing them with time in periphery (Figure 3.49). The anxiety level analyses were related to placing the animals in an open area, and new environment with social isolation. Apart from anxiety-level testing, the locomotor and exploratory activities of the animals could be tested, as well (Nordquist *et al*. 2017). The previous studies with 8- and 12-month-old

Galgt-/- mice, it was shown that the time spent along the walls by escaping from the center was increased (Chiavegatto *et al*. 2000). Thus, in this study, the results supported these results with a decrease in time spent in the center while the increase in the movement in periphery was detected for this model. Moreover, Neu3-/-Galgt-/- mice also indicated a reduction in time in center but an increased time in periphery (Figure 3.49). The absence complex gangliosides could alter the activities of limbic system and olfactory cortex regions of central nervous system (Stafstrom 2006).

Finally, the passive avoidance test was generated in order for evaluating fear-controlled learning and memory aspects of the animal models. The fear related memory was controlled by the actions of amygdala while cerebellum, hippocampus and prefrontal cortex brain regions were related with the recognition memory and learning (Thompson and Kim 1996). In this study, the effects of the lack of complex gangliosides and Neu3 sialidase were assessed by performing passive avoidance task. The levels to escape from dark box related with electric pulse were reduced in Galgt-/- and Neu3-/-Galgt-/- mice in the testing day (Figure 3.50). The studies with transgenic Galgt models showed reduced levels of long-term potentiation in CA1 neurons of hippocampus due to lack of especially b-series complex gangliosides like G_{M1}. The resulting phenotype was related to the failure in learning in this model (Ikarashi *et al*. 2011). Therefore, through the altered learning pattern, the formation of memory could be altered in Galgt enzyme deficient models, as well (Figure 3.50). The decreasing neuron number in hippocampus region in especially older aged groups would be correlated with this phenotype. Neu3 mice G_{M1} levels could not enough for controlling long-term-potentiation in this model. However, for understanding of fear-motivated effects in Galgt-/- and Neu3-/-Galgt-/-, the amygdala region would be further evaluated by measuring the myelin volume, ganglioside content, and neuron number in this region detailly since the nerve degeneration, altered axon-myelin interactions and so reduced conduction velocity of signals due to lack of complex gangliosides would alter signal transduction for forming memory in these models (Figure 3.50).

CHAPTER 5

CONCLUSION

The regulation of the composition and the quantities of gangliosides by the actions of glycosyltransferases or neuraminidases, the cellular fate determination through these glycosphingolipids could be performed. The changes in their local quantities on cell membranes direct cells to either cellular proliferation or programmed cell death. Therefore, the regulations in their patterns are tightly controlled by synthesis enzymes - glycosyltransferases- and neuraminidases acting for catabolism. In this study, one of the four mammalian sialidases called Neuraminidase 3 and a glycosyltransferase named as Galgt were used by generating a double deficient model in order to understand the significance of gangliosides and those ganglioside specific enzymes in the functioning of nervous system. In addition to those aims, through the absence of these enzymes in mouse models, the novel ganglioside pathways could be understood (Chiavegatto *et al*. 2000; Papini *et al*. 2004).

According to previous investigations, Neu3 enzyme was presented to elevate in the cancerous cells for the prevention of apoptosis. The mice model created for studying colon cancer did not shown pathological abnormalities but this could not be an evidence for ignoring the importance of this enzyme in the ganglioside metabolism (Yamaguchi *et al*. 2012). Thus, Seyrantepe *et al*. generated early-onset Tay-Sachs disease mouse model and revealed the crucial role of sialidase Neu3 in a by-pass mechanism found in the mouse brain in contrast to human patients. The removal of this enzyme from the mouse brain led to accumulation of G_{M2} ganglioside (Seyrantepe *et al*. 2018). The Galgt enzyme deficiency causing the loss of complex gangliosides was initially studied in younger mice that did not show altered brain functioning (Takamiya *et al*. 1996). Later, the older aged mouse groups with *Galgt* deficiency presented a progressive worsening in CNS and PNS activity (Chiavegatto *et al*. 2000). Therefore, the significance of complex gangliosides in normal brain physiology was understood. After those investigations, in order to assess the presence of Neu3 sialidase in other parts of ganglioside catabolism pathway in the absence of complex gangliosides, the double deficient animal model would serve as a valuable tool.

In this study, TLC results showed G_{D3} and o-acetyl G_{D3} elevation in *Galgt* deficient mice groups as Galgt-/- and Neu3-/-Galgt-/-. The elevation in the levels was higher in Neu3-/-Galgt-/- compared to Galgt-/- mice. The lack of all other complex gangliosides was possibly compensated by the actions of those gangliosides in cortex and cerebellum tissues according to TLC results (Figure 3.4 and 3.8). Moreover, LacCer levels were elevated in brain regions of *Galgt* deficient models (Figure 3.7 and 3.11). In the absence *Neu3*, there were reduction in most of the complex gangliosides compared to WT mice in cortex (Figure 3.5 A) while in the cerebellum, except G_{M1}, complex gangliosides were reduced (Figure 3.9 A). The elevation in the levels of G_{D3} in Neu3-/-Galgt-/- would be correlated the absence of Neu3 sialidase that was previously investigated to hydrolyze G_{D3} in colon cancer to act as an antiapoptotic molecule. Absence of Neu3 sialidase in Neu3-/-Galgt-/- mice would lead to higher levels of G_{D3} ganglioside in especially cerebellum tissue (Figure 3.10 A). However, in Galgt-/-, the levels of Neu3 sialidase would not be enough to rapidly degrade this ganglioside since a substantial quantity of G_{D3} were also detected in *Galgt* deficient mice. The other contradictory result as the accumulating LacCer in *Galgt* deficient models could be concluded with the absence of Galgt enzyme to produce complex gangliosides (Figure 3.7 and 3.11).

Since accumulating G_{D3} and G_{M1} was previously associated with the apoptotic cell death as the consequence of locally changing concentrations, the further analyses in this study were performed to understand whether the apoptosis was present in the brains of the animal models or not. Moreover, these gangliosides were shown to affect intracellular mechanisms like ER-stress and oxidative stress so in this study, those pathways were also evaluated. The studies were initiated by doing western blot of apoptotic and ER-stress related proteins in addition to examining expression levels of the ER-stress, oxidative stress, and apoptosis associated markers by RT-PCR. According to analyses, it was shown that in cortex tissue of Galgt-/- and Neu3-/-Galgt-/- mice, the G_{D3} activated Bax induced Caspase 3 activity. The release of ER-stress related pore opening in mitochondria caused oxidative stress, as well. For the cerebellum tissue, Neu3 deficiency in Neu3-/- and Neu3-/-Galgt-/- mice could probably lead to apoptosis induction in terms of Caspase levels while Bax levels of Galgt mice was the highest. The apoptosis in Neu3-/- and Neu3-/-Galgt-/- deficient mice was deduced to the absence of antiapoptotic Neu3 sialidase and elevation of G_{M1} and G_{D3} gangliosides (Sano *et al*. 2009). However, the caspases might be activated by the changes in Ca^{2+} content of cytosol affecting mitochondria pores. The Bax activation in Galgt-/- mice was correlated with the increasing levels of ER stress

leading to mitochondrial pore opening via the increase in calcium ions so that certain apoptogenic and oxidative stress factors were released into cytosol. However, the contradictory results in Galgt-/- mice were checked by further analyses like TUNEL assay because the levels of Bcl-2 and Bax were the evidences for the apoptosis in Galgt-/- mice. Then, the thalamus region was evaluated but there was not an explanatory result in terms of the western blot data of apoptosis but for Galgt-/- mice, the presence of ER stress and subsequent oxidative stress in terms of SOD2 was concluded. In the light of those studies, the apoptosis probably altered nerve cells in the brain of especially 6-month-old Neu3-/-, Galgt-/-, and Neu3-/-Galgt-/- mice. These results were further assayed by TUNEL assay, anti-NeuN, anti-CNPase and histopathologic analyses.

The TUNEL results concluded the presence of apoptosis in the cortex of Galgt-/- mice because this assay enabled more region-specific manner by showing fluorescently labeled DNA fragments. The cerebellum tissue TUNEL results were correlated with RT-PCR and western blot analyses and the results in Galgt-/- would be concluded. The thalamus TUNEL positive cells were also deduced to be higher in Neu3-/- and Galgt-/- mice while Neu3-/-Galgt-/- levels were higher than only WT. Finally, hippocampus region was also affected by apoptotic nuclei in all genotypes. Therefore, it could be thought that the arrangements in the ganglioside patterns in different brain regions might result in differentially induced apoptotic pathways (Figure 3.36 and 3.37).

The histopathology analyses showed the altered Purkinje cell layers, degenerating neurons and edema in Galgt-/- and Neu3-/-Galgt-/- mice in Cresyl Echt Violet and Hematoxylin Eosin staining concluding the negative effects of apoptosis in those mice models (Figure 3.38 and 3.39). The Neu3-/- mice showed little effects in histopathology. In addition to histopathology analyses, anti-NeuN staining results were the extension of TUNEL assay with the reduced levels of neuron number in especially 6-month-old Galgt-/- mice for every brain region. In the Neu3-/-mice, the decrease in neuron number in thalamus and cerebellum was correlated with TUNEL positive nuclei. The cortex, thalamus, and cerebellum regions of double deficient mice were also altered in neuron number as a consequence of apoptotic cell death (Figure 3.42 and 3.43). Finally, the anti-CNPase results were evaluated since oligodendrocytes were affected by the apoptosis through the elevation of G_{D3} ganglioside (Figure 3.44 and 3.45). The myelin content, thus, was reduced in Galgt-/- and Neu3-/-Galgt-/- mice so those animal models suffering from decreased myelination in CNS had altered brain functioning affecting balance and coordination (Sha *et al*. 2014). Moreover, the thalamus and cerebellum regions of Neu3-

/- mice showed a decreased myelination directed by G_{M1} regulated cell death in oligodendrocytes, as well. The Luxol Fast Blue assay (Figure 3.41) also supported the anti-CNPase results in 6-month-old Galgt-/- and Neu3-/-Galgt-/- mice. Finally, the PAS staining did indicate accumulating glycosphingolipids in Galgt-/- and Neu3-/-Galgt-/- mice in addition to Neu3-/- mice with the low levels of G_{M1} accumulation.

Then, behavioral analyses were performed to investigate the results of pathological abnormalities in the mice models. In line with the previous examinations, in this study, Galgt-/- mice showed the problems in balance and coordination evaluated by Rotarod test (Sha *et al*., 2014) (Figure 3.48). The absence of Neu3 sialidase was not enough to reverse the negative effects of the loss of complex gangliosides so the double deficient mice presented the altered balance, as well. Furthermore, the memory problems were detected previously. Thus, the passive avoidance performed showed the most worsened short-term memory formation in Galgt-/- and Neu3-/-Galgt-/- mice while the lack of Neu3 could not heal this problem (Figure 3.49). Finally, the anxiety related behaviors were assessed by Open Field Test that evidenced the increased levels of anxious behaviors in Galgt-/- and Neu3-/-Galgt-/- mice in especially 6-month-old group while Neu3-/- could not prevent the occurrence of these alterations (Figure 3.50).

In conclusion, the gangliosides were important regulators of nerve cells by localizing into certain membrane structures together with other membrane proteins. The local changes in their structures, compositions, or concentrations were the causes of the regulation of certain signaling events like cellular proliferation or cellular death. The regulators of cell membrane associated gangliosides were sialidases and glycosyltransferases from which Neu3 and Galgt were stepped forward in this study. The absence of complex gangliosides leading altered brain functions in the mouse model was combined with the defective Neu3 activity. The problems in the mice model were shown to be age-dependent and increased with aging. The alterations at the level of neuron morphology and number shown in especially 6-month-old Galgt-/- mice were similar or decreased in Neu3-/-Galgt- mice that indicated the loss of Neu3 enzyme activity could not show fatal outcomes or the reversal of Galgt-/- pathophysiology. Since the absence of Neu3 sialidase had no lethality effects in the ganglioside metabolism, it could have a potential role to degrade simple gangliosides in Galgt-/- mice in terms of the changes in G_{D3} levels compared to double deficient mice model.

As future direction, the lipid and ganglioside content analyses from the total brains of mice models could be assayed by the mass spectrometry in order for obtaining the

complete primary and secondary changes in the levels of the complex and simple gangliosides in a detailed manner in this study. Moreover, age groups could be chosen as neo-natal to show developmental effects of single and double deficiencies of Neu3 and Galgt enzymes whereas to show progressive effects of the enzyme deficiencies, older aged mice models could also be used. In addition to changes in age of mice models, the fibroblast cell lines of the mice could be generated for assessing oxidative stress or apoptosis levels by Flow Cytometry.

REFERENCES

Babcock, Donner F, and Bertil Hille. (1998). “Mitochondrial Oversight of Cellular Ca2+ Signaling.” Current Opinion in Neurobiology 8 (3): 398–404.

Berridge, Michael J., Martin D. Bootman, and H. Llewelyn Roderick. (2003). “Calcium Signalling: Dynamics, Homeostasis and Remodelling.” Nature Reviews Molecular Cell Biology 4 (7): 517–29.

Bonilla, Myriam, Kristin K. Nastase, and Kyle W. Cunningham. (2002) "Essential role of calcineurin in response to endoplasmic reticulum stress." The EMBO Journal 21 (10): 2343-2353.

Bortner, Carl D., Nicklas B.E. Oldenburg, and John A. Cidlowski. (1995). “The Role of DNA Fragmentation in Apoptosis.” Trends in Cell Biology 5 (1): 21–26.

Boukhris, Amir, Rebecca Schule, José L. Loureiro, Charles Marques Lourenço, Emeline Mundwiller, Michael A. Gonzalez, Perrine Charles, et al. (2013). “Alteration of Ganglioside Biosynthesis Responsible for Complex Hereditary Spastic Paraplegia.” The American Journal of Human Genetics 93 (1): 118–23.

Boya, P, I Cohen, N Zamzami, H L A Vieira, and G Kroemer. (2002). “Endoplasmic Reticulum Stress-Induced Cell Death Requires Mitochondrial Membrane Permeabilization.” Cell Death & Differentiation 9 (4): 465–67.

Chen, Yanfeng, Ying Liu, M. Cameron Sullards, and Alfred H. Merrill. (2010). “An Introduction to Sphingolipid Metabolism and Analysis by New Technologies.” NeuroMolecular Medicine 12 (4): 306–19.

Chiavegatto, Silvana, Ji Sun, Randy J. Nelson, and Ronald L. Schnaar. (2000). “A Functional Role for Complex Gangliosides: Motor Deficits in GM2/GD2 Synthase Knockout Mice.” Experimental Neurology 166 (2): 227–34.

Cohen-Tannoudji, M., P. Marchand, S. Akli, S. A. Sheardown, J. P. Puech, C. Kress, P. Gressens, et al. (1995). “Disruption of Murine Hexa Gene Leads to Enzymatic Deficiency and to Neuronal Lysosomal Storage, Similar to That Observed in Tay-Sachs Disease.” Mammalian Genome 6 (12): 844–49.

Collins, Brian E., Lynda J.-S. Yang, Gitali Mukhopadhyay, Marie T. Filbin, Makoto Kiso, Akira Hasegawa, and Ronald L. Schnaar. (1997). “Sialic Acid Specificity of Myelin-Associated Glycoprotein Binding.” Journal of Biological Chemistry 272 (2): 1248–55.

d'Azzo, A., A. Tessitore, and R. Sano. (2006). "Gangliosides as apoptotic signals in ER stress response." Cell Death & Differentiation 13 (3): 404-414.

De Maria, R. (1997). “Requirement for GD3 Ganglioside in CD95- and Ceramide-Induced Apoptosis.” Science 277 (5332): 1652–55.

Elmore, Susan. (2007). “Apoptosis: A Review of Programmed Cell Death.” Toxicologic Pathology 35 (4): 495–516.

Ferreira, Carlos R., and William A. Gahl. (2017). "Lysosomal storage diseases." Translational science of rare diseases 2, no. 1-2: 1-71.

Fougeray, Sophie, Julien Fleurence, Sébastien Faraj, Meriem Bahri, Denis Cochonneau, Mickaël Terme, Marc-David Leclair, Estelle Thébaud, François Paris, and Stéphane Birklé. (2016). "O-acetylated gangliosides: Structure, biosynthesis, immunogenicity, functions and their potential for cancer immunotherapy."

Furukawa, Keiko, Wei Aixinjueluo, Takeshi Kasama, Yuki Ohkawa, Michiko Yoshihara, Yusuke Ohmi, Orie Tajima, Akio Suzumura, Daiji Kittaka, and Koichi Furukawa. (2008). “Disruption of GM2/GD2 Synthase Gene Resulted in Overt Expression of 9-O-Acetyl GD3 Irrespective of Tis21.” Journal of Neurochemistry 105 (3): 1057–66.

García-Ruiz, Carmen, Anna Colell, Raquel París, and J. C. Fernández-Checa. (2000). “Direct Interaction of GD3 Ganglioside with Mitochondria Generates Reactive Oxygen Species Followed by Mitochondrial Permeability Transition, Cytochrome c Release, and Caspase Activation.” The FASEB Journal 14 (7): 847–58.

Ha, Ki-Tae, Young-Choon Lee, Seung-Hak Cho, June-Ki Kim, and Cheorl-Ho Kim. (2004). "Molecular Characterization of Membrane Type and Ganglioside-specific Sialidase (Neu3) Expressed in E. coli." Molecules & Cells (Springer Science & Business Media BV) 17, no. 2.

Hamm, Robert J., Brian R. Pike, DIANNE M. O'DELL, Bruce G. Lyeth, and Larry W. Jenkins. (1994). "The rotarod test: an evaluation of its effectiveness in assessing

motor deficits following traumatic brain injury." Journal of Neurotrauma 11 (2): 187-196.

Harding, Heather P, Isabel Novoa, Yuhong Zhang, Huiqing Zeng, Ron Wek, Matthieu Schapira, and David Ron. (2000). “Regulated Translation Initiation Controls Stress-Induced Gene Expression in Mammalian Cells.” Molecular Cell 6 (5): 1099–1108.

Hasegawa, Takafumi, Kazunori Yamaguchi, Tadashi Wada, Atsushi Takeda, Yasuto Itoyama, and Taeko Miyagi. (2000). “Molecular Cloning of Mouse Ganglioside Sialidase and Its Increased Expression in Neuro2a Cell Differentiation.” Journal of Biological Chemistry 275 (11): 8007–15.

Heffer-Lauc, Marija, Gordan Lauc, Leonardo Nimrichter, Susan E. Fromholt, and Ronald L. Schnaar. (2005). "Membrane redistribution of gangliosides and glycosylphosphatidylinositol-anchored proteins in brain tissue sections under conditions of lipid raft isolation." Biochimica et Biophysica Acta (BBA)-Molecular and Cell Biology of Lipids 1686 (3): 200-208.

Hirabayashi, Yoshio. (2012). "A world of sphingolipids and glycolipids in the brain—Novel functions of simple lipids modified with glucose—." Proceedings of the Japan Academy, Series B 88 (4): 129-143.

Holst, O., and S. Müller-Loennies. (2007). "Microbial polysaccharide structures, p 123–179. InKamerling H (ed), Comprehensive glycoscience."

Huang, Jing-Qi, Jacquetta M. Trasler, Suleiman Igdoura, Jean Michaud, Nobuo Hanai, and Roy A. Gravel. (1997). "Apoptotic cell death in mouse models of GM2 gangliosidosis and observations on human Tay-Sachs and Sandhoff diseases." Human molecular genetics 6 (11) : 1879-1885.

Ikarashi, Kotaro, Hiroki Fujiwara, Yoshihiko Yamazaki, Jun-Ichi Goto, Kenya Kaneko, Hiroshi Kato, Satoshi Fujii et al. (2011). "Impaired hippocampal long-term potentiation and failure of learning in β1, 4-N-acetylgalactosaminyltransferase gene transgenic mice." Glycobiology 21 (10): 1373-1381.

Iwabuchi, Kazuhisa, Hitoshi Nakayama, Ami Oizumi, Yasushi Suga, Hideoki Ogawa, and Kenji Takamori. (2015). “Role of Ceramide from Glycosphingolipids and Its Metabolites in Immunological and Inflammatory Responses in Humans.” Mediators of Inflammation 2015: 1–10.

Kappagantula, Sunil, Melissa R. Andrews, Menghon Cheah, José Abad-Rodriguez, Carlos G. Dotti, and James W. Fawcett. (2014) "Neu3 sialidase-mediated ganglioside conversion is necessary for axon regeneration and is blocked in CNS axons." Journal of Neuroscience 34 (7): 2477-2492.

Kolter, Thomas. (2012). "Ganglioside Biochemistry." ISRN Biochemistry: 1–36.

Kopitz, Jurgen, Carolina Vonreitzenstein, Claudia Muhl, and Michael Cantz. (1994). "Role of plasma membrane ganglioside sialidase of human neuroblastoma cells in growth control and differentiation." Biochemical and biophysical research communications 199 (3): 1188-1193.

Kopitz, Jürgen, Carolina von Reitzenstein, Maria Burchert, Michael Cantz, and Hans-Joachim Gabius. (1998). "Galectin-1 Is a Major Receptor for Ganglioside GM1, a Product of the Growth-Controlling Activity of a Cell Surface Ganglioside Sialidase, on Human Neuroblastoma Cells in Culture." Journal of Biological Chemistry 273 (18): 11205–11.

Kopitz, Jürgen, Christian Oehler, and Michael Cantz. (2001). "Desialylation of Extracellular GD1a-Neoganglioprotein Suggests Cell Surface Orientation of the Plasma Membrane-Bound Ganglioside Sialidase Activity in Human Neuroblastoma Cells." FEBS Letters 491 (3): 233–36.

Ledeen, Robert W., and Gusheng Wu. (2002). "Ganglioside function in calcium homeostasis and signaling." Neurochemical research 27, no. 7-8: 637-647.

Lee, Jae-Min, Chang-Ju Kim, Jong-Min Park, Min Song, and Youn-Jung Kim. (2018). "Effect of Treadmill Exercise on Spatial Navigation Impairment Associated with Cerebellar Purkinje Cell Loss Following Chronic Cerebral Hypoperfusion." Molecular medicine reports 17 (6): 8121-8128.

Liu, Mei-qing, Zhe Chen, and Lin-xi Chen. (2016). "Endoplasmic Reticulum Stress: A Novel Mechanism and Therapeutic Target for Cardiovascular Diseases." Acta Pharmacologica Sinica 37 (4): 425–43.

Liu, Yujing, Ryuichi Wada, Hiromichi Kawai, Kazunori Sango, Chuxia Deng, Tadashi Tai, Michael P. McDonald, et al. (1999). "A Genetic Model of Substrate Deprivation Therapy for a Glycosphingolipid Storage Disorder." Journal of Clinical Investigation 103 (4): 497–505.

Malisan, Florence, and Roberto Testi. (2002). “GD3 Ganglioside and Apoptosis.” Biochimica et Biophysica Acta (BBA) - Molecular and Cell Biology of Lipids 1585 (2–3): 179–87.

MATSUDA, Junko, Marie T. VANIER, Iuliana POPA, Jacques PORTOUKALIAN, and Kunihiko SUZUKI. (2006). “GD3-and O-Acetylated GD3-Gangliosides in the GM2 Synthase-Deficient Mouse Brain and Their Immunohistochemical Localization.” Proceedings of the Japan Academy, Series B 82 (6): 189–96.

McCullough, Karen D., Jennifer L. Martindale, Lars-Oliver Klotz, Tak-Yee Aw, and Nikki J. Holbrook. (2001). "Gadd153 sensitizes cells to endoplasmic reticulum stress by down-regulating Bcl2 and perturbing the cellular redox state." Molecular and cellular biology 21 (4): 1249-1259.

Miljan, Erik A., and Eric G. Bremer. (2002). “Regulation of Growth Factor Receptors by Gangliosides.” Science Signaling 2002 (160): re15–re15.

Miyagi, Taeko, Tadashi Wada, Akihiro Iwamatsu, Keiko Hata, Yuko Yoshikawa, Satoru Tokuyama, and Masashi Sawada. (1999). “Molecular Cloning and Characterization of a Plasma Membrane-Associated Sialidase Specific for Gangliosides.” Journal of Biological Chemistry 274 (8): 5004–11.

Monti, Eugenio, Augusto Preti, Bruno Venerando, and Giuseppe Borsani. (2002). "Recent development in mammalian sialidase molecular biology." Neurochemical research 27, no. 7-8: 649-663.

Monti, Eugenio, Erik Bonten, Alessandra D'Azzo, Roberto Bresciani, Bruno Venerando, Giuseppe Borsani, Roland Schauer, and Guido Tettamanti. (2010). "Sialidases in vertebrates: a family of enzymes tailored for several cell functions." In Advances in carbohydrate chemistry and biochemistry, vol. 64, pp. 403-479. Academic Press, 2010.

Ngamukote, Sathaporn, Makoto Yanagisawa, Toshio Ariga, Susumu Ando, and Robert K. Yu. (2007). “Developmental Changes of Glycosphingolipids and Expression of Glycogenes in Mouse Brains.” Journal of Neurochemistry 103 (6): 2327–41.

Nordquist, Rebecca E., Ellen Meijer, Franz J. van der Staay, and Saskia S. Arndt. (2017). "Pigs as Model Species to Investigate Effects of Early Life Events on Later Behavioral and Neurological Functions." In Animal Models for the Study of Human Disease, Academic Press, pp. 1003-1030.

Oehler, Christian, Jürgen Kopitz, and Michael Cantz. (2002). "Substrate specificity and inhibitor studies of a membrane-bound ganglioside sialidase isolated from human brain tissue." Biological chemistry, 383 (11): 1735-1742.

Ohanian, J., and V. Ohanian. (2001). "Sphingolipids in Mammalian Cell Signalling." Cellular and Molecular Life Sciences 58 (14): 2053–68.

Palmano, Kate, Angela Rowan, Rozey Guillermo, Jian Guan, and Paul McJarrow. (2015). "The Role of Gangliosides in Neurodevelopment." Nutrients 7 (5): 3891–3913.

Pan, Xuefang, Camila De Britto Pará De Aragão, Juan P. Velasco-Martin, David A. Priestman, Harry Y. Wu, Kohta Takahashi, Kazunori Yamaguchi, et al. (2017). "Neuraminidases 3 and 4 Regulate Neuronal Function by Catabolizing Brain Gangliosides." The FASEB Journal 31 (8): 3467–83.

Papini, Nadia, Luigi Anastasia, Cristina Tringali, Gianluigi Croci, Roberto Bresciani, Kazunori Yamaguchi, Taeko Miyagi, et al. (2004). "The Plasma Membrane-Associated Sialidase MmNEU3 Modifies the Ganglioside Pattern of Adjacent Cells Supporting Its Involvement in Cell-to-Cell Interactions." Journal of Biological Chemistry 279 (17): 16989–95.

Patil, Chris, and Peter Walter. (2001). "Intracellular Signaling from the Endoplasmic Reticulum to the Nucleus: The Unfolded Protein Response in Yeast and Mammals." Current Opinion in Cell Biology 13 (3): 349–55.

Phaneuf, Daniel, Nobuaki Wakamatsu, Jing-Qi Huang, Anita Borowski, Alan C. Peterson, Sheila R. Fortunato, Gerd Ritter et al. (1996). "Dramatically Different Phenotypes in Mouse Models of Human Tay-Sachs and Sandhoff Diseases." Human Molecular Genetics 5 (1): 1–14.

Pralhada Rao, Raghavendra, Nanditha Vaidyanathan, Mathiyazhagan Rengasamy, Anup Mammen Oommen, Neeti Somaiya, and M. R. Jagannath. (2013). "Sphingolipid Metabolic Pathway: An Overview of Major Roles Played in Human Diseases." Journal of Lipids 2013: 1–12.

Rippo, Maria Rita, Florence Malisan, Luigi Rayagnan, Barbara Tomassini, Ivano Condo, Paola Costantini, Santos A. Susin, et al. 2000. "GD3 Ganglioside Directly Targets Mitochondria in a Bcl-2-controlled Fashion." The FASEB Journal 14 (13): 2047–54.

Robert K, Yu, Yi-Tzang Tsai, Toshio Ariga, and Makoto Yanagisawa. (2011). "Structures, biosynthesis, and functions of gangliosides-an overview." Journal of Oleo Science 60, no. 10: 537-544.

Sandhoff, K., and K. Harzer. (2013). "Gangliosides and Gangliosidoses: Principles of Molecular and Metabolic Pathogenesis." Journal of Neuroscience 33 (25): 10195–208.

Sandhoff, Roger, Stefan T. Hepbildikler, Richard Jennemann, Rudolf Geyer, Volkmar Gieselmann, Richard L. Proia, Herbert Wiegandt, and Hermann-Josef Gröne. (2002). "Kidney Sulfatides in Mouse Models of Inherited Glycosphingolipid Disorders." Journal of Biological Chemistry 277 (23): 20386–98.

Sano, Renata, Ida Annunziata, Annette Patterson, Simon Moshiach, Elida Gomero, Joseph Opferman, Michael Forte, and Alessandra d'Azzo. (2009). "GM1-Ganglioside Accumulation at the Mitochondria-Associated ER Membranes Links ER Stress to Ca2+-Dependent Mitochondrial Apoptosis." Molecular Cell 36 (3): 500–511.

Schröder, Martin, and Randal J. Kaufman. (2005). "The mammalian unfolded protein response." Annu. Rev. Biochem. 74: 739-789.

Scorrano, Luca, Valeria Petronilli, Fabio Di Lisa, and Paolo Bernardi. (1999). "Commitment to Apoptosis by GD3 Ganglioside Depends on Opening of the Mitochondrial Permeability Transition Pore." Journal of Biological Chemistry 274 (32): 22581–85.

Seyrantepe, Volkan, Maryssa Canuel, Stéphane Carpentier, Karine Landry, Stéphanie Durand, Feng Liang, Jibin Zeng, et al. (2008). "Mice Deficient in Neu4 Sialidase Exhibit Abnormal Ganglioside Catabolism and Lysosomal Storage." Human Molecular Genetics 17 (11): 1556–68.

Seyrantepe, Volkan, Secil Akyildiz Demir, Zehra Kevser Timur, Johanna Von Gerichten, Christian Marsching, Esra Erdemli, Emin Oztas, et al. (2018). "Murine Sialidase Neu3 Facilitates GM2 Degradation and Bypass in Mouse Model of Tay-Sachs Disease." Experimental Neurology 299 (Pt A): 26–41.

Sha, Sha, Libin Zhou, Jun Yin, Koga Takamiya, Keiko Furukawa, Koichi Furukawa, Masahiro Sokabe, and Ling Chen. (2014). "Deficits in cognitive function and hippocampal plasticity in GM2/GD2 synthase knockout mice." Hippocampus 24 (4): 369-382.

Sheikh, K. A., J. Sun, Y. Liu, H. Kawai, T. O. Crawford, R. L. Proia, J. W. Griffin, and R. L. Schnaar. (1999). “Mice Lacking Complex Gangliosides Develop Wallerian Degeneration and Myelination Defects.” Proceedings of the National Academy of Sciences 96 (13): 7532–37.

Solovyeva, Valeriya V., Alisa A. Shaimardanova, Daria S. Chulpanova, Kristina V. Kitaeva, Lisa Chakrabarti, and Albert A. Rizvanov. (2018). “New Approaches to Tay-Sachs Disease Therapy.” Frontiers in Physiology 9 (November).

Stafstrom, Carl E. (2006). "Behavioral and cognitive testing procedures in animal models of epilepsy." In Models of seizures and epilepsy, pp. 613-628. Elsevier Inc.

Storz, Gisela, and James A. Imlayt. (1999). "Oxidative stress." Current opinion in microbiology 2 (2): 188-194.

Sugiura, Y., K. Furukawa, O. Tajima, S. Mii, T. Honda, and K. Furukawa. (2005). “Sensory Nerve-Dominant Nerve Degeneration and Remodeling in the Mutant Mice Lacking Complex Gangliosides.” Neuroscience 135 (4): 1167–78.

Sun, Angela. (2018). “Lysosomal Storage Disease Overview.” Annals of Translational Medicine 6 (24): 476.-476.

Takamiya, Kogo, Akihito Yamamoto, Keiko Furukawa, Shuji Yamashiro, Masashi Shin, Masahiko Okada, Satoshi Fukumoto et al. (1996). “Mice with Disrupted GM2/GD2 Synthase Gene Lack Complex Gangliosides but Exhibit Only Subtle Defects in Their Nervous System.” Proceedings of the National Academy of Sciences 93 (20): 10662–67.

Thompson, Richard F., and Jeansok J. Kim. (1996). “Memory Systems in the Brain and Localization of a Memory.” Proceedings of the National Academy of Sciences 93 (24): 13438–44.

Valaperta, Rea, Vanna Chigorno, Luisa Basso, Alessandro Prinetti, Roberto Bresciani, Augusto Preti, Taeko Miyagi, et al. 2006. “Plasma Membrane Production of Ceramide from Ganglioside GM3 in Human Fibroblasts.” The FASEB Journal 20 (8): 1227–29.

Vyas, Alka A., Himatkumar V. Patel, Susan E. Fromholt, Marija Heffer-Lauc, Kavita A. Vyas, Jiyoung Dang, Melitta Schachner, and Ronald L. Schnaar. (2002). "Gangliosides are functional nerve cell ligands for myelin-associated

glycoprotein (MAG), an inhibitor of nerve regeneration." Proceedings of the National Academy of Sciences 99 (12): 8412-8417.

Wakil, S. M., D. M. Monies, K. Ramzan, S. Hagos, L. Bastaki, B. F. Meyer, and S. Bohlega. (2014). "Novel B4GALNT1 mutations in a complicated form of hereditary spastic paraplegia." Clinical genetics 86 (5): 500-501.

Wang, Peng, Ji Zhang, Hong Bian, Ping Wu, Reshma Kuvelkar, Ted T. Kung, Yvette Crawley, Robert W. Egan, and M. Motasim Billah. (2004). "Induction of lysosomal and plasma membrane-bound sialidases in human T-cells via T-cell receptor." Biochemical Journal 380 (2): 425-433.

Woods, Amina S., Benoit Colsch, Shelley N. Jackson, Jeremy Post, Kathrine Baldwin, Aurelie Roux, Barry Hoffer et al. (2013). "Gangliosides and ceramides change in a mouse model of blast induced traumatic brain injury." ACS chemical neuroscience 4 (4): 594-600.

Wu, Gusheng, Zi-Hua Lu, Neil Kulkarni, Ruchi Amin, and Robert W. Ledeen. (2011). "Mice Lacking Major Brain Gangliosides Develop Parkinsonism." Neurochemical Research 36 (9): 1706–14.

Xu, You-Hai, Sonya Barnes, Ying Sun, and Gregory A. Grabowski. (2010). "Multi-System Disorders of Glycosphingolipid and Ganglioside Metabolism." Journal of Lipid Research 51 (7): 1643–75.

Yamaguchi, Kazunori, Kazuhiro Shiozaki, Setsuko Moriya, Koichi Koseki, Tadashi Wada, Hiroo Tateno, Ikuro Sato, Masahide Asano, Yoichiro Iwakura, and Taeko Miyagi. (2012). "Reduced Susceptibility to Colitis-Associated Colon Carcinogenesis in Mice Lacking Plasma Membrane-Associated Sialidase." Edited by Markus M. Heimesaat. PLoS ONE 7 (7): e41132.

Yamanaka, S., M. D. Johnson, A. Grinberg, H. Westphal, J. N. Crawley, M. Taniike, K. Suzuki, and R. L. Proia. (1994). "Targeted Disruption of the Hexa Gene Results in Mice with Biochemical and Pathologic Features of Tay-Sachs Disease." Proceedings of the National Academy of Sciences 91 (21): 9975–79.

Yamashita, Tadashi, Yun-Ping Wu, Roger Sandhoff, Norbert Werth, Hiroki Mizukami, Jessica M. Ellis, Jeffrey L. Dupree, Rudolf Geyer, Konrad Sandhoff, and Richard L. Proia. (2005). "Interruption of ganglioside synthesis produces central nervous system degeneration and altered axon–glial interactions." Proceedings of the National Academy of Sciences 102 (8): 2725-2730.

Yao, Denggao, Rhona McGonigal, Jennifer A. Barrie, Joanna Cappell, Madeleine E. Cunningham, Gavin R. Meehan, Simon N. Fewou, et al. (2014). "Neuronal Expression of GalNAc Transferase Is Sufficient to Prevent the Age-Related Neurodegenerative Phenotype of Complex Ganglioside-Deficient Mice." The Journal of Neuroscience 34 (3): 880–91.

Zanchetti, Gabriele, Paolo Colombi, Marta Manzoni, Luigi Anastasia, Luigi Caimi, Giuseppe Borsani, Bruno Venerando, et al. (2007). "Sialidase NEU3 Is a Peripheral Membrane Protein Localized on the Cell Surface and in Endosomal Structures." Biochemical Journal 408 (2): 211–19.